Modeling ion and water permeation through narrow biological channels

by

Artem B. Mamonov

M.Sc., Moscow State University, 1999

Submitted to the Graduate Faculty of

Arts and Sciences in partial fulfillment

of the requirements for the degree of

Doctor of Philosophy

University of Pittsburgh

2006

UNIVERSITY OF PITTSBURGH

School of Arts and Sciences

This dissertation was presented

by

Artem B. Mamonov

It was defended on

9 June 2006

and approved by

Sunil Saxena, Ph. D.

Kenneth D. Jordan, Ph. D.

Michael Cascio, Ph. D.

Dissertation Director: Rob D. Coalson, Ph. D.

Modeling ion and water permeation through narrow biological channels

Artem B. Mamonov, Ph. D.

University of Pittsburgh, 2006

Standard Poisson-Nernst-Planck (PNP) theory is modified by adding contributions due the Dielectric Self Energy and dynamic relaxation of a protein channel in response to ion permeation. This approach is utilized to predict ionic currents through the Gramicidin A (GA) channel, in which the applicability of conventional continuum theories is questionable. The Potential of Mean Force for K^+ and Cl^- ions in GA are obtained by combining an equilibrium molecular dynamics (MD) simulation that samples dynamic protein configurations with a continuum electrostatic calculation of the free energy. The results of our study show that the channel response to the permeating ion produces significant electrostatic stabilization of K^+ inside the channel.

The local diffusion constant of K^+ inside the GA channel has been calculated using four different computational methods based on MD simulations: Mean Square Displacement (MSD), Velocity Autocorrelation Function (FACF), Second Fluctuation Dissipation Theorem (SFDT) and analysis of the Generalized Langevin Equation for a Harmonic Oscillator (GLE-HO). All methods were tested and compared in bulk water and all predicted the correct diffusion constant. Inside GA, MSD and VACF methods were found to be unreliable because they are biased by the systematic force exerted by the channel system. SFDT and GLE-HO methods properly unbias the influence of systematic force and predicted a similar diffusion constant of K^+ inside GA, namely, *ca.* 10 times smaller than in the bulk.

A simplified three-dimensional model of ClC chloride channel was constructed to couple the ion permeation to the motion of a glutamate side chain which acts as the putative fast gate. Dynamic Monte Carlo (DMC) simulations were carried out using this model channel to investigate the dependence of the gate closing rate on internal and external chloride concentration as well as the gate charge. Our simulation results were in qualitative agreement with experimental observations and consistent with the “foot-in-the-door” mechanism.

Osmotic and diffusion permeabilities of H_2O and D_2O in Aquaporin 1 (AQP1) were calculated using MD simulations and, subsequently, osmotic permeabilities were measured experimentally. The combined computational and experimental results suggest that D_2O permeability through AQP1 is similar to that of water.

TABLE OF CONTENTS

PREFACE ..... **XIV**

1.0 INTRODUCTION **1**

2.0 THE ROLE OF THE DIELECTRIC BARRIER IN NARROW BIOLOGICAL CHANNELS: A NOVEL COMPOSITE APPROACH TO MODELING SINGLE CHANNEL CURRENTS. **14**

2.1 ABSTRACT **14**

2.2 INTRODUCTION **15**

2.3 THEORY AND SIMULATION METHODS **17**

2.3.1 Potential-of-Mean-Force-Poisson-Nernst-Planck (PMFPNP) approach to calculate ion currents through the channel **17**

2.3.2 A Continuum approach to calculate the electrostatic free energy **20**

2.3.3 A Combined Molecular Dynamics/Continuum Electrostatics approach to calculate free energy **21**

2.4 THE SIMULATION PROCEDURE **23**

2.4.1 The model system **23**

2.4.2 MD/continuum simulation of an ion in the GA channel **25**

2.4.3 MD calculation of the diffusion coefficients **28**

2.5 RESULTS AND DISCUSSION **28**

2.5.1 Continuum dielectric theory: the role of the dielectric response **28**

2.5.2 Free energy of ion-channel association from combined MD simulations and continuum electrostatics method: the role of channel relaxation **32**

2.5.3 Calculation of diffusion constants **47**

2.5.4 Ion current **49**

2.6 CONCLUSIONS **55**

APPENDIX **57**

2.7 ACKNOWLEDGMENTS **58**

3.0 DIFFUSION CONSTANT OF K^+ INSIDE GRAMICIDIN A: A COMPARATIVE STUDY OF FOUR COMPUTATIONAL METHODS **59**

3.1 ABSTRACT **59**

3.2 INTRODUCTION **60**

3.3 METHODS **63**

3.3.1 Theory **63**

3.3.2 MD simulations **66**

3.4 RESULTS AND DISCUSSIONS **68**

3.4.1 Calculation of diffusion constant of K^+ in bulk water **68**

3.4.2 Analytic test of $\hat{D}(s)$ behavior at small *s* in bulk water **71**

3.4.3 Calculation of K^+ PMF in the GA channel **73**

3.4.4 Calculation of the K^+ diffusion constant inside the GA channel **75**

3.5 CONCLUSIONS **84**

3.6 ACKNOWLEDGMENTS **84**

4.0 MODELING THE FAST GATING MECHANISM IN CLC CHLORIDE CHANNELS **85**

4.1 ABSTRACT **85**

4.2 INTRODUCTION **86**

4.3 METHODS **88**

4.3.1 Model channel **88**

4.3.2 Dynamic Monte Carlo **92**

4.4 RESULTS AND DISSCUSION **95**

4.4.1 Test of the gate motion using a simple analytical model **95**

4.4.2 Dependence of the gate open time on internal and external [Cl^-] **97**

4.4.3 Effect of a negatively charged gate on the gate open time **100**

4.4.4 Effect of D_{gate} and E_{act} **102**

4.4.5 Approximate Factorization of the Gate Closure Mechanism **105**

4.4.6 Factorized model for gate closure mechanism **106**

4.5 CONCLUSIONS **109**

5.0 WATER AND DEUTERIUM OXIDE PERMEABILITY THROUGH AQUAPORIN 1: MD PREDICTION AND EXPERIMENTAL VERIFICATION 112
5.1 ABSTRACT 112
5.2 INTRODUCTION 113
5.3 METHODS 114
5.3.1 MD simulations 114
5.3.2 Reconstitution of AQP1 into liposomes. 116
5.3.3 Measurement of osmotic water permeability. 117
5.4 RESULTS AND DISCUSSION 117
5.5 CONCLUSIONS 123
5.6 ACKNOWLEDGMENTS 124
BIBLIOGRAPHY 125

LIST OF TABLES

Table 1. The value of the $\Delta G_{SIP}^{K^+}$ barrier calculated by numerical solution of the Poisson equation for a rigid NMR configuration of GA (as prescribed by Eq. 2.5)..... 30
Table 2. Distances between K^+ and the nearest backbone carbonyl oxygen atoms are reported for NMR (R_{NMR}), MD_GA (R_{MD_GA}) and MD_GA_K ($R_{MD\_GA\_K}$) configurations..... 42
Table 3. Same as in Table 2 but for NMR, MD_GA and MD_GA_K configurations with K^+ ion placed 9 Å away from the center of the channel..... 43
Table 4. Backbone carbonyl groups angles with respect to the bilayer normal are reported for NMR (θ_{NMR}), MD_GA (θ_{MD_GA}) and MD_GA_K ($\theta_{MD\_GA\_K}$) configurations..... 43
Table 5. The same as in Table 4 but for NMR, MD_GA and MD_GA_K configurations with K^+ ion placed 9Å away from the center of the channel 44
Table 6. Diffusion constants of K^+ in bulk water calculated using the four methods described in the "Theory"..... 69
Table 7. Best fit parameters for analytic memory function of K^+ in bulk SPC/E water fitted from fixed ion MD simulations (cf. Eq. 3.5). 73
Table 8. Diffusion constants of K^+ inside the Gramicidin A channel calculated using the four methods describes in the Theory section. 78
Table 9. Diffusion constants of K^+ inside the Gramicidin A channel calculated using the four methods describes in the Theory section. 80
Table 10. Comparison of the mean value of the squared random force in bulk SPC/E water and inside GA. 81
Table 11. Parameters used in our DMC simulations. Rate constant was calculated using Eq. 4.9. 91
Table 12. Force field parameters of TIP3P-HW model..... 120

Table 13. Results of equilibrium MD simulations. 122
Table 14. Results of applied pressure MD simulations for H_2O 123
Table 15. Results of applied pressure MD simulations for D_2O 123

LIST OF FIGURES

Figure 1. Membrane motif. 2

Figure 2. Snapshot of the GA channel with a K^+ ion embedded in a model membrane and solvated with water after a 300 ps MD simulation as described in text. 24

Figure 3. 2D center-cut of the 3D space-dependent dielectric constant function used for numerical solution of the Poisson equation. 27

Figure 4. Electrostatic free energy of the K^+-GA binding [$\Delta G_{SIP}^{K+}(\vec{r})$ (PMF) is calculated here for the rigid channel with different dielectric constants]. $\Delta G_{SIP}^{K^+}$ is plotted as a function of the ion displacement from the center of the GA channel along the channel axis. 31

Figure 5. $\Delta G_{SIP}^{K^+}$ calculated for different protein structures which are collected during the MD simulation. 34

Figure 6. Dependence of $\Delta G_{SIP}^{K^+}$ on $\boldsymbol{\varepsilon}_w^{ch}$ plotted for several snapshots taken from the MD trajectory. n is the index labeling snapshots along the MD trajectory. 34

Figure 7. The total free energy profile calculated for K+ ion in the channel using the flexible channel from MD trajectory as described in "A Combined Molecular Dynamics/continuum electrostatics approach to calculate free energy", this is averaged $\Delta G_{SIP}^{K^+}$ for a flexible protein.. 37

Figure 8. (*a*) Average free energy of K^+-flexible GA binding $\Delta G_{SIP}^{K^+}$, i.e. with partial charges on GA atoms (●), and $\Delta G_{DSE}^{K^+}$, i.e. without partial charges on the GA atoms (♦). 38

Figure 9. Root Mean Square Deviation (RMSD) of GA backbone carbonyl oxygen atoms in the MD simulation. 39

Figure 10. The average configuration of GA in MD simulation without the ion (*orange peptide*) is superimposed with the average configuration of GA in MD simulations with the K^+ ion (*green peptide*). 45

Figure 11. Average $\Delta G_{SIP}^{Cl^-}$ for a flexible GA (●) and for a rigid one (♦). 46

Figure 12. Calculated diffusion coefficient for K^+ ion inside of the GA channel (●), and in bulk SPC/E water (solid line). Only the D_z component of the diffusion coefficient of the ion in the channel is calculated. 48

Figure 13. Current-voltage relations predicted by PMFPNP model are compared to experimental results [133] (*upper left inset*). 51

Figure 14. Current-Concentration relations as predicted by PNP (♦) and PMFPNP (●) models. The external potential difference was set to 100mV. 52

Figure 15. $\psi_i(\vec{r})$ profile along the channel axes for K^+ and Cl^- is plotted for several bulk electrolyte concentrations and 100 mV applied voltage: *a* , *c* calculated using PNP; *b*, *d* calculated using PMFPNP. 53

Figure 16. Ion concentration profile along the channel axis for K^+ and Cl^- is plotted for several bulk electrolyte concentrations: *a* and *c* calculated using PNP; *b* and *d* calculated using PMFPNP. 54

Figure 17. A snapshot from an MD simulation of Gramicidin A embedded in a model hydrophobic membrane and solvated by 1020 SPC/E water molecules. 68

Figure 18. Calculation of K^+ diffusion constants in bulk water using four methods described in the Theory section. 70

Figure 19. Analytic test of $\hat{D}(s)$ behavior at small s for K^+ in bulk water. 72

Figure 20. PMF profile of K^+ along *z* (channel) direction inside GA. The origin of the coordinate system coincides with in the center of the channel. 74

Figure 21. MSDs of K^+ released at several different locations inside GA. 79

Figure 22. (A) Velocity Autocorrelation Function (VACF) of K^+ in z direction in bulk water (circles) and in the center of GA (squares). (B) VACF in *x* (circles), *y* (diamonds) and *z* (squares) direction for K^+ released in the center of GA. 79

Figure 23. Force Autocorrelation Function (FACF) (jagged line on the bottom) for K^+ fixed in the center of GA, and integrals of the FACF with error bars for K^+ fixed in the center of the

channel (squares), 2.5 Å away from the center of the channel (circles), and 11.5 Å away from the center of the channel (diamonds). 80
Figure 24. $\hat{D}(s)$ function calculated using GLE-HO method for K^+ in bulk water (squares) and in the center of GA (circles) along with extrapolations from 15<s<35 range (the extrapolation range used in Ref. [65]). 81
Figure 25. $\hat{D}(s)$ function calculated using GLE-HO method i.e. Eq. 3.12, for K^+ restrained with different harmonic restraints in the center of GA. 82
Figure 26. $\hat{D}(s)$ function calculated using GLE-HO method for K^+ restrained at three different locations along the channel (z axis) with harmonic constant of 40 kcal/mol/Å^2: 5.2 Å away from the center (diamonds), 2.4 Å away from the center (squares) and in the center of the channel (circles). 83
Figure 27. Schematic depiction of the DMC simulation model. 90
Figure 28. Free energy profile of the fast gate used in our model. θ=0 degrees corresponds to the closed state and θ=120 degrees to the open state of the fast gate. 91
Figure 29. 1D Potential of mean force (PMF) of Na^+ (solid line) and Cl^- (dashed line) along the channel (z) axis. 92
Figure 30. Dependence of the neutral gate probability to be open on time for parameter Set 6 (Table 11) calculated using Kramer's rate theory (circles) and DMC (diamonds). The error bars for DMC data are smaller than symbol labels. 96
Figure 31. Dependence of the gate open time on the internal [Cl^-] for the neutral gate and parameter Set 6 (Table 11) calculated using DMC. Result of the experimental measurements [74] are shown in the inset. 99
Figure 32. Dependence of the gate open time on the external [Cl^-] (squares) for neutral gate with parameter Set 6 (Table 11) calculated using DMC. For comparison, dependence of the gate open time on the internal [Cl^-] is also shown (circles). 100
Figure 33. Dependence of the gate open time on the internal [Cl^-] for neutral gate (circles) and negatively charged gate (squares) calculated using DMC with parameter Set 6 (Table 11). 101
Figure 34. Dependence of the gate open time on the internal [Cl^-] for neutral gate calculated using DMC. 104

Figure 35. Dependence of the normalized neutral gate open time on internal [Cl^-] calculated using DMC. 105
Figure 36. The average number of Cl^- ions along the channel axis for several different internal Cl^- concentrations calculated using DMC for parameter Set 6 (Table 11). 108
Figure 37. Dependence of gate open time on the internal [Cl^-] for neural gate and parameter Set 8 (Table 11). Results of DMC simulations (open squares) are compared with analytical model using Eq. 4.11 (solid line). 109
Figure 38. Osmotic permeability of H_2O and D_2O. Shown is the time course of relative volume (volume at time *t* divided by initial volume) change of AQP1 containing vesicles and control lipid vesicles on abrupt exposure to a doubling of external osmotic pressure in H_2O (A) and D_2O (B). 120
Figure 39. A snapshot from MD simulation of AQP1/H_2O system. Only one monomer and channel water is shown. Note the single file arrangement of water molecules inside the channel. 121
Figure 40. Concentration profile of H_2O along z axis (channel axis) at equilibrium conditions (black line) and 100 MPa applied hydrostatic pressure (red line). Note the low concentration region between approximately z=-11 Å and z=+11 Å: this is the "channel pore region" discussed in the text. 121
Figure 41. Flux versus applied hydrostatic pressure with error bars for H_2O (A) and D_2O (B). Circles represent the calculated (average) data point values, which are shown along with the best-fit line. 122

PREFACE

I would like to express my greatest gratitude to my academic adviser Professor Rob Coalson for inviting me to join his research group and for all his help and support during graduate school. It was an honor and a valuable learning experience to work with one of the best scientists in the field. Rob is an example for highest professional standards and critical thinking.

I am deeply grateful to my parents whose continuous support was invaluable during all these past years.

1.0 INTRODUCTION

Cells of living organisms are surrounded by membranes whose main function is to separate the internal environment from the external. Membranes are made of a phospholipid bilayer that can contain different proteins and molecules such as cholesterol. Due to lipid hydrophobic properties, membranes have low permeability for charged and polar species. However, cells need to exchange their chemical material with the outside environment to carry out diverse metabolic functions. Nature has developed a variety of elaborate ways to transport compounds across the membrane (Figure 1). There are three main classes of transmembrane proteins that perform transport functions: channels, carriers and pumps [1]. Both channels and carriers facilitate the passive transport of chemical species down their electrochemical gradients across the membrane while pumps transport chemical species against their electrochemical gradients by consuming chemical energy stored in ATP or light. Channels have well defined water-filled pores and selectively facilitate the transport of ions and molecules at almost barrier free rates. A single channel can transport as many as millions of solute species per second. Another intrinsic property of channels is that they can open and close in the response to external factors such as ligand binding and membrane potential. What distinguishes carriers from channels is that carriers do not have well defined water-filled pores. The mechanism of carrier conductance is still poorly understood and presumably involves binding/unbinding of solute species to specific sites that due to conformational changes become available to one or the other side of the membrane. Because carriers can transport only one or few species per cycle they are much slower than channels. There are several classes of pumps based on transport mechanism as well as genetic and structural homology. The reaction mechanism for P-class ion pumps involves transient covalent modification of the protein inducing large conformational changes. At one step of the reaction cycle, phosphate is transferred from ATP to the carboxyl of a glutamate or aspartate side-chain, forming “high energy” anhydride linkage. At the later step the phosphate is released

by hydrolysis. Due to the induced conformation changes solute species bound to the protein on one side of the membrane get transported to the other side of the membrane.

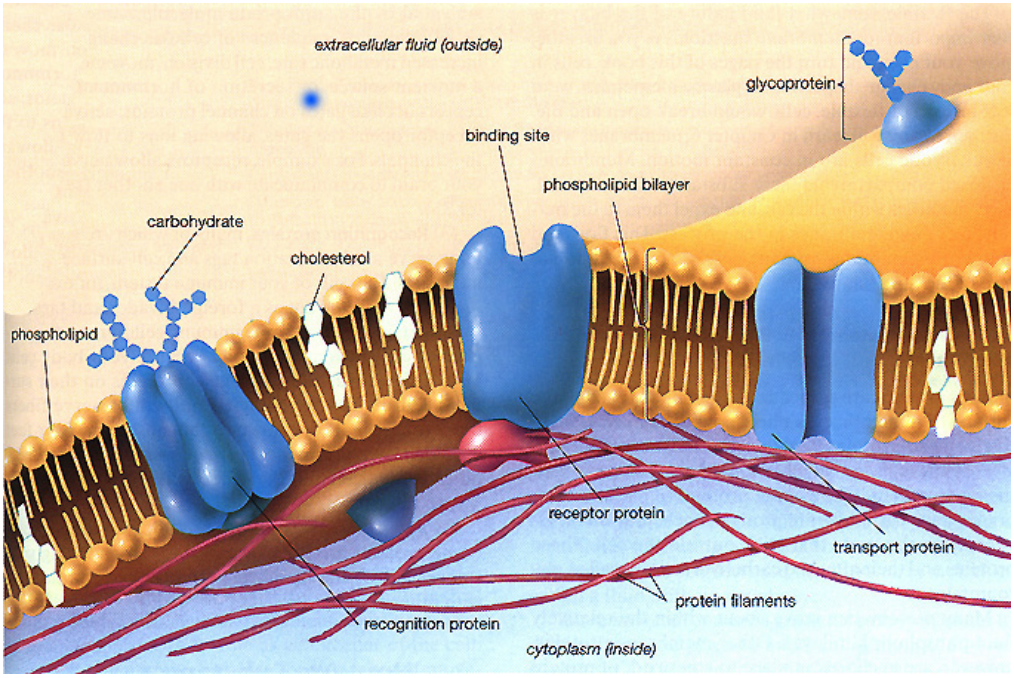

Figure 1. Membrane motif.
(http://sun.menloschool.org/~cweaver/cells/c/cell_membrane/)

Although the history of ion channels is only about 50 years old, it has been characterized by rapid progress, leading to the award of three Nobel Prizes [2]. The hypothesis of the existence of selective pathways for ions in the membrane started to emerge during the classical electrophysiological studies of action potential propagation in nerve cell axons in 1930s-1950s. The squid giant axon was particularly popular to use because of its large size. The squid giant axon can be up to 1 mm in diameter, which is 100-1000 times larger than mammalian axons. The discovery of the squid axon made it much easier for the experimentalists to conduct electrophysiological studies i.e., to insert electrodes inside the cell and make reliable electrical measurements. These studies involved the stimulating of the axon with electric current and measuring the change in the membrane potential caused by such stimulations. Unfortunately, this did not allow the experimentalists to control the membrane potential and had limited application for the studies of the action potential. The development of the voltage clamp technique in the late 1940s was a breakthrough in channel research [3, 4]. Using the feedback amplifier device it

allowed the voltage across the membrane to be "clamped" and the transmembrane currents to be directly measured. Using this technique Hodgkin and Huxley demonstrated in 1952 that permeabilities of K^+ and Na^+ contribute separately to the action potential of the squid giant axon by varying both the membrane potential and extracellular electrolyte composition [5, 6]. The analysis of electrical responses led them to distinguish and separately measure ion currents carried by K^+ and Na^+. Membrane permeabilities for these ions were characterized by different selectivity and separable kinetics but they both were voltage dependent. This study let Hodgkin and Huxley to conclude that there are separate ionic pathways for K^+ and Na^+ in the membrane. Hodgkin and Huxley summarized their experimental data in an empirical kinetic model [7]. This model accurately predicted different features of the action potential in terms of permeability changes. It correctly described the basic property of the ion channels that ions passively move across the membrane down their electrochemical gradients and suggested some features of ion channel gating. Hodgkin and Huxley were awarded the Nobel Prize in medicine in 1963 for their work elucidating the ionic mechanism of nerve cell excitation.

The next major advances in ion channel research came with the discovery of specific channel blocking agents in the 1960s. One of these is tetrodotoxin, which is found in fugu puffer fish and some other species [8]. Tetrodotoxin drew some medical attention in Japan because fugu puffer fish is considered a delicacy there - with occasional lethal consequences. Tetrodotoxin blocks voltage gated sodium channels responsible for generation of action potentials, paralyzing the victim unfortunate enough to eat it. Another natural toxin, saxitoxin, is a chemical analog of tetrodotoxin produced by some dinoflagellate species that are a component of marine plankton. In fertile seasons the population of microscopic dinoflagellates blooms, discoloring the water with their reddish color: this phenomenon is known as "red tide". Shellfish feeding on filtering the water get contaminated with accumulated toxin and it becomes very dangerous to eat them because cooking does not destroy the toxin. Public health authorities control the commercial harvest of shellfish to prevent this type of poisoning. It was also found that tetraethyl ammonium is an effective agent for blocking voltage dependent potassium pathways [9]. The discovery of specific channel blocking agents made it possible to study sodium and potassium channels separately from each other and provided further evidence that permeability of different ions is controlled by separate ion pathways. Later, in the 1980s neurotoxins became crucial for biochemical isolation and purification of ion channels.

The final and most compelling evidence establishing the existence of ion channels as distinct membrane entities came from the studies of Hladky and Haydon in 1972 [10]. They incorporated small amounts of the antibiotic gramicidin into an artificial membrane and observed that ionic permeability of the membrane dramatically increased with stepwise fluctuations in the ionic current. This suggested that each step in the current recording corresponds to opening or closing of an individual ion channel.

Until the 1970s it was possible to study ion channels only collectively. The breakthrough came in 1976 when Erwin Neher and Bert Sakmann invented "patch clamp" technique, which allowed isolation and characterization of individual ion channels [11]. In this method a tiny glass pipette filled with salt solution is placed against a cell membrane where it is believed a single ion channel is. If this is the case, then the current is recorded by the measuring device. This method makes it possible to detect currents which are smaller than 10^{-12} amps i.e., sensitive enough to measure ion flow through single ion channel protein. Patch clamping became possible in part because of improvement in amplifiers, as well as in cell culturing techniques. The slightly modified version of the patch clamp technique called "gigaseal" still remains one of the most important experimental methods for studying ion channels [12]. In the gigaseal method a slight suction is applied to seal the microelectode to the membrane, which considerably reduces the noise level due to formation of resistance to extraneous ion flow. It also allowed different modifications of this technique to be used, including "cell attached", "whole cell", "inside-out" and "outside-out" configurations. The importance of the development of patch clamp technique for ion channel research was reflected in the Nobel Prize awarded to Neher and Sakmann for Physiology and Medicine in 1991.

Patch clamp recordings provided unprecedented opportunities in assessing ion channel function, but mechanistic understanding was still limited to cartoon models. The mechanistic understanding relies on the knowledge of detailed three-dimensional (3D) structure that can explain permeability, selectivity and gating. New methods started to be applied to reveal the structure of ion channels and relate it to function. The amino-acid sequence of nicotinic acetylcholine receptor channel was determined in 1982 by applying recombinant DNA techniques [13]. Combining these data with methods for predicting secondary structure [14] and regions of hydrophobicity [15], provided the first robust hypothesis for ion channel architecture

[16]. Another important method called site directed mutagenesis allowed mutation of selected residues in order to understand their role in permeability, selectivity and gating [17].

The first atomic structure of an ion channel was obtained by Arseniev's group in 1985 for Gramicidin A incorporated in sodium dodecyl sulfate micelles using solution state Nuclear Magnetic Resonance (NMR) [18]. Gramicidin A is a 17 residue peptide with alternating D- and L-amino acids which is selectively permeable only to monovalent cations. It is secreted by organisms in the defense response against foreign bacterial cells by "punching holes" in their cell membranes. The structure revealed that the channel is a head-to-head right handed β-helix dimer that is formed by hydrogen bonding between carbonyl and amino groups six residues apart. The two monomers are held together by the "locking" of six hydrogen bonds so that the total length of the channel is ca. 25 Å and its radius is ca. 2 Å.

Structures provide important information about the mechanism of channel functions at the molecular level. They also serve as important input data to any rigorous theoretical model that aims to elucidate the molecular mechanism of permeation, selectivity or gating. Unfortunately, the rapid progress in determining the high resolution structures (at the atomic detail) of globular proteins has not transpired in the case of ion channels. By present, there is only handful of high resolution structures available for ion channels. This situation has arisen because obtaining high resolution structures relies on using x-ray crystallography, which provides superior signal-to-noise ratio. Ion channels have a hydrophobic exterior, rendering them insoluble in aqueous solutions and, therefore, hard to crystallize. The NMR method is limited to determining structures of small peptides or protein segments and cannot be used to resolve the structure of large channel complexes. The first structure of a physiologically relevant KcsA potassium channel, was resolved by MacKinnon's group in 1998 at 3.2 Å resolution using x-ray crystallography [19]. It provided a great deal of information about how "real" channels look like. The structure revealed that the selectivity filter is a narrow cylinder near the channel's external mouth, ca. 15 Å long, that accommodates two potassium ions. An aqueous cavity was found in the middle of the channel containing one potassium ion. The crystal structure of bacterial ClC channel resolved by MacKinnon's group at 3 Å was reported in 2002 [20]. Surprisingly, the structure of ClC channel was significantly different from any other known ion channel, but consistent with an early "double barrel" model [21]. MacKinnon was awarded a Nobel Prize in Chemistry in 2003 for structural and mechanistic studies of ion channels.

Electron microscopy (EM) is another useful technique for obtaining structures of ion channels at medium to low resolution (typically *ca.* 5-20 Å) [22]. The structure of nicotinic acetylcholine receptor at 4 Å resolution, obtained by Unwin and collaborators in 2003, has helped to elucidate the mechanism of ligand gating [23]. Several structures of physiological relevant ion channels have been resolved at medium and low resolution by the cryogenic EM method including the calcium-release channel of skeletal muscle ryanodine receptor 1 (RyR1) at 9.6 Å resolution [24], voltage gated L-type calcium channel at 23 Å [25] and sodium channel at 19 Å [26].

Many ion channels have been identified since the first voltage clamp studies by Hodgkin and Huxley on voltage dependent sodium and potassium channels. Classification of ion channels is based on selectivity and gating [1]. Some channels are permeable only by certain ions (e.g., the potassium channel KscA is permeable only by K^+ [27]), by a certain class of ions (e.g., Gramicidin A is permeable only by small monovalent cations [28]) or not selective at all (e.g., gap junctions [1]). Classification based on gating includes what kind of physical modulation controls their gating activity. There are channels whose opening or closing is activated by ligand binding (e.g. nicotinic acetylcholine receptor [1]), by a change in the membrane potential, or by membrane tension (e.g. mechanosensitive MscL channel). There are also channels that are not gated at all (e.g. gap junctions, OmpF porin [29]).

It was generally assumed for a long time that water passes biological membranes by simple diffusion through the lipid bilayer [30]. The discovery of Aquaporin 1 (AQP1) in red cells and renal tubules ended the controversies about the existence of molecular water channels [31, 32]. Although water can be transported by different membrane proteins in varying degree, it is now known that water transport across the membrane can be regulated independently of solute transport due to unique properties of the aquaporins. Since the discovery of AQP1 in 1992 around 200 members of the aquaporin family have been identified at all levels of life: bacteria, plants, animals and humans [33]. Eleven aquaporins, designated AQP0-AQP11, have been found in mammals [34]. Aquaporins are expressed differently in many types of cells and tissues in the human body and their mutations are responsible for a wide range of pathological diseases [34].

As experimental methods developed, so did theoretical methods to explain the mechanism of channel functions. Early theoretical studies relied on cartoon structures. These studies treated water-channel-membrane as a problem of electrostatics aimed at discriminating

between different qualitative pictures of ion permeation [35, 36]. For example, it was found that the model describing the channel as the water-filled pore had the most favorable energy for ion permeation compared to other putative models. Several methods for modeling ionic currents across the membrane were proposed [37]: the Poisson-Nernst-Planck (PNP) theory, reaction rate theory [38], Brownian dynamics [37] and Molecular Dynamics [39, 40].

In late 1880s Nernst [41] and Planck [42] independently derived an electro-diffusion equation by combining Fick's law of diffusion with Kohlrausch's electrophoretic equation. In Nernst-Planck theory ions are represented by continuum average concentrations whose time evolution is described as drift down the electrostatic potential gradient accompanied by diffusion. The ionic flux J_i of species i is described by the following one-dimensional (1D) Nernst-Planck equation:

$$J_i = -D_i\left[\frac{dc_i}{dx} + \frac{z_i e}{k_B T} c \frac{d\psi}{dx}\right], \tag{1.1}$$

where D_i is the diffusion constant, c_i is the concentration and z_i is the valence of ionic species i; e is the elementary charge, k_B is the Boltzmann constant, T is the absolute temperature and ψ is the electrostatic potential. Goldman [43], Hodgkin and Katz [44] introduced three assumptions that helped them to derive analytical equations for ion current and zero-current potential across the membrane using 1D Nernst-Planck equation, namely, 1) the electrostatic potential drops linearly across the membrane (constant-field), 2) each ion is not influenced by any other ions and 3) the diffusion coefficients do not vary along the channel.

In a more rigorous approach, the electrostatic potential in the Nernst-Planck equation is not presupposed in advance but calculated from the first principles using Poisson's law:

$$\frac{d}{dx}\left(\varepsilon \frac{d\psi}{dx}\right) = -4\pi\left[\rho_f + \sum_{i=1}^{N} z_i e c_i\right], \tag{1.2}$$

where ε is the dielectric constant of the medium, ρ_f is the density of fixed charges, N is the number of the ion species in the solution. The resulting method in which Poisson and Nernst-Planck equations are solved self-consistently is called Poisson-Nernst-Planck theory [45-47]. 1D PNP was useful for modeling ion currents for channel with unknown atomic structure. For channels with known atomic structure, a 3D version was developed [48]. The numerical algorithm for solving the 3D PNP equations consists of independently solving a set of partial differential equations, namely Nernst-Planck (one for each ionic species) and Poisson [47].

Among different numerical methods for solving partial differential equations, finite difference and finite elements are the most popular. In the finite difference approach the electric potential, charge distribution and spatially dependent dielectric constant are discretized onto a 3D lattice. The relaxation algorithm involves cycling around the interior lattice points and updating them based on an appropriate average over the nearest neighbors. 3D PNP was tested for channels with different radii and it was found that 3D PNP is reliable for channels with medium and large radii but implementation for narrow ion channels encountered several serious weaknesses relates to its mean-field nature [29, 47, 49-51]. In PNP ions are infinitesimal in size and, therefore, the change in the solvation energy as the ion moves from the high dielectric medium provided by the aqueous solution into the low dielectric environment of the channel and membrane is not taken into account. This change in the free energy, known as a dielectric barrier (or dielectric self energy (DSE)), imposes a significant obstruction for ion permeation across the membrane. Numerical calculations based on the Poisson equation revealed that in a narrow cylindrical channel the dielectric barrier for a single ion is very high (*ca.* 15 k_BT) and, therefore, cannot be neglected [49, 50]. Another serious weakness of PNP is that ion-ion interactions are treated only on the mean-field level, which does not properly describe the physical interactions between ions in the channel. It can be especially severe for channels that are occupied by several ions and whose permeation mechanism relies on "knocking" of one ion by another [47, 51]. In its standard implementation, PNP does not take into account flexibility of the protein in response to ion permeation [47, 51]. Furthermore, in the narrow cylindrical channels, which characterize biological channels, the dielectric constant of water may be ill-defined.

In the reaction rate model, the ionic pathway through the channel is described by series of energy wells and barriers [38]. The wells represent specific sites where ions prefer to be localized with barriers separating these sites. Ion permeation consists of a series of "hops" from one site to another. In order to hop an ion must gain enough thermal energy to overcome the imposed energy barrier. Thus, ion permeation is described by a set of kinetic rate equations:

$$\ldots a_{n-1} \underset{k^b_{n-1}}{\overset{k^f_{n-1}}{\rightleftharpoons}} a_n \underset{k^b_{n}}{\overset{k^f_{n}}{\rightleftharpoons}} a_{n+1} \ldots , \tag{1.3}$$

where a_{n-1}, a_n, a_{n+1} represent the ion's favored ("binding") sites, and k^f and k^b represent forward and backward rate constants respectively for hoping between the sites. The rate constants can be calculated using the transition-state theory:

$$k = k_0 \exp\left(-\frac{\Delta G}{k_B T}\right), \tag{1.4}$$

where the pre-exponential factor k_0 is the attempt frequency for the barrier crossing and ΔG is the free energy of activation. In the case of dilute gas-phase reactions, according to the absolute reaction rate theory the prefactor k_0 is equal to $\frac{k_B T}{h}$. In a condensed phase environment such as aqueous solution, the reactants suffer continuous damping interactions with the fluctuating environment and the absolute reaction rate constant cannot be used [1, 37]. A great deal of the statistical mechanics work beginning with Kramers [52] focused on the deriving the appropriate form of the prefactor for reactions in condensed phases. The following equation for prefactor due to Kramers [52] is often used for aqueous solutions $k_0 = \frac{D\sqrt{k_w k_b}}{2\pi k_B T}$, where k_w and k_b are constants of the harmonic potential function ($\frac{1}{2}kx^2$) that describe the curvature of the potential energy near the well and the barrier respectively. Nernst-Planck theory is considered to be superior to the absolute reaction rate theory because the latter theory constitutes a gross simplification of complex microscopic events that captures some important part of a problem while ignoring many others [1, 37, 53]. Nevertheless, standard 1D Nernst-Planck theory does not allow the channel conductance to be interpreted in terms of the actual channel geometry and electrostatics. It can be used if one simply wants to parameterize the channel using the available experimental data.

In Brownian Dynamics ions are treated explicitly but the solvent is replaced by a continuum whose interactions with the ions are modeled via a friction coefficient and a dielectric constant [37, 54]. The protein is held fixed. With these assumptions the 3D movement of ion i can be described by the Langevin equation [55]:

$$m_i \frac{d^2 \vec{r}_i(t)}{dt^2} = \vec{F}^{sys} - \gamma_i \frac{d\vec{r}_i(t)}{dt} + \vec{R}(t), \tag{1.5}$$

where m_i is mass of ionic species i, $\vec{r}_i(t)$ is its 3D position, $\vec{F}^{sys}$ is systematic force acting on ion including the externally applied electric field, electric field due to partial charges on the protein atoms, all other ions, and induced charges from the discontinuity in the dielectric constant at the boundaries between the protein, water and lipid. Furthermore, γ_i is the friction coefficient and $\vec{R}(t)$ is the random force representing the effect of collisions with the water and the channel

wall. The electric potential at each ion position can be calculated using Poisson's law. Because the dynamics of the water and the protein are no longer computed, relatively long time steps can be taken for the ion motion (*ca.* 1 ps). A major advantage of BD method compared to 3D PNP is that it allows direct simulation of ion-ion interactions [49-51]. One difficulty with this approach is that because of the induced charges at the membrane, channel and water interfaces, the calculation of the electrostatic energy at each step requires time-consuming calculations. Several approaches were developed to make such calculations faster. In one approach the electrostatic potential of one, two and if necessary more ions inside the channel is calculated in advance, stored on the computer and used during the BD simulations [56]. In another approach a simple empirical equation was found to accurately describe pairwise electrostatic interactions between ions in a model channel and used in BD simulations [57].

The concept of Molecular Dynamics (MD) is rooted in the Born-Oppenheimer approximation [58]. This approximation states that the motion of electronic and nuclear degrees of freedom in molecules can be separated. Therefore, the motion of nuclei can be solved independently of the motion of electrons. The Born-Oppenheimer approximation implies that the motion of the nuclei occurs in the average field exerted by the electrons called the potential energy surface. Because the mass of nuclei is much heavier than the mass of electrons, the motion of nuclei can be often described using classical laws of motion. In MD, time evolution of the atomic coordinates is calculated by integrating Newton's equation of motion in the potential energy surface described by molecular force fields [59]. These force fields describe the physical interactions between atoms such as repulsion at short distances, electrostatic interactions between partially charged atoms and ions, bond stretching, the opening and closing of angles and rotations about single bonds. Force field models of physical interactions often rely on simple functions such as Hooke's laws [59].

The first detailed MD simulation of an ion channel was reported by Wilson's group in 1984 for the Gramicidin A channel after a reasonable structure became available [60]. The full atomic structure of Gramicidin A was simulated along with approximately 13 water molecules and one ion. Four different ions Li^+, Na^+, K^+, Cs^+ were studied. This study provided important insights about the mechanism of ion solvation, energy stabilization inside the channel and the single-file concerted motion of an ion with the channel water molecules. Nowadays, MD simulations are routinely used to study channels with known atomic structures. The simulations

systems contain as many as tens and even hundreds of thousands of atoms with explicit representation of a phospholipid bilayer and external electrolyte solutions [61-63]. Using MD simulations, accurate free energy curves (in 1D) or surfaces (in 2D) and diffusion constants of solute species can be calculated [61, 64, 65]. Unfortunately, MD is still too slow for calculating solute or solvent fluxes through the channels although several attempts have been made [39, 40, 62, 66]. The approximate time of ion permeation at physiological conditions is in the range of 10-100 ns [1]. Hundreds of ion permeation events must be simulated to obtain statistically reliable results. This would require microseconds of MD time – still far unreachable by standard MD method. However, several MD simulations at high ion concentrations and applied voltages were reported [39, 40, 62]. In the method called Non-equilibrium Molecular Dynamics (NEMD) an electric field is applied to all charged species in the simulation box along the channel axis forcing ions to move through the channel. By averaging the number of ions that crossed the channel over the time period, an ionic current can be calculated. To simulate osmotic fluxes of solvent molecules through channels, a different version of NEMD was developed in which a hydrostatic pressure gradient is established across the membrane by applying extra force to a layer of solvent molecules parallel to the membrane interface [66]. However, the same sampling problem remains and the fluxes can be calculated only at unrealistically high osmotic pressures.

The further development of the field has been made and Chapter 2 addresses improvements of the standard PNP theory for modeling ionic current through narrow ion channels. Gramicidin A was chosen as a test system due to its mature state of experimental and theoretical characterization. A hybrid molecular dynamics–PNP model was developed, termed PMFPNP, which properly accounts for dielectric barrier and channel relaxation effects. In this approach molecular dynamics was used to generate snapshots along the equilibrium MD trajectory for an ion (K^+ and Cl^-) fixed at several different positions along the channel. Subsequently, these snapshots were used to calculate the free energy of transferring the ion from the bulk into the particular point inside the channel by numerical solution of the Poisson equation and averaging the energy over the MD snapshots. Single ion potentials for K^+ and Cl^- ions calculated in this fashion were used to compute ionic currents by solving the appropriately modified 3D PNP equation. The calculated ionic currents were in reasonable agreement with the available experimental data. The new PMFPNP method even predicted saturation of ion current with increase of bulk ion concentration, an effect which is completely missed by the standard

PNP theory. This saturation can be attributed to "clogging" of the channel by the ions as the ionic concentration increases in the bulk solutions. However, this success should be taken with some caution because it is hard to estimate the accuracy of the mean-field approximation and more work is needed to fully asses the model's reliability. In general, mean-field theories have a habit of working better than one might expect (e.g., Debye-Huckel theory, Born theory of solvation) and remain invaluable to the present day [47].

PNP and Brownian dynamics in their approximations rely on the magnitude of the diffusion constant of ions inside the channel. To date there are no direct experimental measurements of the diffusion constant of ions in narrow pores. Indirect experimental data reveals that they are much smaller than in bulk solution [67]. This is reasonable to expect because the mobility of ions and water molecules is suppressed in the confined environment of a narrow ion channel; ions and water molecules form a single file and must move in concert to pass the channel [1]. Therefore, one must rely on theory to predict the diffusion constants and, indeed, several theoretical methods have been developed for this purpose. They are widely used for calculating diffusion properties of ions and molecules in bulk phase [68-70], but the applicability of some of these methods to narrow ion channels is questionable. Currently, there is no consensus in the biophysical literature about the magnitude of the diffusion constants of ions inside narrow pores [65, 67, 71-73]. Different methods and authors predicted a wide range of diffusion constants. In Chapter 3 the diffusion constant of K^+ was calculated inside the Gramicidin A channel using four computational methods based on molecular dynamics simulations, specifically: Mean Square Displacement (MSD), Velocity Autocorrelation Function (FACF), Second Fluctuation Dissipation theorem (SFDT) and Generalized Langevin equation for a Harmonic Oscillator (GLE-HO). All methods were first tested and compared for K^+ in bulk water – all predicted the correct diffusion constant. Inside GA, the MSD and VACF methods were found to be unreliable because they are biased by the systematic force exerted by the membrane channel system on the ion. It was found that SFDT and GLE-HO techniques properly unbias the influence of the systematic force on the diffusion properties and predicts a similar diffusion constant of K^+ inside GA, namely, *ca.* 10 times smaller than in the bulk. A similar diffusion constant inside the channel, namely, 8.5 times smaller compared to the bulk was used in Chapter 2 to calculate ion currents using PMFPNP model. The results were in reasonable agreement with experimental data.

In Chapter 4 the Dynamic Monte Carlo method (essentially equivalent to Brownian Dynamics) was used to study the fast gating of the ClC-0 channel. According to experimental measurements the gate open time of ClC-0 depends strongly on the intracellular concentration, but only weakly on the extracellular concentration [74-76]. To explain this dependence, a "foot-in-the-door" mechanism was proposed [74, 75]. According to this mechanism a permeating Cl^- ion blocks the fast gate from closing by occupying a binding site that would be occupied by the fast gate in the closed state. Recently, Dutzler et al. [77] presented a structural basis for this mechanism and suggested a possible way of coupling ion permeation to ClC channel gating. To test this experimental hypothesis a simplified three-dimensional ClC chloride channel was constructed to couple the ion permeation to the motion of a glutamate side chain which acts as the putative fast gate in the ClC-0 channel. The simulation results were in qualitative agreement with experimental observations and consistent with the "foot-in-the-door" mechanism.

In Chapter 5 NEMD was used to predict diffusion and osmotic permeabilities of water (H_2O) and heavy water (D_2O) through the AQP1 channel. The molecular mechanism of water permeation and selectivity in the AQP channels was recently revealed using MD simulations [63, 78]. Quite recently, an experimental interest arose to study the permeability of heavy water across AQP channels [79] because D_2O properties are almost the same as H_2O and it would be reasonable to expect that their permeabilities are the same too. This hypothesis was first tested using MD simulations in which the diffusion and osmotic permeabilities of H_2O and D_2O through AQP1 were calculated. The simulation results were subsequently confirmed by experimental measurements: indeed, the diffusion and osmotic permeabilities of H_2O and D_2O are very similar through the AQP1 channel.

2.0 THE ROLE OF THE DIELECTRIC BARRIER IN NARROW BIOLOGICAL CHANNELS: A NOVEL COMPOSITE APPROACH TO MODELING SINGLE CHANNEL CURRENTS.

Mamonov, A. B., R. D. Coalson, A. Nitzan, and M. G. Kurnikova. Biophys. J. 2003, vol. 84, p. 3646-3661.

2.1 ABSTRACT

A composite continuum theory for calculating ion current through a protein channel of known structure is proposed, which incorporates information about the channel dynamics. The approach is utilized to predict current through the Gramicidin A ion channel, a narrow pore in which the applicability of conventional continuum theories is questionable. The proposed approach utilizes a modified version of Poisson-Nernst-Planck (PNP) theory, termed Potential-of-Mean-Force-Poisson-Nernst-Planck theory (PMFPNP), to compute ion currents. As in standard PNP, ion permeation is modeled as a continuum drift-diffusion process in a self-consistent electrostatic potential. In PMFPNP, however, information about the dynamic relaxation of the protein and the surrounding medium is incorporated into the model of ion permeation by including the free energy of inserting a single ion into the channel, i.e., the potential of mean force along the permeation pathway. In this way the dynamic flexibility of the channel environment is approximately accounted for. The PMF profile of the ion along the Gramicidin A channel is obtained by combining an equilibrium molecular dynamics (MD) simulation that samples dynamic protein configurations when an ion resides at a particular location in the channel with a continuum electrostatics calculation of the free energy. The diffusion coefficient of a potassium ion within the channel is also calculated using the MD trajectory. Therefore, except for a

reasonable choice of dielectric constants, no direct fitting parameters enter into this model. The results of our study reveal that the channel response to the permeating ion produces significant electrostatic stabilization of the ion inside the channel. The dielectric self-energy of the ion remains essentially unchanged in the course of the MD simulation, indicating that no substantial changes in the protein geometry occur as the ion passes through it. Also, the model accounts for the experimentally observed saturation of ion current with increase of the electrolyte concentration, in contrast to the predictions of standard PNP theory.

2.2 INTRODUCTION

Ion permeation through narrow protein channels is a topic of considerable current interest [80-85]. The importance of ion transport for many vital cell functions is difficult to overestimate. Processes in which substantial ionic currents are generated in membrane channels include maintenance of ionic concentration gradients across the cell membrane, generation of action potentials in neurons and auto-waves in heart muscle to name just three. Moreover, many modern drugs target ionic channels to modify their action [86-89]. Therefore, in addition to extensive experimental effort, there is much theoretical interest in understanding mechanisms of ion channel function at the molecular level. Recent advances in solving 3D structures of membrane proteins in general and channel proteins in particular [90] have enabled attempts at detailed molecular level modeling of ion current through protein channels [48, 91, 92] (see also recent reviews of the subject [85, 93]). A first attempt to perform a full scale non-equilibrium Molecular Dynamics (MD) simulation of ion current through a simplified model channel at very high ion concentrations and applied voltage has been reported recently [40, 94]. However, non-equilibrium MD simulations are too expensive for realistic biological ion channel systems at physiological conditions because of the many different time-scales and length-scales involved. Instead, several Dynamic Monte-Carlo (DMC) [50, 95] and Brownian Dynamics (BD) studies [91, 96-100] of current-voltage relations through different natural and model channels have been recently reported. A key conclusion drawn from these studies is that the dielectric self-energy (DSE) which arises when an ion moves through a relatively narrow channel with diameter of up to ca.1 nm greatly affects the dynamics of ion permeation [49, 50, 95, 101]. A charged particle

which moves from a highly polarizable medium such as water solution into a low polarity medium such as a protein surrounded by a lipid bilayer experiences a dielectric barrier or dielectric self-energy (DSE). Several studies have demonstrated that transport through a narrow channel is greatly reduced or even completely inhibited by the presence of a dielectric barrier [49, 50, 95, 97]. In contrast, experimentally observed currents through narrow channels such as Gramicidin A (GA) are not negligible but, on the contrary, quite substantial - measured in tens of millions of ions per second [1]. Therefore, these relatively small and simple molecular structures function very efficiently as ion channels. One thus suspects that a rigid model of a narrow membrane channel is inadequate for describing its ionic permeability. What is obviously missing from this oversimplified model is the motion of the channel structure itself. The importance of this aspect of ion-channel operation has been clearly demonstrated in equilibrium simulations [102]. In this paper we propose a modeling approach that takes into account the dynamic implication of this motion for the transport of ions under nonequilibrium conditions. The proposed approach can describe ion currents (a long-time scale process) while accounting for the molecular flexibility of the channel protein (fast conformational changes on a short time-scale) which forms the channel. We examine the possible mechanisms by which a functional channel overcomes the impediment of a dielectric barrier and devise a model of an ion channel that is free of fitting parameters (except for a reasonable choice of dielectric constants) and realistic enough to yield ion currents which are compatible with experimental observations. We employ a combination of modeling methods that span a range of molecular resolutions (particle dynamics, continuum electrostatics), thus enabling treatment of ion channel permeation from first principles.

Ion permeation is slow on a molecular time scale. As an ion passes through the channel, the protein channel molecule has time to adjust its local geometry to the presence of the ion "instantaneously" on the time scale of the ion transport [102-105]. We have performed an equilibrium MD study of protein channel relaxation with an ion placed at various positions inside the channel. Our simulations reveal that the introduction of an ion into the channel causes only small changes in the 3D structure of the protein in agreement with previous studies of an Na^+ ion in Gramicidin A channel [106]. These small structural changes, however, substantially alter the ion-protein electrostatic interaction energy, leading to the relative stabilization of the ion-channel complex. This observation forms the basis for the numerical approach proposed herein.

The remainder of this paper is organized as follows. In "Theory and Simulation Methods" section the theoretical formulation is discussed and the simulation methods used are outlined. The "Simulation Procedure" section describes the system studied and provides details of the numerical modeling. Our results are presented and discussed in "Results and Discussion" section, followed by a "Conclusions" section. An Appendix is provided with a summary of terms and abbreviations used throughout the article.

2.3 THEORY AND SIMULATION METHODS

2.3.1 Potential-of-Mean-Force-Poisson-Nernst-Planck (PMFPNP) approach to calculate ion currents through the channel

In continuum theory electrolyte ions are treated as a continuous charge distribution characterized by the concentrations $\{c_i(\vec{r})\}$ of the ionic species involved. The electric charge of the i^{th} ionic species is q_i and the associated charge density is $q_i c_i(\vec{r})$. The distribution of these concentrations is governed by a set of drift-diffusion equations, also called Nernst-Planck equations, one for each ionic species i present in solution. In particular, $\vec{j}_i$, the flux of species i at a given point in space is given by

$$\vec{j}_i(\vec{r}) = -D_i(\vec{r})\left[\frac{\partial c_i(\vec{r})}{\partial \vec{r}} + c_i(\vec{r})\frac{\partial}{\partial \vec{r}}(\beta\psi_i(\vec{r}))\right], \tag{2.1a}$$

and the concentration of species i evolves in accordance with the continuity equation $\frac{\partial c_i}{\partial t} = -div\ \vec{j}_i$. In Eq. 2.1a D_i is the position dependent diffusion coefficient of species i, $\beta = (kT)^{-1}$ is the inverse temperature, k is the Boltzmann constant and T is the absolute temperature. Finally, $\psi_i(\vec{r})$ is the free energy of ions of species i in solution. At steady-state,

$$div\ \vec{j}_i = 0, \tag{2.1b}$$

and thus all quantities in Eq. 2.1 are time-independent. The second term on the right-hand side of Eq. 2.1a is the drift term due to the forces acting on a charged particle of species i from both ion-

ion interactions and external sources. The latter include interactions with fixed charges on the protein system and the externally imposed electric field. Eq. 2.1 is supplemented by concentration boundary conditions that account for the external bulk ionic concentrations of species i (which may be different on different boundary "faces", particularly if concentrations in the bathing solutions on the two sides of the membrane differ).

In a continuum model $\psi_i(\vec{r})$ depends on the electrostatic charge distribution in the system and on the (generally position dependent) dielectric response function $\varepsilon(\vec{r})$. It is convenient to separate the ion free energy into two contributions:

$$\psi_i(\vec{r}) = q_i\phi_{mobile}(\vec{r}) + \Delta G^i_{SIP}(\vec{r}), \tag{2.2}$$

where $\phi_{mobile}(\vec{r})$ is the electrostatic potential due to all mobile ions and the applied electric field associated with external electrodes, and $\Delta G^i_{SIP}(\vec{r})$ is the potential of mean force (PMF) [55] for a single test ion [hence "Single Ion Potential" (SIP)]. In an inhomogeneous dielectric medium $\phi_{mobile}(\vec{r})$ is determined by the Poisson equation:

$$\vec{\nabla}\cdot(\varepsilon(\vec{r})\vec{\nabla}\phi_{mobile}(\vec{r})) = -4\pi\sum_i q_i c_i(\vec{r}), \tag{2.3}$$

subject to Dirichlet boundary conditions, i.e., values of the electrostatic potential are fixed on the boundaries of the computational box [48]. In reality, these boundary conditions are imposed by the electrodes. In numerical models practical considerations often dictate the use of smaller subsystems, for which the computational boundary conditions need to be taken to reflect the effect of the actual ones using theoretical considerations [50]. In the simplest approximation that was introduced in the field of channel modeling by Eisenberg and coworkers [107] the term $\Delta G^i_{SIP}(\vec{r})$ is disregarded. In an obvious generalization $\Delta G^i_{SIP}(\vec{r})$ may include the electrostatic potential due to partial charges fixed on the protein and lipid atoms, i.e. $\Delta G^i_{SIP}(\vec{r}) = q_i\phi_{protein}(\vec{r})$ [48, 92, 108, 109]. Equations 2.1 and 2.3 are coupled nonlinearly via the c_i and ϕ_{mobile} variables. In the general case of a protein of arbitrary geometry and distribution of partial charges on protein atoms, they have no analytical solution and must be solved numerically to self-consistency [48]. Equations 2.1-2.3 with $\Delta G^i_{SIP}(\vec{r}) = q_i\phi_{protein}(\vec{r})$ comprise the so-called Poisson-Nernst-Planck (PNP) theory.

It is important to note that PNP theory invokes a mean field approximation in which the ion responds to the average concentrations of all mobile ions and its integrity as a particle is not accounted for. In particular, it was recognized recently that the change in solvation energy of a single ion when it moves in an inhomogeneous dielectric medium provides an important contribution to the drift flux term of Eq. 2.1 but is missing from the PNP definition of $\Delta G^i_{SIP}(\vec{r})$ [49, 50, 110]. This change in the free energy of a single ion defined with respect to the free energy of that ion in a bulk solvent was termed the dielectric-self energy (or dielectric barrier) $\Delta G^i_{DSE}(\vec{r})$ [50, 95]. When the DSE is taken into account, $\Delta G^i_{SIP}(\vec{r})$ is modified to

$$\Delta G^i_{SIP}(\vec{r}) = q_i \phi_{protein}(\vec{r}) + \Delta G^i_{DSE}(\vec{r}) . \tag{2.4}$$

Recent studies have shown that ΔG^i_{DSE} in a narrow channel strongly influences the resulting current [50, 95]. Therefore, a careful assessment of $\Delta G^i_{SIP}(\vec{r})$ is essential for modeling realistic channel behavior. PNP-like theory that implements $\Delta G^i_{SIP}(\vec{r})$ as defined in Eq. 2.4 will be termed Dielectric-Self-Energy-Poisson-Nernst-Planck (DSEPNP) theory [95]. It was found that using this model to calculate ion transport through narrow channels such as Gramicidin A leads to very low permeability due to the high dielectric self-energy barrier, and cannot account for the observed relatively efficient ionic permeation through such channels. Note however that ΔG^i_{SIP} as defined by Eq. 2.4 still disregards a potentially important contribution to the free energy of inserting an ion at some location in the channel that results from the induced change in the channel geometry. A better calculation of ΔG^i_{SIP} is clearly needed.

In general, calculating free energy differences in bio-molecular processes is a challenging task. Several approaches have been adopted for various problems in molecular modeling. These theoretical methodologies span a wide range of molecular resolution—from estimating electrostatic free energies on a continuum level by solving the Poisson equation [101, 111-113] to full atomistic Molecular Dynamics simulations [102, 114]. In this paper we adopt a methodology to calculate $\Delta G^i_{SIP}(\vec{r})$ for an ion entering the channel which is both cost–effective in terms of computational power and can account for the most essential properties of the system, including efficient ion permeation, when the function $\Delta G^i_{SIP}(\vec{r})$ thus estimated is utilized in a

PNP-like kinetic theory. The general approach of combining the precalculated PMF for a single ion with the self-consistent PNP approach to estimate ion currents will be termed PMFPNP.

The electrostatic free energy of transferring an ion from the bulk solution into the channel is defined by

$$\Delta G^{i}_{SIP}(\vec{r}) = G^{complex}(\vec{r}) - G^{protein} - G^{ion}, \tag{2.5}$$

where $G^{complex}$ is the energy of an ion plus protein/membrane complex embedded in the solvent (water) with the ion located at a point $\vec{r}$ inside the channel, $G^{protein}$ is the energy of the protein/membrane system (without the ion) embedded in the same solvent and G^{ion} is the energy of a single ion in the bulk solvent. The conventional continuum electrostatic approach for calculating $\Delta G^{i}_{SIP}(\vec{r})$, based on Eq. 2.4, is outlined in the next subsection. A combined MD/continuum approach, which takes into account the channel flexibility, is presented in the following subsection. In subsequent sections we present results of applying both methodologies to first determine a plausible set of dielectric constants and then simulate current through the Gramicidin A channel.

2.3.2 A Continuum approach to calculate the electrostatic free energy

In the absence of external fields, the electrostatic energy *G* of a collection of point charges can be found as $G = \frac{1}{2}\sum_i q_i \phi_i$, where the summation is over all electrostatic charges q_i in the system and ϕ_i is the value of the electrostatic potential at the position of charge *i*. The electrostatic potential $\phi(\vec{r})$ needed to calculate G can be found from the corresponding Poisson equation:

$$\vec{\nabla} \cdot (\varepsilon(\vec{r})\vec{\nabla}\phi(\vec{r})) = -4\pi \sum_j q_j \delta(\vec{r} - \vec{r}_j) \tag{2.6}$$

supplemented by Dirichlet boundary conditions with the boundary potential set to zero. In Eq. 2.6 δ is the three-dimensional Dirac delta-function and $\vec{r}_j$ is the position of charge q_j. We have recently shown [50, 95] that for channels as narrow as 4 Å in radius, a continuum description of ion permeation described by DSEPNP, i.e. Eqs. 2.1-2.6, compares well with results of Dynamic Monte-Carlo (DMC) simulations in which ions are treated as charged particles that diffuse in an inhomogeneous dielectric medium with a prescribed diffusion coefficient. As already mentioned,

such particle based simulation models of narrow rigid channels [50, 91] exhibit very small superlinear currents for voltages up to 200 mV. The insignificance of these currents can be traced to the presence of a DSE barrier of several *k*T in such. In contrast, real biological channels of similar size and shape exhibit substantial ionic current at low voltages, with nearly linear or sublinear current-voltage characteristics. A detailed analysis of DSEPNP and DMC particle simulations suggests that the effective polarizability of the channel environment (loosely defined as the ability of the local protein environment to adjust in order to stabilize an extra electric charge) must be higher than implied by the "standard" model utilized in both DMC and DSEPNP studies reported previously. Both approaches for simulating ion motions across channels suffer from the following two major limitations, related to the insufficient flexibility assigned to the description of the channel. First, the solvent polarizability is accounted for by a single parameter (a dielectric constant), while in reality solvent response in the confined channel environment may vary with the position in the channel in a way that cannot be determined from the bulk solvent properties. Second, the protein structure is taken to be rigid (usually at its average NMR configuration), while in reality the protein structure responds to the ionic presence. Below we will investigate the consequences of both limitations.

2.3.3 A Combined Molecular Dynamics/Continuum Electrostatics approach to calculate free energy

$\Delta G^{i}_{SIP}(\vec{r})$ can, in principle, be found from an atomistic simulation in which all atoms on the protein, the lipid membrane and the solvent are treated explicitly. Several attempts to calculate the free energy of an ion in a Gramicidin A channel by MD simulation have been reported [102, 106, 115]. Such calculations obviously rely on a parameterized potential function [116] and require complete sampling of the system configuration space. Improvements in the available parameterizations of potential functions have been slow in recent years [116]. Fortunately, an alternative method of dealing with the second problem, namely the limited sampling of the environment configurational space, has recently been introduced. Since a large portion of the configuration space required for quantitative calculation of the free energy of an ion in a solvent is due to the solvent itself, it was recently proposed [114, 117] that the computationally expensive sampling of solvent configurations may be replaced by considering solvent effects via

an appropriate approximate averaging procedure. A similar procedure was applied to model a polyglycine analogue of Gramicidin A channel [118]. Following the approach of Kollman et al. [114] a full-scale equilibrium Molecular Dynamics (MD) trajectory of the protein in an atomistic solvent is generated to sample the protein conformational space (with and without ion in the channel). The resulting sequence of N protein/water configurations is used to obtain a corresponding sequence of dielectric continuum models of these systems, in which the fixed protein charges are embedded in their corresponding atomic positions. These continuum dielectric configurations, obtained with the permeating ion fixed in a given position, are then used to compute the electrostatic free energy of inserting the ion at that position [111]. Adapting the procedure introduced by Kollman et al, [114] the free energy of ion-protein complex formation is calculated as an average over all n=1,...,N configurations:

$$\Delta G_{SIP}^{i} = \frac{1}{N}\sum_{n=1}^{N} \Delta G_{SIP}^{i(n)} \,, \tag{2.7}$$

where $\Delta G_{SIP}^{i(n)}$ has the same meaning as in Eq. 2.5, calculated for the n-th configuration. The method thus combines an MD simulation to obtain atomistic configurations of the membrane-protein-ion complex with a continuum dielectric representation of each configuration in order to obtain a simple estimate of $\Delta G_{SIP}^{i(n)}$ for that configuration, followed by the average indicated in Eq. 2.7. This approach allows us to account for solvent effects on average, i.e. at a mean field level, and to reduce the noise in the free energy calculations due to insufficient sampling of solvent configurations. The procedure described above, in which the potential of mean force ΔG_{SIP} is calculated via Eq. 2.7 and then used in the PNP formalism, will be termed Potential-of-Mean-Force-Poisson-Nernst-Planck (PMFPNP). We should note that this calculation still disregards contributions to the free energy due changes in the protein internal energy and accounts only approximately (through the temperature dependence of the dielectric functions) for entropic contributions. These missing contributions are expected to be small because deformation of the protein is minimal during the ion permeation (see the results and discussion sections), and because the changes in configuration entropy in these processes are typically small. (A similar number of degrees of freedom are constrained independent of the ion position in the channel).

2.4 THE SIMULATION PROCEDURE

2.4.1 The model system

The approach outlined above was implemented in a series of calculations performed for a model Gramicidin A (GA) channel. GA is an antibiotic peptide widely used in single-channel experiments on passive ion-current permeation through a lipid membrane. It is a robust narrow channel with a relatively rigid structure. It reconstructs into a lipid bilayer by forming head-to-head dimers of betta-helical polypeptides. Due to its unusual primary sequence of alternating L and D amino acids it forms a helix with all the amino acid side-groups extending away from the backbone helix, which forms the channel. Therefore, the channel is lined with backbone carbonyl and amide groups, generating a hydrophilic environment inside the channel. Figure 2 shows a 3D GA ion channel structure incorporated into a crude model of a lipid bilayer membrane, with the membrane/protein channel system solvated in water. This snapshot is taken from an MD simulation performed as described in the next section. As has been noted by several workers [50, 101, 119] the dielectric self-energy is very large for channels less than 5 Å in radius, implying the conundrum discussed above in modeling their permeability. We have chosen to work with GA, the narrowest known ion channel, to emphasize our goal of understanding the permeability of such narrow channels. It has also been pointed out [93, 120] that the selectivity filter of the potassium channel possesses certain similarities to the GA channel and thus our study of GA may help to understand the energetics of the potassium channel selectivity filter as well as other narrow channels.

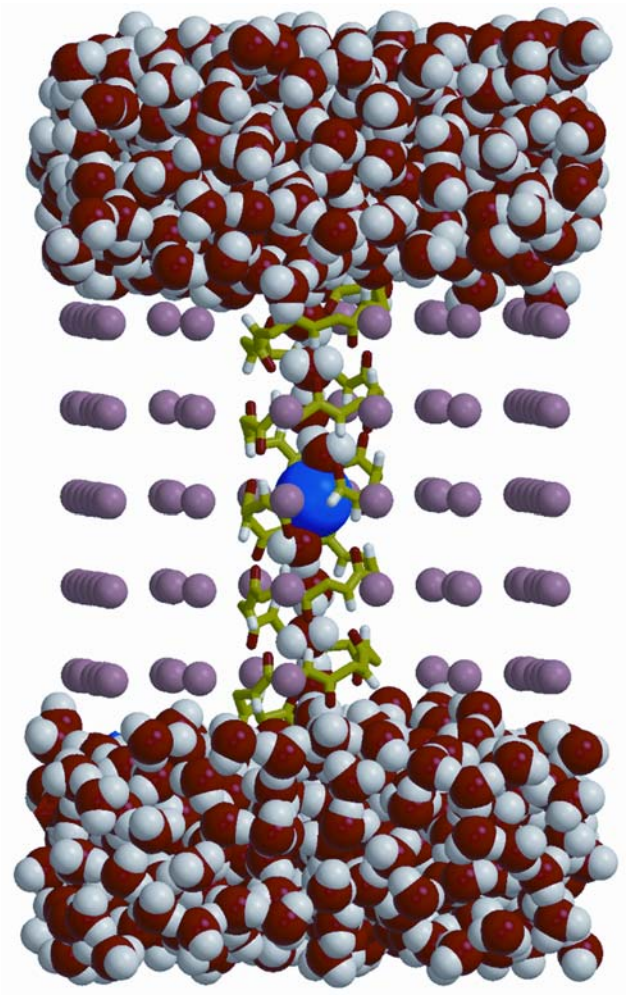

Figure 2. Snapshot of the GA channel with a K^+ ion embedded in a model membrane and solvated with water after a 300 ps MD simulation as described in text.

The model lipid bilayer is represented by pink spheres (the radius of the pink sphere in a picture does not reflect its Lennard-Jones parameters). The K^+ ion is shown as the blue sphere in the center of the channel. Only backbone atoms of the peptide chains are shown.

2.4.2 MD/continuum simulation of an ion in the GA channel

We have performed a set of Molecular Dynamics (MD) simulations of a single potassium ion and a single chloride ion fixed at various positions in a Gramicidin A channel. GA was incorporated into a slab of heavy (mass=100 au) spheres with Lennard-Jones parameters ε=0.05 kcal/mol and σ=4.45 Å, and no partial charge. The slab of these dummy spheres represents a lipid bilayer by providing a non-polar environment for the channel molecule. This channel-membrane model system was then immersed in a box of 738 SPC/E water molecules. Eight water molecules in random configurations were placed inside the GA pore. This system was subjected to energy minimization followed by a 200 ps constant pressure MD equilibration run at 300 K. Positions of the dummy atoms and GA atoms were constrained in space with 200 kcal/mol/Å^2 harmonic spring forces. After the GA-water equilibration was completed, an ion (K^+ or Cl^-) was introduced into the channel. A force constant of 200 kcal/mol/Å^2 was again applied to the positions of the dummy atoms and a 10 kcal/mol/Å^2 force constant was applied to the backbone atoms of the GA. The energy of each system thus prepared was minimized, followed by a 30 ps equilibration period when the harmonic constraints on the GA backbone atoms were gradually reduced from 10 kcal/mol/Å^2 to 0.5 kcal/mol/Å^2. Subsequently, 300 ps production runs were performed with constant volume dynamics at 300 K. 0.5 kcal/mol/Å^2 harmonic constraints were maintained on each of the backbone C and N atoms of GA. The coordinate of the ion along the channel axis (z axis) was held fixed, while its x, y coordinates were allowed to fluctuate. The coordinates of the protein atoms were collected every 2 ps. For every such time point along the MD trajectory the coordinates of the protein molecule and the ion were used to calculate the appropriate electrostatic free energy by solving the Poisson equation as described in "A Continuum Approach to Calculate the Electrostatic Free Energy".

An MD trajectory of GA without K^+ was also generated as described above. All MD simulations were performed using the AMBER 6 software package and Cornell et al. force field [121]. The Lennard-Jones parameters for the potassium ion were taken from work of Aqvist [122]. Bonds involving hydrogen atoms were constrained via the SHAKE algorithm. A 12 Å cut-off distance was used for all non-bonded interactions. The MD time step was set to 2 fs.

For the continuum electrostatics calculations, partial charges on the GA atoms were taken from the Cornell et al. force field [121]. The dielectric response profile $\varepsilon(\vec{r})$ and the positions of the partial charges represent the molecular system in a continuum representation. In the numerical solution of Eq. 2.6, these functions are discretized on a uniform 3D grid as described in [48]. The radii of potassium and chlorine ions, estimated by fitting experimental enthalpies of hydration, were chosen to be R_{K^+}=2.17 Å [101] and R_{Cl^-}=1.81 Å [123]. The electrostatic energy was calculated using our 3D PNP program [48], modified to allow the assignment of several arbitrary values of dielectric constant parameters to different regions of space. For all results reported in the following sections, the grid dimensions of the simulation box were 151^3 with a linear scale of 3 grid points per Å. The width of the membrane was set to 33 Å to mimic a glycerilmonoolein (GMO) bilayer. In Figure 3, a two-dimensional slice of $\varepsilon(\vec{r})$ shows how different dielectric constants are assigned to membrane (ε_m), protein (ε_p), bulk (ε_w), and channel (ε_w^{ch}) regions. The set of calculations described above was repeated with the potassium ion fixed at 18 different positions along one GA monomer at spatial increments of 1 Å, and the chloride ion fixed at 7 different positions at spatial increments of 3 Å.

All calculations were performed on a set of IBM RS6000 workstations. It took ~12.5 h to complete a 300 ps MD simulation and ~27 h to solve a set of Poisson equations as prescribed by Eq. 2.7 for *N*=150.

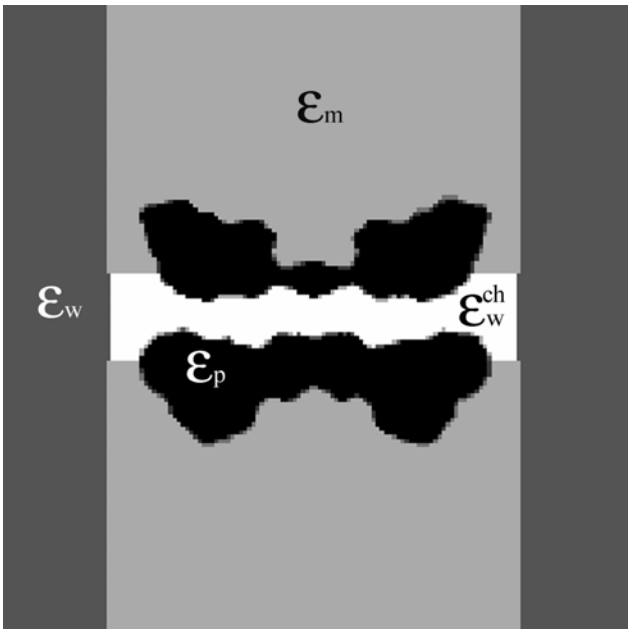

Figure 3. 2D center-cut of the 3D space-dependent dielectric constant function used for numerical solution of the Poisson equation.

The simulation system is divided into four regions: the protein and the ion (ε_p), the bulk water (ε_w), the membrane (ε_m) and the channel water (ε_w^{ch}).

2.4.3 MD calculation of the diffusion coefficients

The diffusion coefficients of the ion were calculated from the all atom MD simulation using the force-force autocorrelation function [55, 68]. According to the fluctuation-dissipation theorem for a Brownian particle moving in thermal equilibrium, the 1D friction coefficient is:

$$\gamma_z(\vec{r}) = \frac{\beta}{2}\int_{-\infty}^{\infty} < F_z(\vec{r},0) \times F_z(\vec{r},t) > dt\,, \tag{2.8}$$

where $F_z(\vec{r},t)$ is the random force on the particle at position $\vec{r}$ along the channel axis. The space-dependent diffusion coefficient $D(\vec{r})$ for the ion can then be extracted using the Stokes-Einstein relation $D(\vec{r}) = \left(\beta\gamma(\vec{r})\right)^{-1}$.

The input needed for Eq. 2.8 was obtained from equilibrium MD simulations with the potassium ion fixed in space. All parameters needed for the MD simulation were set as described in section 3.2. Starting with equilibrated systems of K^+ fixed in the GA channel at a particular position along the channel axis, a 1 ns trajectory was generated and the forces acting on the ion were collected. This calculation was repeated at 18 K^+ ion positions selected as indicated above. A similar MD simulation of a potassium ion in bulk water was also performed. In the latter simulation the K^+ ion was immersed in a box of 735 SPC/E water molecules, the system was equilibrated, and finally, a 1 ns constant volume equilibrium trajectory was generated.

2.5 RESULTS AND DISCUSSION

2.5.1 Continuum dielectric theory: the role of the dielectric response

In continuum modeling of biological channels the position dependent dielectric response function plays a prominent role. The most common choice for the dielectric constant of the membrane and the protein molecule is $\varepsilon_m=\varepsilon_p=2\text{-}5$. Water is usually represented as a dielectric medium with dielectric constant $\varepsilon_w=80$. The choice of these parameters for calculating

electrostatic free energies of binding in solution has been intensively scrutinized in recent literature on globular proteins and organic molecules [111, 124, 125]. However, the appropriate choice of dielectric constants for membrane proteins and membrane environments is relatively unexplored. We have examined the dependence of the electrostatic binding free energy $\Delta G_{SIP}^{K^+}$ in the GA channel, calculated as described in "A Continuum Approach to Calculate the Electrostatic Free Energy", on the choice of the dielectric constant values of the channel environment (as in Figure 3). Indeed, the two-ε model predicts a huge solvation barrier for an ion in a narrow channel. Figure 4 shows via the solid line with filled circles $\Delta G_{SIP}^{K^+}$ for a potassium ion in a GA channel, as a function of the ion position along the channel axis, for a set of ε values in the range indicated above, namely, $\varepsilon_w=\varepsilon_w^{ch}=80$, $\varepsilon_m=\varepsilon_p=4$. The 3D channel structure reported by Arsen'ev et al. [126] was employed in these calculations. Note the high barrier of ~14 *k*T to bring the ion into the center of the channel which results from this choice of parameters. Such a barrier would completely block ion current [95], in contrast to experimental observation. Since the GA channel is very efficient in passing simple cations, one should ask what other properties of the channel and its environment must be incorporated into the model to describe its interaction with the ion at least qualitatively correctly. It is widely believed that the environment around a biological channel is highly inhomogeneous in its electrostatic properties and therefore cannot be described adequately by just two dielectric constant regions. One possibility is that simply employing a better description of the dielectric response function may yield a more realistic permeability model. A protein is a polarizable medium and ε_p values between 4 and 20 have recently been suggested to represent a protein molecule[1] [127-129]. Therefore, the dielectric constant ε_p was increased in several increments up to $\varepsilon_p=30$, keeping $\varepsilon_w=\varepsilon_w^{ch}$ and ε_m as 80 and 4, respectively. Figure 4 shows results for $\Delta G_{SIP}^{K^+}$ obtained under these conditions. We see that even for ε_p as high as 30 the barrier $\Delta G_{SIP}^{K^+}$ is still ~2.5 *k*T. Note that the mobility of water inside the channel is highly restricted and its dielectric response is probably substantially lower than that of

[1] It should be emphasized that this separation of the single ion potential into two contributions, one associated with explicit charges in the environment (in this case the protein) and the other arising from the dielectric self energy, is to some extent arbitrary and reflects our choice of the electrostatic model for the protein.

bulk water. Still, we find that the ion penetration free energy is rather insensitive to the water dielectric constant value in this region. This is shown in Table 1, in which ε_w^{ch} was varied between 40 and 200. It appears that for a narrow channel confined within a low dielectric constant ($\varepsilon<6$) membrane, a substantial dielectric barrier exists even if the protein and/or the channel region are assigned unphysically high dielectric constants. Our recent DMC studies of ion current in a model cylindrical channel [50] indicate that an energetic barrier as low as 2 kT effectively inhibits any appreciable ionic current at low applied voltages [50, 95]. Therefore, other mechanisms by which the environment can polarize in response to the presence of a permeating ion must exist. As outlined in the Introduction, a likely mechanism entails local conformational changes in the protein as the ion moves through the channel. The next subsection considers this possibility.

Table 1. The value of the $\Delta G_{SIP}^{K^+}$ barrier calculated by numerical solution of the Poisson equation for a rigid NMR configuration of GA (as prescribed by Eq. 2.5).

ε_w^{ch}	$\Delta G_{SIP}^{K^+}$ (kT)
40	7.2
80	6.4
200	5.4

The dielectric constant of the channel water is varied while dielectric constants of other parts of the system are kept fixed with epsilon of bulk water ε_w=80, membrane ε_m=4, and protein ε_p=10.

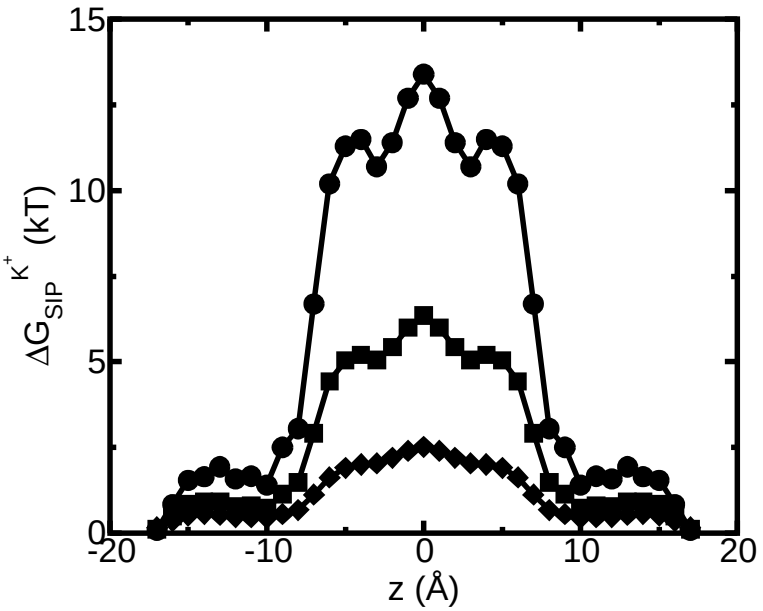

Figure 4. Electrostatic free energy of the K^+-GA binding [$\Delta G_{SIP}^{K+}(\vec{r})$ (PMF) is calculated here for the rigid channel with different dielectric constants]. $\Delta G_{SIP}^{K^+}$ is plotted as a function of the ion displacement from the center of the GA channel along the channel axis.

The energy is calculated by numerical solution of the Poisson equation for a configuration of GA taken from the PDB data bank [126] (Eq. 2.5-2.6). The dielectric constant of the bulk water is ε_w=80, the membrane ε_m=4 and the channel water ε_w^{ch}= 80. The dielectric constant of the protein was taken to be ε_p=4 (●), 10 (■) and 30 (♦). See Figure 3 for the assignment of regions with different dielectric constants.

2.5.2 Free energy of ion-channel association from combined MD simulations and continuum electrostatics method: the role of channel relaxation

In order to elucidate the influence of the protein molecule itself on the passage of an ion through the channel, the free energy $\Delta G_{SIP}^{K^+}$ associated with transferring a K^+ ion from the bulk electrolyte solution to a particular point $\vec{r}$ inside the GA channel was calculated as described above in "A Combined Molecular Dynamics/Continuum Electrostatics Approach to Calculate Free Energy". Namely, a sample of GA configurations was obtained from equilibrium MD simulations with a K^+ ion at various positions along the channel, followed by continuum dielectric model calculations of the free energy associated with transferring the potassium ion into the channel. The results obtained from these simulations are shown in Figures 5-8. Figure 5 shows $\Delta G_{SIP}^{K^+}$ as a function of time calculated along the MD trajectory for the complex with the ion positioned in the center of the channel as in Figure 2, starting from an initial protein structure taken as the NMR geometry. The values of the dielectric constants used in the electrostatic part of this calculation are ε_p=2, ε_m=4, ε_w^{ch}=40 and ε_w=80. The initial relaxation of energy at the onset of the simulation is shown in Figure 5*a*. The free energy drops below zero on average in a fraction of a pico-second. This result clearly demonstrates the short time-scale required for the protein to adjust to the insertion of the ion. The equilibrium state is reached after a longer time. Electrostatic calculations in the equilibrated part of the trajectory, presented in Figure 5*b*, were performed using ε_p=4 (solid line) and ε_p=2 (dashed line), keeping ε_m and ε_w^{ch} as above: note that $\Delta G_{SIP}^{K^+}$ is characterized by large fluctuations between positive and negative values. That is, the protein fluctuates between "permeable" and "non-permeable" structures in rapid succession. On average, however, more configurations that favor ion binding inside the channel occur and the resulting average energy is negative, i.e. favorable for ion permeation into the channel. Another important observation that can be drawn from Figure 5*b* is that the dependence of the calculated energy on the value of ε_p is different for different configurations. For some structures e.g. the initial NMR structure, $\Delta G_{SIP}^{K^+}$ increases as ε_p decreases in the same manner as observed in Figure

4. For others, however, the energy decreases with decreasing ε_p, resulting in tighter binding of the ion-protein complex. This is somewhat counterintuitive and demonstrates that for any particular spatial distribution of the dielectric response function $\varepsilon(\vec{r})$ it is impossible to predict a priori how the polarization of the media around the charge will influence the calculated electrostatic energy in the system. The dependence of $\Delta G_{SIP}^{K^+}$ on the choice of ε_w^{ch} and ε_m is shown in Figure 6, *a* and *b*, respectively, for several snapshots from the MD simulation. $\Delta G_{SIP}^{K^+}$ depends very weakly on ε_w^{ch} (Figure 6*a*) and varies monotonically with ε_m (Figure 6*b*).

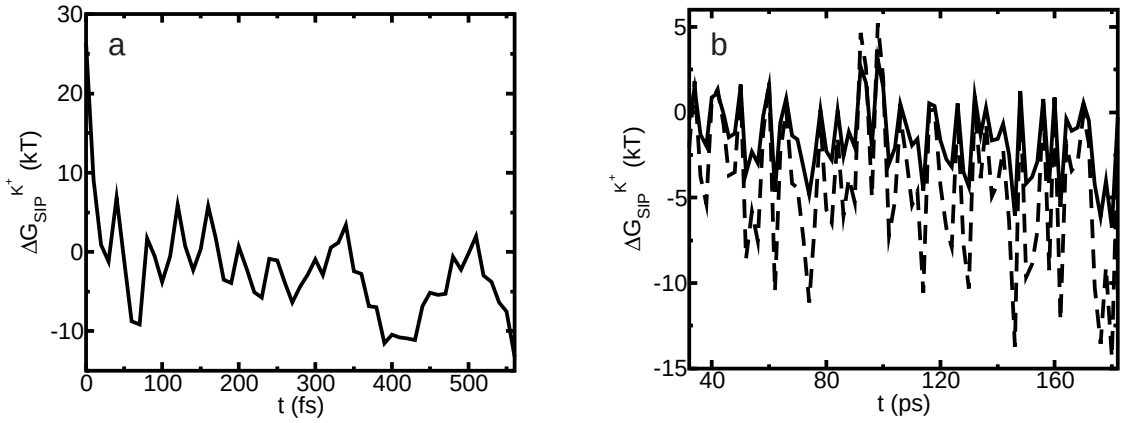

Figure 5. $\Delta G_{SIP}^{K^+}$ calculated for different protein structures which are collected during the MD simulation.

Note how the energy fluctuates between positive and negative values, indicating ion-permeable and impermeable structural conformations of the protein (see explanation in text). In both panels ε_w^{ch}=40, ε_w=80, ε_m=4. (*a*) Initial relaxation. ε_p=2. (*b*) A portion of the equilibrium trajectory. Solid line shows the calculations with ε_p=4 and dashed line is for ε_p=2.

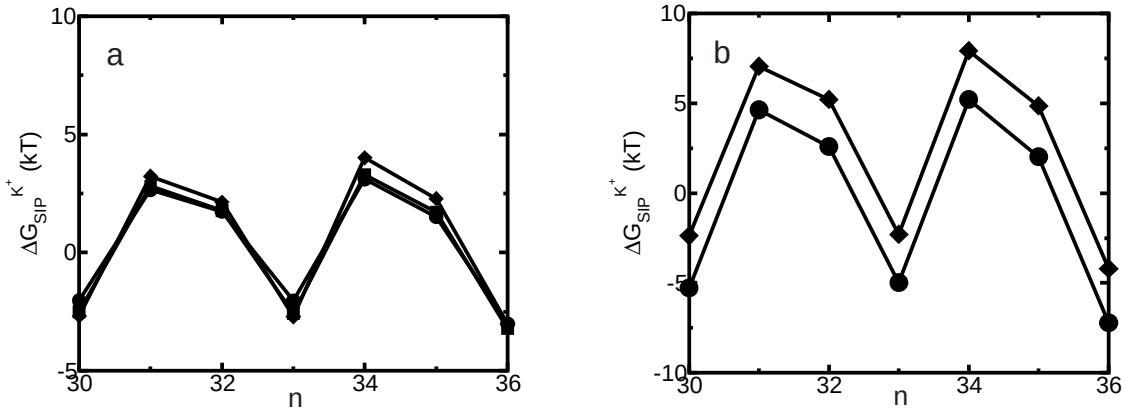

Figure 6. Dependence of $\Delta G_{SIP}^{K^+}$ on ε_w^{ch} plotted for several snapshots taken from the MD trajectory. n is the index labeling snapshots along the MD trajectory.

The following set of dielectric parameters was used ε_p=ε_m=4, ε_w=80. The dielectric constant of the channel water was set to ε_w^{ch}=20 (♦), 40 (■) and 80 (●). See Figure 3 for the assignment of regions with different dielectric constants. (b) Dependence of $\Delta G_{SIP}^{K^+}$ on ε_m plotted for several snapshots taken from the MD trajectory. The following set of dielectric parameters was used ε_p=2, ε_w=80, ε_w^{ch}=40. The dielectric constant of the membrane was set to ε_m=2 (♦) and 4 (●).

$\Delta G_{SIP}^{K^+}$ was shown for individual channel configurations in Figures 4-6. In what follows we consider the corresponding free energy averages over the entire equilibrium MD trajectory according to Eq. 2.7. The following values of dielectric parameters were used to obtain the results presented in the remainder of the paper: $\varepsilon_m=\varepsilon_p=4$, and $\varepsilon_w=\varepsilon_w^{ch}=80$. Figure 7 shows this trajectory-averaged free energy as a function of ion position along the channel axis. Deep wells in the $\Delta G_{SIP}^{K^+}$ profile indicate cation stabilization (and thus possible ion binding sites). The energy minima located closer to the entrance to the channel are deeper than the two energy minima near the center of the channel. It is important to emphasize the large difference between the free energy for ion insertion calculated for the relaxed channel and for the NMR configuration. In Figure 8*a* the trajectory-averaged $\Delta G_{SIP}^{K^+}(\vec{r})$ in the relaxed channel with K^+ is shown (again) along with $\Delta G_{DSE}^{K^+}(\vec{r})$. The electrostatic free energy of transferring an ion from the bulk solution into the channel for the (unrelaxed) NMR channel geometry, calculated via Eq. 2.5, is shown in Figure 8*b*. In Figure 8*c* we show the electrostatic free energy of transferring K^+ from the bulk solution into an averaged structure obtained by first equilibrating the GA protein in an MD simulation with only water inside. Comparing Figure 8*a* to either Figure 8*b* or Figure 8*c*, it is clearly seen that the relaxation of the channel environment in the ion's presence during the MD simulation leads to a huge decrease in the cost of introducing an ion into the channel. If the channel is kept in its NMR geometry or in an average geometrical structure obtained by pre-equilibrating the channel with water but without K^+, an ion entering the channel experiences a significant energetic barrier. Thus, it is favorable for the ion to bind into channel that was allowed to relax in response to the ion's presence, as is the case in Nature. This relaxation evidently leads to a dramatic decrease of the electrostatic free energy, which may become negative. Further inspection of the DSE term in Figure 8 (diamonds) and the total $\Delta G_{SIP}^{K^+}(\vec{r})$ (circles) reveals that when channel flexibility is allowed in the ion's presence (Figure 8*a*) only minor changes in the dielectric-self-energy (DSE) term occur, whereas the total complex association energy $\Delta G_{SIP}^{K^+}(\vec{r})$ decreases significantly. The latter observation indicates that for our choice of the electrostatic model of the protein the main effect of the small structural changes in the channel molecule, which occur as a result of the local relaxation around the permeating ion, is to modify the direct electrostatic interactions of the permeating ion with the nearby partial

charges on the protein groups. The effect of protein relaxation on $\Delta G_{DSE}^{K^+}(\vec{r})$ is small. The direct ion-protein electrostatic interactions become significantly stronger in a flexible channel and can compensate the large DSE, thus rendering the channel permeable.

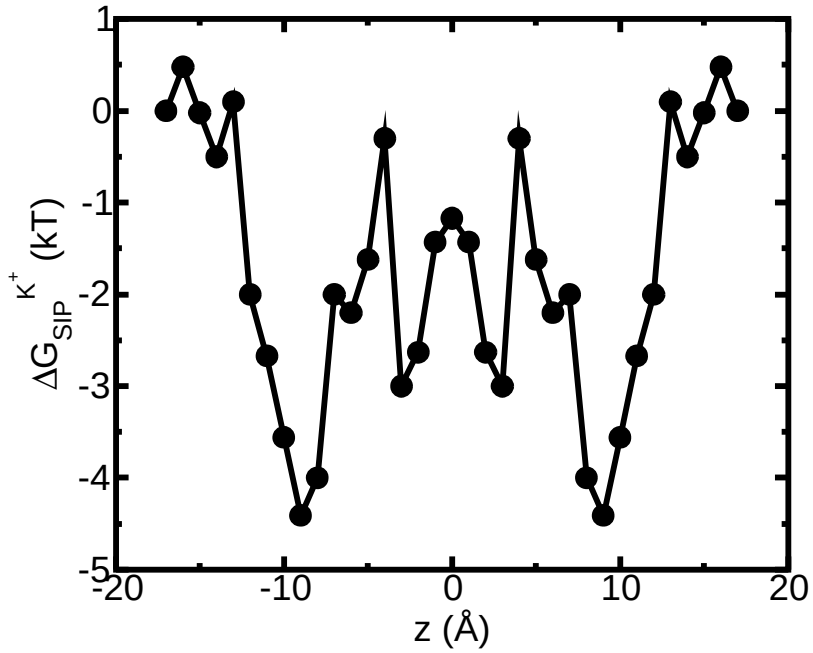

Figure 7. The total free energy profile calculated for K+ ion in the channel using the flexible channel from MD trajectory as described in "A Combined Molecular Dynamics/continuum electrostatics approach to calculate free energy", this is averaged $\Delta G_{SIP}^{K^+}$ for a flexible protein.

Each point in the plot is the average of N=150 calculations along the 300 ps MD trajectory as prescribed by Eq 2.7. The following set of dielectric parameters was used: $\varepsilon_p=\varepsilon_m=4$, $\varepsilon_w=\varepsilon_w^{ch}=80$.

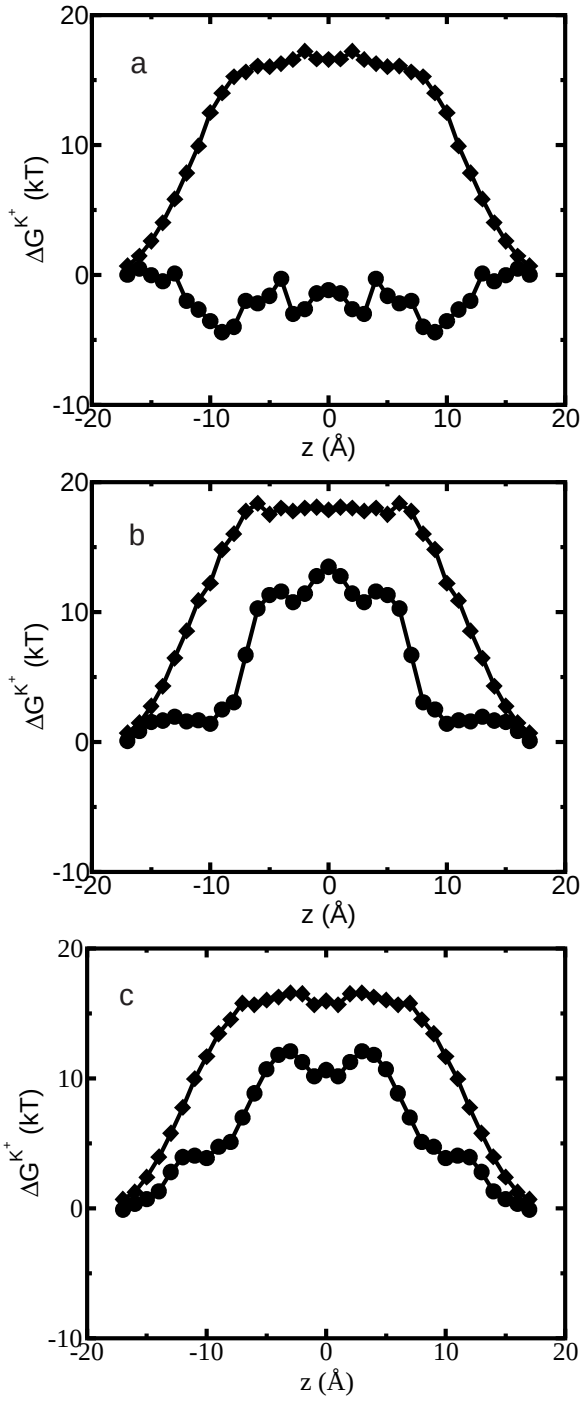

Figure 8. (*a*) Average free energy of K^+-flexible GA binding $\Delta G_{SIP}^{K^+}$, i.e. with partial charges on GA atoms (●), and $\Delta G_{DSE}^{K^+}$, i.e. without partial charges on the GA atoms (♦).

Each point is the average of N=150 calculations along the 300 ps MD trajectory as prescribed by Eq. 2.7. (b) The same as in (a) but for the rigid NMR geometry of GA as prescribed by Eq. 2.5. (c) The same as in (b) but for average MD geometry of GA equilibrated with only water (no ion) in the channel.

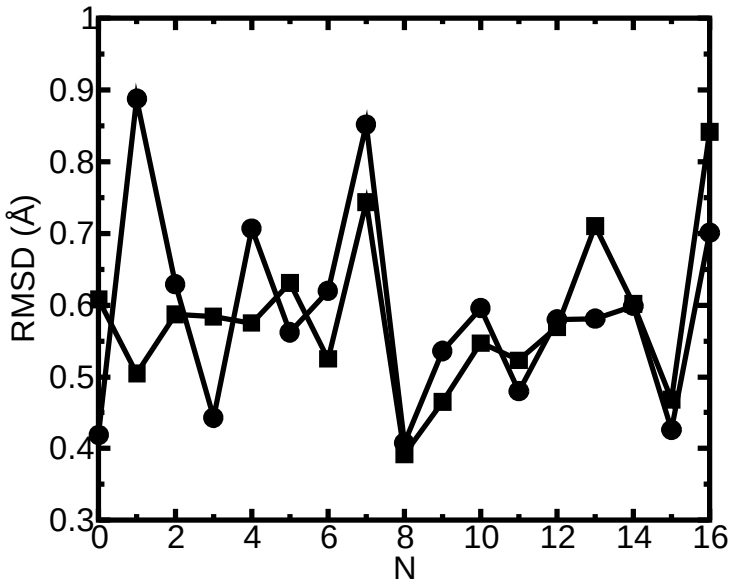

Figure 9. Root Mean Square Deviation (RMSD) of GA backbone carbonyl oxygen atoms in the MD simulation. The numbers of the residues in the protein sequence are indicated on the abscissa. Circles correspond to the simulation with a K^+ ion placed in the center of the channel (●). The curve with the squares is for the GA channel without K^+ (■). Each RMSD curve is calculated along the 300 ps MD trajectory relative to the corresponding average MD structure.

Next, we investigate how the structure of the protein is affected on average by the presence of an ion in the protein channel. The central part of the GA channel is formed when two alpha-helical monomers are stacked on top of each other in the membrane. They are held together only by hydrogen bonds, and, therefore, the center is the most flexible part of the channel, which is fairly rigid in other parts [106]. We have found that deviations from the average atom positions due to the ion presence are relatively small even in the center of the channel. Therefore, we report only the results corresponding to the ion position in the center of the channel to demonstrate that the influence of the ion on the channel structure is small even in this case. In Figure 9 the root mean square deviation (RMSD) from the average equilibrium geometry of the backbone carbonyl oxygen atoms lining the channel pore, accumulated over the course of the MD simulation, is shown. Comparison of the RMSD for a channel simulated with and in the absence of K^+ ion further supports the conclusion that the average geometry of the protein molecule remains essentially unchanged as the ion is introduced into the channel. Direct comparison of the NMR and average MD structures indeed reveals only small changes in the average positions of the protein atoms. This is further illustrated in Figure 10, *a* and *b*, where we have superimposed the average MD coordinates of the GA-K^+ system (ion inside the channel) with the average MD coordinates of the GA system (no ion in the channel). It can be seen from these figures that the largest changes in atomic positions between the two structures occur for carbonyl oxygen atoms closest to the ion. In particular, carbonyl groups near the ion have tilted towards it, as indicated by arrows. Other workers studying narrow channels, e.g. GA and K^+ channels [102, 103, 105, 115, 130] have observed that ions distorted the positions of the carbonyl oxygens to achieve proper solvation. The average positions of most other GA atoms have not changed significantly. Tables 2-5 report various configurational changes that occur in the channel when an ion is placed in different positions along the channel's aqueous pore. The average distances and magnitudes of distortion between the potassium ion and the nearest carbonyl groups are within the range of changes reported earlier in NMR and MD analyses of Na^+ ion migration through GA [106]. There are four carbonyl oxygens whose distances from the ion decrease substantially when the ion is introduced into the center of the GA channel. Even for the largest distortions reported here, it can be seen that the hydrogen bonds among the backbone atoms of GA remain intact, i.e. the additional tilt angle of carbonyl groups involved remains small (see Figure 10).

The shape of the free energy profile in Figure 7 suggests that there are four energy wells in the GA channel. Two of them, represented by the deeper minima, are located at a distance of ~9 Å from the center of the channel. This observation agrees well with previous experimental and theoretical studies of GA binding sites [48, 106, 115]. Two other, energetically shallower, energy minima reside approximately 3 Å from the center of the channel [48].

Finally we consider the free energy profile for a chloride ion in the GA channel. As in the K^+ case, when the GA channel is allowed to relax as described above the free energy barrier calculated for a Cl^- ion decreases (see Figure 11). However, the magnitude of the net barrier in the center of the channel is still much too large to expect any significant Cl^- current through the channel.

Table 2. Distances between K^+ and the nearest backbone carbonyl oxygen atoms are reported for NMR (R_{NMR}), MD_GA (R_{MD_GA}) and MD_GA_K ($R_{MD\_GA\_K}$) configurations.

Name and no. of the residue	R_{NMR} (Å)	R_{MD_GA} (Å)	$R_{MD\_GA\_K}$ (Å)	ΔR_{NMR} (Å)	ΔR_{MD} (Å)	$\Delta\alpha_{MD}$ (deg)
FOR0	3.95	4.30	4.25	0.30	-0.05	6
VAL1	4.03	4.01	3.30	-0.73	-0.71	24
ALA3	3.07	3.35	2.87	-0.20	-0.48	14
FOR17	3.95	3.99	4.03	0.08	0.04	17
VAL18	4.04	4.11	3.13	-0.91	-0.98	33
ALA20	3.09	3.35	2.89	-0.2	-0.46	15

For the NMR configuration K^+ was placed in the center of the channel, for the MD_GA configuration Gramicidin A was equilibrated with only water in the channel, then the average configuration over the trajectory was generated, and a K^+ ion placed in the center of the channel. To generate the MD_GA_K configuration gramicidin A was equilibrated by MD simulation with K^+ placed at the center of the channel, fixing the coordinate in the axial direction: then the average configuration over the trajectory was generated. Changes in K^+-carbonyl oxygen distances between NMR and MD_GA_K (ΔR_{NMR}) configurations and between MD_GA and MD_GA_K (ΔR_{MD}) configurations are also given in the table, as are changes in the carbonyl group angles ($\Delta\alpha_{MD}$) between MD_GA and MD_GA_K configurations. The name and the number of the corresponding residues are given in the first column of the table and are enumerated as in the original file (1GRM) taken from the protein data bank (www.rcsb.org).

Table 3. Same as in Table 2 but for NMR, MD_GA and MD_GA_K configurations with K^+ ion placed 9 Å away from the center of the channel.

Name and no. of the residue	R_{NMR} (Å)	R_{MD_GA} (Å)	$R_{MD\_GA\_K}$ (Å)	ΔR_{NMR} (Å)	ΔR_{MD} (Å)	$\Delta\alpha_{MD}$ (deg)
VAL8	3.64	3.33	2.91	-0.73	-0.42	14
LEU10	3.91	3.76	3.16	-0.75	-0.60	22
TRP11	3.15	3.55	3.26	0.11	-0.29	15
LEU12	5.05	4.73	4.81	-0.24	0.08	15
TRP13	2.55	3.10	2.73	0.18	-0.37	12
TRP15	3.00	2.96	2.78	-0.22	-0.18	0

Table 4. Backbone carbonyl groups angles with respect to the bilayer normal are reported for NMR (θ_{NMR}), MD_GA (θ_{MD_GA}) and MD_GA_K ($\theta_{MD\_GA\_K}$) configurations.

Name and no. of the residue	θ_{NMR} (deg)	θ_{MD_GA} (deg)	$\theta_{MD\_GA\_K}$ (deg)
FOR0	5	12	10
VAL1	157	158	155
ALA3	158	161	158
FOR17	174	171	161
VAL18	24	23	26
ALA20	23	18	23

To generate the MD_GA configuration Gramicidin A was equilibrated with only water in the channel, then the average configuration over the trajectory was computed, and a K^+ ion placed in the center of the channel. For the MD_GA_K configuration gramicidin A was equilibrated by MD simulation with K^+ placed at the center of the channel, fixing the coordinate in the axial direction: then the average configuration over the trajectory was computed.

Table 5. The same as in Table 4 but for NMR, MD_GA and MD_GA_K configurations with K^+ ion placed 9Å away from the center of the channel[2].

Name and no. of the residue	θ_{NMR} (deg)	θ_{MD_GA} (deg)	$\theta_{MD\_GA\_K}$ (deg)
VAL8	15	13	17
LEU10	9	4	23
TRP11	155	155	144
LEU12	19	8	5
TRP13	150	155	146
TRP15	142	144	147

[2] It is worth noting that the carbonyl group angle with respect to the bilayer normal does not fully characterize the actual degree of protein motion. For example, from Table 2 the distance between carbonyl oxygen of VAL18 and K^+ decreases by ~1Å when the ion is placed in the center of the channel and the carbonyl group changes its angle by ~33°. On the other hand, as seen in table 4, the carbonyl group angle with respect to the bilayer normal has not changed significantly. The reason is that the carbonyl group has flipped, so that the change in interatomic distances occurred not due to the change of the angle with respect to the bilayer normal but due to the change of the angle in the plane of the bilayer. We have also noticed that the potassium ion changes its position in the bilayer plane relative to the center of the channel by ~0.2Å when it has been equilibrated in the center of the channel and by ~0.3Å when it has been equilibrated at 9Å away from the center.

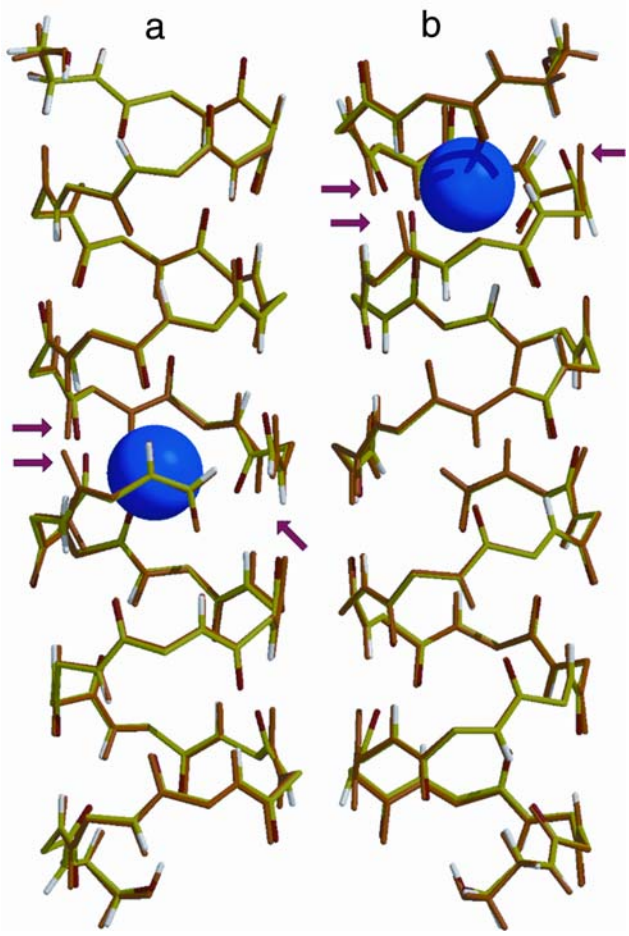

Figure 10. The average configuration of GA in MD simulation without the ion (*orange peptide*) is superimposed with the average configuration of GA in MD simulations with the K^+ ion (*green peptide*).

K^+ is shown as a blue sphere. Arrows indicate the carbonyl oxygens that bent toward the K^+ due to favorable electrostatic interactions. (a) During the MD simulation, an ion was in the center of the channel; (b) K^+ is at 9 Å from the center of the channel, the predicted position of the binding cite (cf. Figure 7).

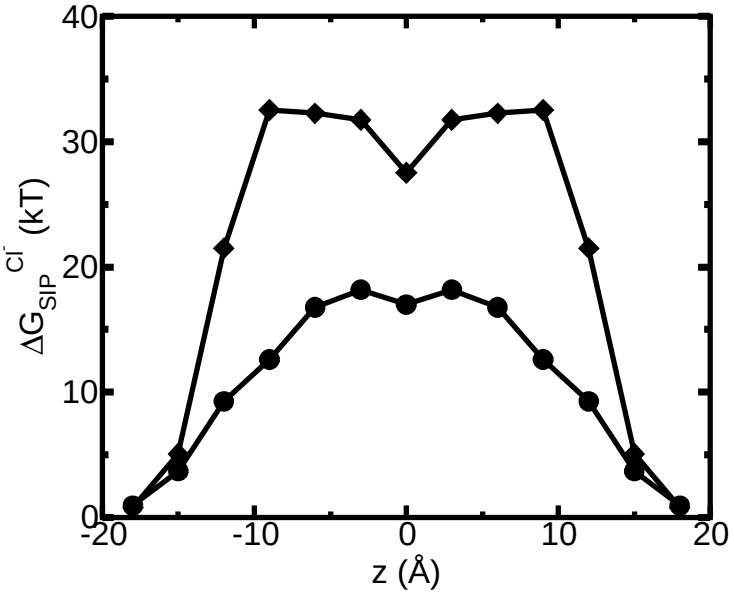

Figure 11. Average $\Delta G_{SIP}^{Cl^-}$ for a flexible GA (●) and for a rigid one (♦).

For the flexible protein each point in the plot is the average of N=150 calculations along the 300 ps MD trajectory as prescribed by Eq 2.7. The NMR geometry of the GA was used for the rigid channel. The following set of dielectric parameters was used for both calculations: $\varepsilon_p=\varepsilon_m=4$, $\varepsilon_w=\varepsilon_w^{ch}=80$.

2.5.3 Calculation of diffusion constants

Current calculations using PMFPNP or Brownian Dynamics techniques crucially depend on the magnitude of the diffusion coefficients that characterize the motion of ions in the channel. In the narrow pore of Gramicidin the permeant ion is largely dehydrated and is instead coordinated by backbone carbonyl groups. The mobility of the permeating ion is suppressed not only by the restrictions inherent in its lateral confinement but also by strong electrostatic interactions with these relatively immobile carbonyl oxygens. Moreover, due to the single file arrangement of the ion and water molecules, the motion of the ion is coupled to the motion of surrounding water, which is also inhibited inside the channel [115].

There are no direct experimental measurements of diffusion coefficients of ions inside Gramicidin or other channels. The diffusion coefficient of a potassium ion in bulk water calculated as described in MD Calculation of the Diffusion Coefficients and indicated in Figure 12 is only 13% smaller than the experimentally measured value [131]. Figure 12 also shows the calculated diffusion coefficient of a K^+ ion inside the channel. The resulting values are *ca.* 8.5 times less than in the bulk solution. Several model MD studies of ion diffusion coefficients inside various model channels have been reported recently. All of them find reduction by a factor of 3-10 in the diffusion coefficient when the ion is moved from bulk water into a channel environment [73, 132]. Furthermore, the ion's mobility is expected to be position dependent. In Figure 12 position is measured with respect to the channel center. We see that when an ion leaves the channel (at about 17 Å from the channel center) its diffusion coefficient abruptly increases by a factor of four. At this distance the ion is completely solvated by reservoir water and interaction with the channel is very weak. The small size of the simulation box did not allow us to move the ion to a distance from the channel at which the value of the bulk $D_w^{K^+}$ is completely recovered. In the kinetics calculations described below we have used $D_w^{K^+}$ =1.75x10^{-5} cm^2/s in the bulk region and 0.25x10^{-5} cm^2/s in the channel based on the numerical results shown in Figure 12. A linear interpolation function has been employed to connect bulk and channel diffusion constant at the ends of the GA. The diffusion constants for Cl^- ion were set to the same

values as for the K^+ ion, based on the fact that in bulk water these ions have similar diffusion constants.

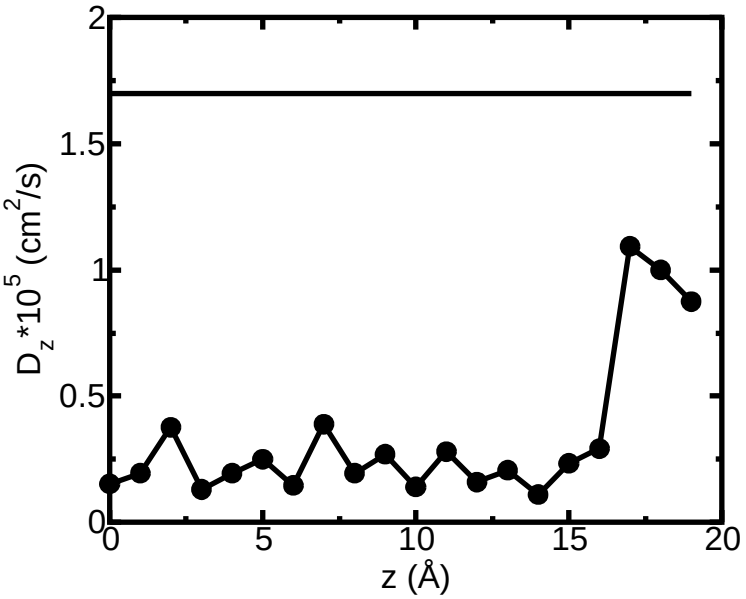

Figure 12. Calculated diffusion coefficient for K^+ ion inside of the GA channel (●), and in bulk SPC/E water (solid line). Only the D_z component of the diffusion coefficient of the ion in the channel is calculated.

2.5.4 Ion current

With the calculated diffusion coefficients and free energies for ion–channel interaction in hand we can now apply the PMFPNP procedure, as prescribed by Eqs. 2.1-2.7, to evaluate ion currents in the GA channel. The SIP potentials for K^+ and Cl^- as reported in Figure 7 and Figure 11, respectively, were used for the ion current evaluation in PMFPNP procedure to model the required PMF potential for permeating ions. The 1D potential along the (z) channel axis extracted from MD/continuum calculation was simply extended in the lateral (x,y) directions. Within the narrow channel, variation in the lateral direction is expected to be minor, and likewise in the bulk solution regions. Near the channel entrances, the SIP will not be strictly independent of x, y position, but again, we expect the error in the I-V curves resulting from the simplified SIP profile employed here to be negligible. The SIP profiles shown in Figure 7 and Figure 11 were used for the K^+ and Cl^- ions, respectively. The dielectric constants were set to $\varepsilon_m=\varepsilon_p=4$, and $\varepsilon_w=\varepsilon_w^{ch}=80$. In Figure 13 the current-voltage characteristic of a GA channel in a GMO membrane is shown for two values of reservoir electrolyte concentrations. The inset to Figure 13 displays experimental measurements of single ion channel currents for this system [133]. Our calculated currents compare rather well with the experimental curves. At 200 mV applied voltage the theory underestimates measured currents for the low bath electrolyte concentration (0.1 M) by about a factor of two. Given that no fitting parameters were employed in our analysis, the agreement with experiment is encouraging.

In Figure 14, ion current is plotted as a function of the electrolyte concentration in the bathing solutions at an applied voltage of 100 mV. At V=100 mV the experimental current data points shown in Figure 13 at concentrations up to 2 M are consistently 2-3 times larger than the prediction of our PMFPNP calculations, but show a similar trend towards saturation. Such saturation of the I-c curves is not observed in simple PNP theory, i.e. with $\Delta G_{DSE}^{K^+}=0$ and a rigid channel (as demonstrated by the line with diamonds in Figure 14). We note that one remaining possible source of error is underestimating the diffusion constants in the channel, and further studies regarding the validity of the procedure that uses Eq. 2.8 in the restricted channel environment are required. In order to understand the mechanism of saturation in PMFPNP we

have plotted the free energy $\psi_i(\vec{r})$ along the channel axis that results from PNP (Figure 15, *a* and *c*) and PMFPNP (Figure 15, *b* and *d*) for several bulk electrolyte concentrations. By comparing Figure 15, *a* and *b*, we observe that the potential profile features several barriers for the positive ion in PMFPNP. The height of the barriers increases as the bulk electrolyte concentration increases. In standard PNP, however, such barriers are not observed (Figure 15*a*). In PMFPNP (see Figure 15, *b* and *d*) negative ions experience a much larger barrier than positive ions in the channel. As indicated in Figure 16, when the bulk ion concentration increases, the positive ion density in the channel also increases and cannot be compensated by negative ions. The resulting effective positive charge in the channel creates a larger effective barrier for the transfer of positive ions and leads to current saturation with increased salt concentration. However, since PMFPNP does not account for direct ion-ion dynamic correlations, it may only partially account for correlation-dependent phenomena such as currents at large bath electrolyte concentrations at high voltages. Clearly, the nature of direct ion-ion correlations in a channel environment is not completely understood and requires further study.

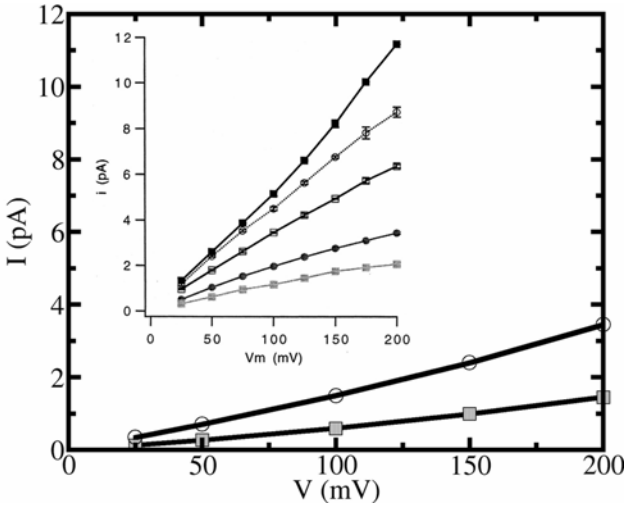

Figure 13. Current-voltage relations predicted by PMFPNP model are compared to experimental results [133] (*upper left inset*).

Bulk KCl concentrations of 0.1 M (*shaded square*) and 1.0 M (*open circle*) were used in the simulations. The experimental curves in the inset correspond to the following concentrations of bulk KCl solutions: shaded square, 0.1 M; filled circle 0.2 M; open square, 0.5 M; open circle, 1.0 M; and filled square, 2.0 M. The analogous experimental and calculated curves are labeled with the same symbols.

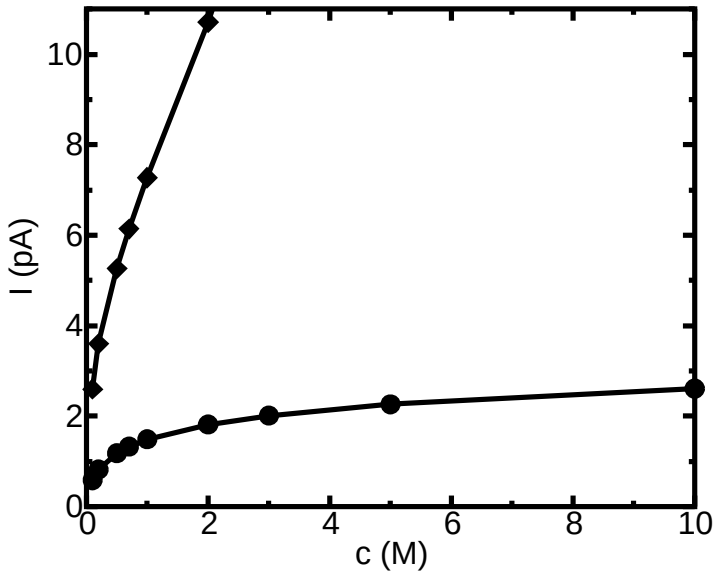

Figure 14. Current-Concentration relations as predicted by PNP (♦) and PMFPNP (•) models. The external potential difference was set to 100mV.

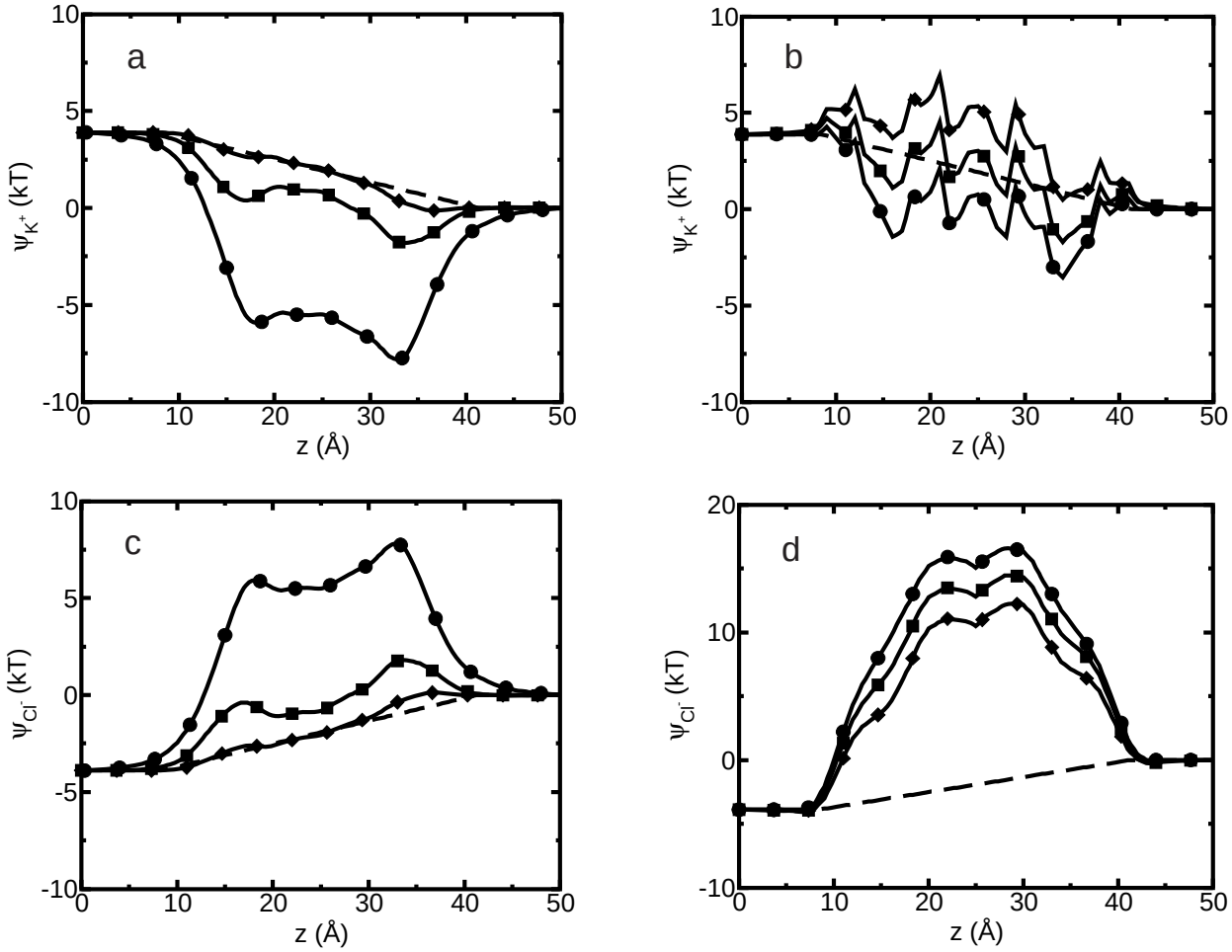

Figure 15. $\psi_i(\vec{r})$ profile along the channel axes for K^+ and Cl^- is plotted for several bulk electrolyte concentrations and 100 mV applied voltage: *a* , *c* calculated using PNP; *b*, *d* calculated using PMFPNP.

The curve with circles is for 0 M, the curve with squares is for 0.5 M and the curve with diamonds is for 10 M electrolyte concentrations. The dashed line is the result of the calculation at 0 M electrolyte concentration in which protein molecule had no partial charges on the atoms. It corresponds to the linear ramp potential caused by the high resistivity of the membrane.

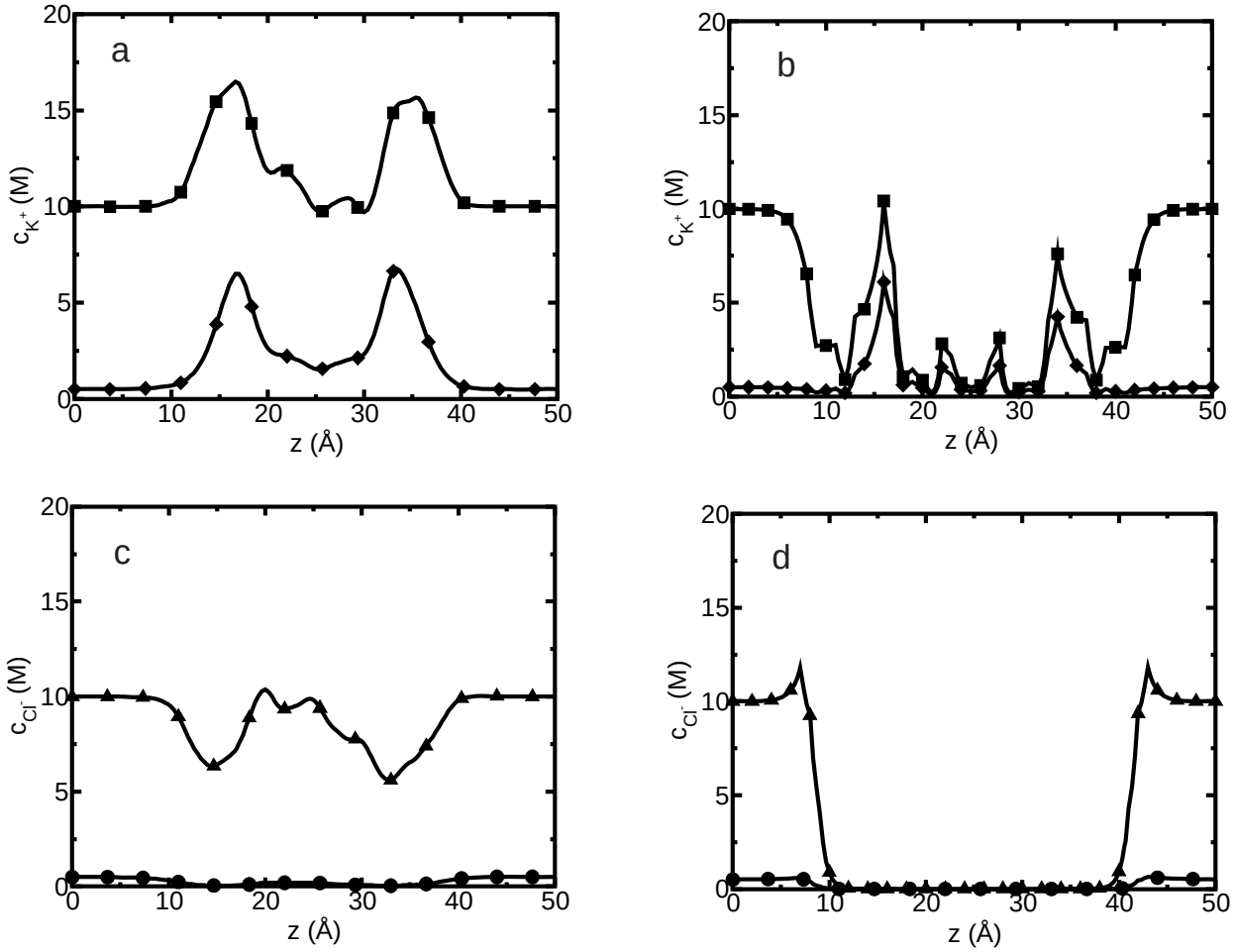

Figure 16. Ion concentration profile along the channel axis for K^+ and Cl^- is plotted for several bulk electrolyte concentrations: *a* and *c* calculated using PNP; *b* and *d* calculated using PMFPNP.

The curves with diamonds and circles are for 0.5M; the curves with squares and triangles are for 10 M electrolyte concentrations.

2.6 CONCLUSIONS

The passage of ions through narrow membrane channels is affected by a combination of interconnected energetic and kinetic factors including the local electric field resulting from the response of the membrane and the channel protein to the externally imposed potential, the energetics (electrostatic and short range interactions) of the ion accommodation in different parts of the channel, the electrostatic interaction between mobile ions in and near the channel and the ion's mobilities in the channel environment. Full-scale MD simulations of this process are not yet practical because of the vastly different time and length-scales involved.

Alternative simplified coarse-grained models have tried to capture the essential physics of the process. The Poisson-Nernst-Planck (PNP) approach focuses on the electrostatic interaction between permeant ions and between one such ion and its rigid inhomogeneous dielectric environment as the main factors that control the channel operation. Calculations of ion transport through the Gramicidin A (GA) channel based on this approach have shown a remarkable agreement with experimental results [48, 92, 134]. The present calculations together with several recent works show, however, that this apparent success is an artifact resulting from the cancellation of two errors that are big for narrow channels such as GA. First, the PNP approach strongly underestimates the dielectric barrier associated with transferring an ion from bulk water into the channel. This would lead to a strong overestimate of the ion current. Second, the PNP model considers the channel protein and the membrane as rigid dielectric environments, disregarding the channel structural response to the presence of the ion and thus implying a relatively small ability of the channel to accommodate the ion and to facilitate its transfer. This alone would lead to the opposite effect of underestimating the ion current. These two errors compensate each other in the final result for ion transport through the GA channel.

In the present paper we have described a hybrid molecular dynamics-continuum electrostatic methodology that makes it possible to combine the convenience and numerical efficiency of a PNP-based calculation with correct accounting for dielectric barrier and channel relaxation effects. This methodology contains several ingredients:

1. The standard PNP approach is corrected by adding the gradient of a suitable single-ion potential to the drift term in the drift-diffusion Eq 2.1. In another work [95], in which this potential is derived from the dielectric response of a rigid membrane-protein complex to the presence of a single ion, we show that this approach provides a good approximation for the dielectric barrier.
2. This electrostatic single-ion potential is further augmented by a contribution arising from the structural response of the channel to the ion. This is done by using atomistic MD simulations to compute this response, while still maintaining numerical simplicity by representing the resulting responsive structure as a dielectric continuum for the purpose of computing the local electrostatic energy.
3. The local diffusion coefficient of the ion is obtained from a first-principles calculation based on MD evaluation of the force-force autocorrelation function associated with the ion positioned at different locations along the channel.
4. The modified PNP equations, including all the above ingredients, now referred to as the Potential of-Mean-Force-Poisson-Nernst-Planck (PMFPNP) model, are used to calculate the ionic current for the imposed potential and concentration biases.

We have seen that this calculation yields results that agree well with available experiments on ion transport through the GA channel, without employing any arbitrary adjustable parameters. This suggests that the present modeling may account for the essential factors that affect ion transport through open membrane channels. Still, one must view this success with some caution. The use of continuum dielectric models for the protein and water with the inevitable introduction of ill-defined dielectric constants and the neglect of restrictions on water mobility in the channel is obviously a serious approximation. Also, dynamic correlations between ions in the channel that possibly affect the dynamics of ion permeation, especially at higher concentrations, are only partially accounted for by this model. Further work is needed to fully assess the model reliability.

APPENDIX

SYMBOLS

$\psi_i(\vec{r})$	Free energy function entering the Nernst-Planck equation (Eq. 2.1a).
$\phi_{mobile}(\vec{r})$	Electrostatic potential due to all mobile ions and the applied electric field.
$\phi_{protein}(\vec{r})$	Electrostatic potential due to partial charges fixed on the protein and lipid atoms.
$\phi(\vec{r})$	Electrostatic potential found from the solution of the corresponding Poisson equation (Eq. 2.6).
$\Delta G^i_{SIP}(\vec{r})$	Potential of mean force for a single test ion [hence "Single ion potential" (SIP)].
$\Delta G^i_{DSE}(\vec{r})$	Dielectric self-energy (DSE) or solvation energy of a single ion.
$G^{complex}(\vec{r})$	Electrostatic free energy of an ion-protein/membrane complex with the ion located at a point $\vec{r}$ inside the channel, calculated by numerical solution of Poisson equation (Eq. 2.6).
$G^{protein}$	Electrostatic free energy of the protein/membrane in the absence of the ion, calculated by numerical solution of Poisson equation.
G^{ion}	Electrostatic free energy of the ion in bulk solvent, calculated by numerical solution of Poisson equation.
$\varepsilon(\vec{r})$	Position dependent dielectric response function (dielectric constant).
ε_p, ε_m, ε_w, ε_w^{ch}	Dielectric constant of protein, membrane, bulk and channel water region (Figure 3).

ACRONYMS

PNP	Poisson-Nernst-Planck theory.
DSEPNP	Dielectric-Self-Energy-Poisson-Nernst-Planck theory.
PMFPNP	Potential-of-Mean-Force-Poisson-Nernst-Planck theory.
DMC	Dynamic Monte-Carlo method.
DSE	Dielectric self-energy.
PMF	Potential of mean force.

2.7 ACKNOWLEDGMENTS

The calculations reported here were carried out on computers at the University of Pittsburgh's Center for Molecular and Materials Simulations (CMMS).

A.N.'s work was supported in part by the Israel Science Foundation and by the Kurt Lion Fund. Work in R.D.C.'s group was supported by NIH Grant R0l GMG1082-03 and American Chemical Society Petroleum Research Fund (ACS-PRF) grant 34754-AC6. M.K. acknowledges the financial support provided by Marquette University.

3.0 DIFFUSION CONSTANT OF K^+ INSIDE GRAMICIDIN A: A COMPARATIVE STUDY OF FOUR COMPUTATIONAL METHODS

Mamonov, A. B., M. G. Kurnikova, and R. D. Coalson. Biophys. Chem. 2006. In press.

3.1 ABSTRACT

The local diffusion constant of K^+ inside the Gramicidin A (GA) channel has been calculated using four computational methods based on molecular dynamics (MD) simulations, specifically: Mean Square Displacement (MSD), Velocity Autocorrelation Function (VACF), Second Fluctuation Dissipation Theorem (SFDT) and analysis of the Generalized Langevin Equation for a Harmonic Oscillator (GLE-HO). All methods were first tested and compared for K^+ in bulk water – all predicted the correct diffusion constant. Inside GA, MSD and VACF methods were found to be unreliable because they are biased by the systematic force exerted by the membrane-channel system on the ion. SFDT and GLE-HO techniques properly unbias the influence of the systematic force on the diffusion properties and predicted a similar diffusion constant of K^+ inside GA, namely, ca. 10 times smaller than in the bulk. It was found that both SFDT and GLE-HO methods require extensive MD sampling on the order of tens of nanoseconds to predict a reliable diffusion constant of K^+ inside GA.

3.2 INTRODUCTION

There is a great deal of interest in studying biological ion channels due to the important roles that they play in the physiology of organelles, cells and tissues. With the availability of detailed atomistic structures of several ion channels (Gramicidin A (GA) [135], KcsA potassium channel [19], α-hemolysin [136], ClC chloride channel [20]) it has become feasible to do accurate theoretical modeling of ion currents in order to understand the mechanisms of ion transport through biological channels. At present, the most popular methods of ion current modeling are Poisson-Nernst-Planck (PNP) [48, 92, 107, 137-139], Brownian Dynamics (BD) [50, 54, 96-98, 140] and Non-equilibrium Molecular dynamics (NEMD) [39, 40, 62]. Of these methods PNP is the most primitive but fastest method. In PNP, ions are represented by continuous densities whose steady state concentrations are calculated in the electrostatic field due to partial charges on the protein and mobile ion charge densities, plus a contribution due to external electrodes, by solving Poisson's equation self-consistently with a Nernst-Planck Equation for each ion species [48]. In BD, ions are modeled explicitly but water is treated implicitly as a continuous medium characterized by dielectric and friction constants. In BD, ions move in the electrostatic field of partial charges on the protein, surface charges induced on dielectric boundaries within the system, externally applied electric fields, pairwise electrostatic interactions with other ions and steric overlap interactions with other ions and the walls of the protein/membrane system [50]. In NEMD the entire system, including water, is modeled explicitly and the dynamics of all atoms is computed by numerical integration of Newton's second law using an atomistic force field [39, 40, 62]. Therefore, NEMD is the most accurate method, but very slow compared to PNP and BD and still not very practical.

For calculating ion currents, both PNP and BD methods rely heavily on the magnitude of the diffusion constant inside the channel, which is a phenomenological input into these theories. To date, there are no direct experimental measurements of diffusion constants of ions inside narrow pores. Therefore, one must rely on simulations to predict diffusion constants, and, indeed, several theoretical methods have been developed for this purpose. They are widely used for calculating diffusion properties of ions and molecules in bulk phases [68-70], but the applicability of some of these methods to narrow ion channels (e.g., Gramicidin A) is questionable. Currently, there is no consensus in the biophysics literature about the magnitude of

diffusion constants of ions inside narrow channels [65, 67, 71-73, 137, 141]. Different methods and authors have predicted a wide range of diffusion constants. Therefore, it is imperative to test and compare different methods to assess their applicability in narrow channels and to estimate the value of the diffusion constants of ions inside such channels.

An important question that has to be addressed first is how to define the diffusion constant. In fact, the diffusion constant can be defined in many different ways depending on the model used to describe transport of ions across the channel. In Brownian (Smoluchowski) Dynamics and PNP-like models the flux $\vec{j}_i(\vec{r},t)$ of ion species *i* is expressed as

$$\vec{j}_i(\vec{r},t) = -D_i\left[\vec{\nabla}c_i(\vec{r},t) + c_i(\vec{r},t)\vec{\nabla}\left(\beta\psi_i(\vec{r})\right)\right], \tag{3.1}$$

where D_i is the diffusion constant for this species, $c_i(\vec{r},t)$ is its concentration and $\psi_i(\vec{r})$ is its free energy or potential of mean force (PMF); furthermore, $\beta = \frac{1}{k_B T}$ (k_B is Boltzmann's constant and T is absolute temperature). The free energy of an ion at a given position in space arises from its interactions with the protein, membrane, and water molecules. In particular, these interaction forces can be attributed to electrostatic interactions of the ion with the partial charges of the protein and membrane, rotational polarization of water, rotational/translational polarization of protein and membrane groups as well as electronic polarization of the protein, membrane and water. It has been shown in several studies that translational/rotational polarization of protein groups is important in electrostatic stabilization of ions inside narrow channels [137, 142]. This is manifested in the flexibility of key protein groups that relax locally around the ion and stabilize it, ultimately rendering permeation more favorable.

Let us briefly review what has been done to date to calculate diffusion constants of ions inside narrow channels. The most widely employed methods for calculating diffusion constants are based on extracting the mean square displacement (MSD) or the velocity autocorrelation function (VACF) from MD simulations. In Ref. [71], the diffusion constants inside smooth cylindrical channels with repulsive walls of different width and length were calculated using the MSD method for Na^+, K^+, Cs^+, Ca^{2+}, F^-, Cl^- and I^- ions. It was observed that the diffusion constants decreased as the radius of the channel decreased. In a 3 Å radius channel the diffusion constant of K^+ was found to be *ca.* 5 times smaller than in the bulk water. This decrease was attributed to two main factors, one being an increase in the mean square of random forces on the

ions as the channel gets narrower and the second an increase in time scale of random force correlations. In Ref. [72], the diffusion constants of K^+ and Na^+ were estimated using the MSD method from MD simulations in hydrophobic cylindrical channels with varying radii, as well as in the KcsA potassium channel. In a 3 Å radius hydrophobic channel the diffusion constants for both K^+ and Na^+ were ca. 12 % of the bulk value. In Ref. [73] mobilities of K^+ and Cl^- were studied by extracting MSD and VACF functions from MD simulations inside five different channels with radii ranging from 2 Å to 6 Å. It was found that the diffusion constants were 2-10 times smaller than in the bulk solution depending on the channel width and the position where the probe ion was released. In a 2 Å radius channel the diffusion constant was found to be on average 10 times smaller than in the bulk. In Ref. [143], friction coefficients of K^+ and Na^+ ions were evaluated by fitting the analytical expression for the VACF of a Brownian harmonic oscillator to the VACF obtained from MD simulations inside the KcsA potassium channel. The authors of this study found diffusion constants of K^+ and Na^+ ca. 3 times smaller inside the channel. In Ref. [67] the effective diffusion constant of K^+ and Na^+ ions was estimated inside a Gramicidin-like β-helix using two methods. The first method utilized the effect that the dependence of the terminal velocity on the external weak force applied to the ion is proportional to the diffusion constant. The other methods used in Ref. [67] was based on the second fluctuation dissipation theorem. Both methods predicted that the effective diffusion constant of K^+ is 3-5 times smaller inside the β-helix compared to the bulk value. In our earlier study [137] the diffusion constant of K^+ inside the Gramicidin A (GA) channel was calculated using the fluctuation dissipation theorem by extracting the force autocorrelation function (FACF) from MD simulations. A reduction of 8.5 times in diffusion constant compared to the bulk value was found inside the channel.

A different approach to calculation of diffusion constants is based on fitting the diffusion constant to reproduce experimental ion currents using BD or PNP. In Ref. [141] the potential energy well depth and barrier height as well as the internal diffusion constant were fit for the GA channel: a best fit was obtained when the diffusion constant inside the channel was taken to be 10 times smaller than in the bulk. It was found that the model did not reproduce the experimentally observed saturation of ion current when the mobile ion concentration in the reservoir was increased beyond 1 M, implying that the value of this constant may critically influence the saturation properties of the channel. In Ref. [92] the internal diffusion constant of

Cs^+ (K^+) had to be decreased 11 (17) times compared to the bulk in calculations of ion currents via the PNP model in order to get agreement with experimental results. The overall conclusion drawn from these studies is that diffusion constants of ions in narrow channels are roughly 3-10 times smaller than in the bulk. In contrast to this conclusion, it was found in Ref. [65] that the diffusion constant of K^+ inside the GA channel is not much different from the bulk. These authors used MD simulations of K^+ restrained with a harmonic potential and mapped this microscopic dynamics to the generalized Langevin equation (GLE). They estimated that the internal diffusion constant was 66 % of its bulk value.

The goal of the present study is to calculate the diffusion constant of K^+ ion inside the GA channel using four different methods based on MD simulations. The paper is organized in the following way. The theoretical basis of the methods and their computational implementation are described in the "Methods" section. The main results of our study are reported in the "Results and Discussion" section, and our main conclusions are summarized in the "Conclusions" section.

3.3 METHODS

3.3.1 Theory

We will compare four methods for calculating diffusion constants of ions in bulk water and inside the GA channel. The first method is based on the MSD of a particle from its initial position [55]:

$$D = \lim_{t\to\infty} \frac{1}{2} \frac{\left\langle \Delta z(t)^2 \right\rangle}{t}, \tag{3.2}$$

where D is the one dimensional diffusion constant[3], and $\left\langle \Delta z(t)^2 \right\rangle$ is the mean square displacement elapsed at time t calculated as an average over all possible time origins along the MD trajectory.

The second method is based on calculation of the VACF [55]:

$$D = \int_0^\infty \left\langle v(0)v(t) \right\rangle dt \,, \tag{3.3}$$

where $v(t)$ is the ion's velocity.

The final two methods are based on the Generalized Langevin Equation (GLE) [55]:

$$m\frac{dv(t)}{dt} = F^{sys} - \int_0^t M(t-\tau)v(\tau)d\tau + R(t)\,, \tag{3.4}$$

where m is the ion's mass, F^{sys} is the systematic force, $R(t)$ is the random force acting on the ion and $M(t)$ is the appropriate memory function.

According to the second fluctuation-dissipation theorem (SFDT), the memory function is related to the random force autocorrelation function (FACF) [68, 144] according to

$$M(t) = \frac{1}{k_B T}\left\langle R(0)R(t) \right\rangle . \tag{3.5}$$

Using Einstein's relation $D = \frac{k_B T}{\gamma}$ and the connection between friction constant and memory function $\gamma = \int_0^\infty M(t)dt$, then:

$$D = \frac{(k_B T)^2}{\int_0^\infty \left\langle R(0)R(t) \right\rangle dt} . \tag{3.6}$$

The last method [65, 145, 146] is based on an analysis of the GLE for a harmonic oscillator (GLE-HO). In Eq. 3.4 F^{sys} can be replaced with the harmonic oscillator force

---

[3] We will consider only one dimensional diffusion because diffusion of ions inside the GA channel is essentially a one dimensional phenomenon. Subscripts *x*, *y* or *z* will be dropped throughout: when necessary it will be explicitly noted in the text which direction is relevant.

$-k\Delta z(t)$, where $\Delta z(t)$ is the displacement of the oscillator from its equilibrium position, and k is an appropriate Hooke's Law spring constant. The GLE then reads:

$$m\frac{dv(t)}{dt} = -k\Delta z(t) - \int_0^t M(t-\tau)v(\tau)d\tau + R(t). \tag{3.7}$$

Using $\Delta z(t) = \int_0^t v(\tau)d\tau$ and various properties of the random force and equilibrium velocity distribution, one finds:

$$m\frac{dC(t)}{dt} = -k\int_0^t C(\tau)d\tau - \int_0^t M(t-\tau)C(\tau)d\tau \tag{3.8}$$

where $C(t) = \frac{\langle v(0)v(t)\rangle}{\langle v(0)^2\rangle}$ is the normalized VACF of an ion. Laplace transforming this equation with $\hat{f}(s) \equiv \int_0^\infty dtf(t)e^{-st}$ gives:

$$m\left[s\hat{C}(s) - 1\right] = -k\frac{\hat{C}(s)}{s} - \hat{M}(s)\hat{C}(s). \tag{3.9}$$

The diffusion constant is related to the $s \to 0$ limit of the Laplace transform of the memory function through the Einstein relation:

$$\hat{D}(s) = \frac{k_B T}{\hat{M}(s)}. \tag{3.10}$$

Substituting $\hat{M}(s)$ from Eq. 3.9 into Eq. 3.10 the following expression is obtained:

$$\hat{D}(s) = \frac{-k_B T\hat{C}(s)}{\hat{C}(s)\left(ms + \frac{k}{s}\right) - m}. \tag{3.11}$$

The Equipartition Theorem [55] for a harmonic oscillator implies that, $k = \frac{k_B T}{\langle \Delta z(0)^2\rangle}$ and $m = \frac{k_B T}{\langle v(0)^2\rangle}$; hence Eq. 3.11 can be rewritten as

$$\hat{D}(s) = \frac{-\hat{C}(s)\left\langle v(0)^2 \right\rangle \left\langle \Delta z(0)^2 \right\rangle}{\hat{C}(s)\left(\left\langle \Delta z(0)^2 \right\rangle s + \frac{\left\langle v(0)^2 \right\rangle}{s} \right) - \left\langle \Delta z(0)^2 \right\rangle}. \tag{3.12}$$

The diffusion constant is then the $s \to 0$ limit of $\hat{D}(s)$:

$$D = \lim_{s \to 0} \hat{D}(s). \tag{3.13}$$

3.3.2 MD simulations

Molecular dynamics (MD) simulations of K^+ ion in bulk water and inside the GA channel were carried out to calculate the diffusion constant of K^+ using the four methods described in the Theory subsection. Two systems were built for the MD simulations: one consisted of K^+ in bulk water, the other one was comprised of a K^+ ion inside the GA channel. For the first system one K^+ ion was solvated by 1077 SPC/E [147] water molecules. For the second system one K^+ ion was placed inside the GA channel, embedded in a slab of 235 randomly positioned neutral Lennard-Jones spheres to mimic the hydrophobic environment of a membrane and solvated by 1020 SPC/E water molecules. One Cl^- ion was placed outside the channel to neutralize the charge of the K^+ ion (see Figure 17). For the starting configuration, we used the NMR structure of GA downloaded from the Protein Data Bank (www.rcsb.org) with pdb code 1GRM [135]. Both systems were equilibrated first at constant volume, then at a constant pressure of 1 atm at 300 K. For all MD simulations, the SANDER module of the AMBER7 software package [148] was used. The modified *Cornell et. al.* force field (*parm99.dat*) [149, 150] was used for the ions and GA. The coordinates of the Lennard-Jones spheres were fixed during all MD simulations. To prevent drifting and misfolding of GA during long MD simulations a weak 1.0 kcal/mol/A^2 harmonic restraining potential was applied to all backbone peptide carbon atoms. The Cl^- ion was also restrained during MD simulations so as to keep it in the middle of the reservoir and thus prevent direct influence on the K^+ motion.

For the MSD MD simulations, K^+ was released and its coordinates collected every 10 fs for 4-6 ns of equilibrium simulation. The diffusion constant was calculated from the slope of the MSD versus time plot according to Eq. 3.2.

For the VACF MD simulations, K^+ was released and the Cartesian components of its velocity were collected every 10 fs for 4-6 ns. VACFs were calculated from the velocity components and then numerically integrated to find the diffusion constant according to Eq. 3.3.

For the SFDT MD simulations, K^+ was fixed at a particular point along the channel axis and the Cartesian components of the total force on the ion collected every 1 fs for 15-27 ns depending on the location. By fixing the ion we employed the infinitely heavy particle approximation [151] to satisfy a condition of the Generalized Langevin equation that the random force does not correlate with the velocity [144]. The random force acting on the ion was extracted by subtracting the time-averaged force from the instantaneous force value. From the random force, the FACF was calculated, numerically integrated and the diffusion constant found according to Eq. 3.6.

For the GLE-HO MD simulations, a harmonic restraint was applied to K^+ and the Cartesian components of the coordinate and velocity of K^+ were collected every 10 fs for 27-42 ns depending on the location and the strength of the harmonic restraint employed. Then the normalized VACF was computed and Laplace transformed numerically to find $\hat{D}(s)$ according to Eq. 3.12. The effect of the harmonic restraint strength on the ion diffusion constant was tested in the $4 \leq k \leq 40$ kcal/mol/Å^2 range (*vide infra*).

The potential of mean force (PMF) of K^+ inside GA was calculated using the Umbrella Sampling technique [152] by restraining the ion in 3D via a harmonic potential of 4 kcal/mol/Å^2 with umbrella windows separated by 0.5 Å. The initial configurations for the umbrella windows were created by placing K^+ at a particular position along the channel and checking for overlapping water molecules. If the ion-water and water-water steric overlaps disappeared in the energy minimization then the system was accepted for further equilibration; otherwise, overlapping water molecules were manually moved to the bulk reservoir and the whole system was energy minimized again. These simulations were carried out for the ion restrained along one monomer only so that a total region of 16 Å was covered with umbrella windows. This was done because the GA channel system is symmetrical relative to the middle of the channel, and thus there is no need to repeat the simulations for the other monomer. For each umbrella window the coordinate of the ion was collected every 10 fs over a 1 ns interval. The PMF profile of K^+ in the *z* direction was reconstructed using Weighted Histogram Analysis Method (WHAM) [153].

These simulations were carried out on 15 Dual AMD Athlon computer nodes and it took 30 h to complete 1 ns MD simulation on 2 CPUs.

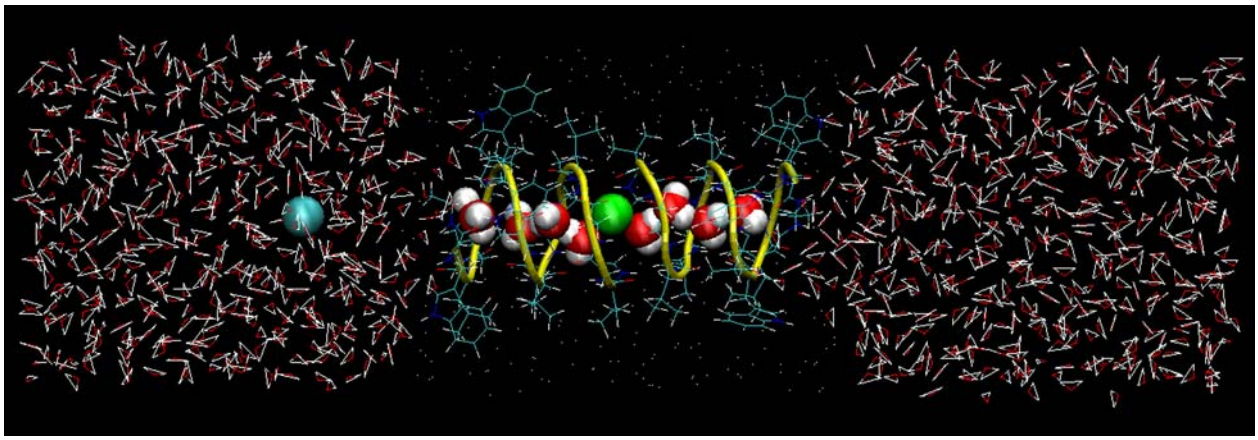

Figure 17. A snapshot from an MD simulation of Gramicidin A embedded in a model hydrophobic membrane and solvated by 1020 SPC/E water molecules.
Potassium ion is shown in green, chloride ion in blue, peptide backbone in yellow, protein side chains in blue and neutral Lennard-Jones spheres (that constitute the membrane mimetic) as white dots.

3.4 RESULTS AND DISCUSSIONS

3.4.1 Calculation of diffusion constant of K^+ in bulk water

The main results of applying the four methods described in the Theory subsection for K^+ in bulk water are reported in Figure 18 and Table 6. MSDs versus time plots of K^+ in x, y and z are illustrated in Figure 18A. The VACF of K^+ in one dimension (the z direction) is shown in Figure 18B. The correlation time of the VACF is *ca.* 1.5 ps. The FACF of K^+ in the z direction is shown in Figure 18C. The correlation time of the FACF is *ca.* 1 ps. The function $\hat{D}(s)$ calculated using the GLE-HO method (Eq. 3.12) is shown in Figure 18D. The harmonic restraining force strength was varied over the range of $4 \leq k \leq 40$ kcal/mol/A^2 and found to have little effect on the shape of $\hat{D}(s)$ in this case. Namely, at s<10 ps^{-1} the $\hat{D}(s)$ function bends down as $s \to 0^+$. In the

10<s<30 range it has a relatively linear shape and bends up at s>30 ps^{-1}. We found that at very small s the smooth shape of $\hat{D}(s)$ function is corrupted by a singularity near s=0, as has been observed previously [154]. We observed that the location of the singularity depends on the amount of MD sampling: longer simulations shifted the singularity to smaller s. For a 30 ns MD simulation the onset of the singularity went down to s=0.05 ps^{-1}. Such dependence of the singularity on the length of the sampling suggests that it arises from numerical errors. Close inspection of Eq. 3.12 shows that at small s the final result depends critically on a delicate balance of arithmetic operations involving small and large numbers in the denominator. Therefore, small numerical errors in $\hat{C}(s)$, $\langle v(0)^2 \rangle$ or $\langle \Delta z(0)^2 \rangle$ may get significantly amplified and lead to large errors in the final result. This assumption was further tested by calculating $\hat{D}(s)$ analytically based on a functional fit to MD data for $M(t)$, so that its shape should not be affected by numerical errors in $\hat{C}(s)$, $\langle v(0)^2 \rangle$ or $\langle \Delta z(0)^2 \rangle$. Results of this test are discussed in the next subsection. In practice, we extrapolated $\hat{D}(s)$ to s=0 from the 0.05<s<0.2 range by ignoring the numerical singularity at s<0.05. This resulted in a diffusion constant of 0.19 Å^2/ps, i.e., the same as predicted by the other three methods (Table 6).

Recently, Hummer [155] proposed an alternative form of expression for Eq. 3.12, which in the limit of an overdamped harmonic oscillator uses the position autocorrelation function $\langle \Delta z(t) \Delta z(0) \rangle$ instead of *C(t)* and avoids this singularity. However, this procedure also requires a long MD simulation, because the position autocorrelation function and its time integral $\int_0^\infty \langle \Delta z(t) \Delta z(0) \rangle dt$ depend delicately on the simulation length.

Table 6. Diffusion constants of K^+ in bulk water calculated using the four methods described in the "Theory".

	MSD	VACF	SFDT	GLE-HO
D (Å^2/ps)	0.2	0.19	0.18	0.19

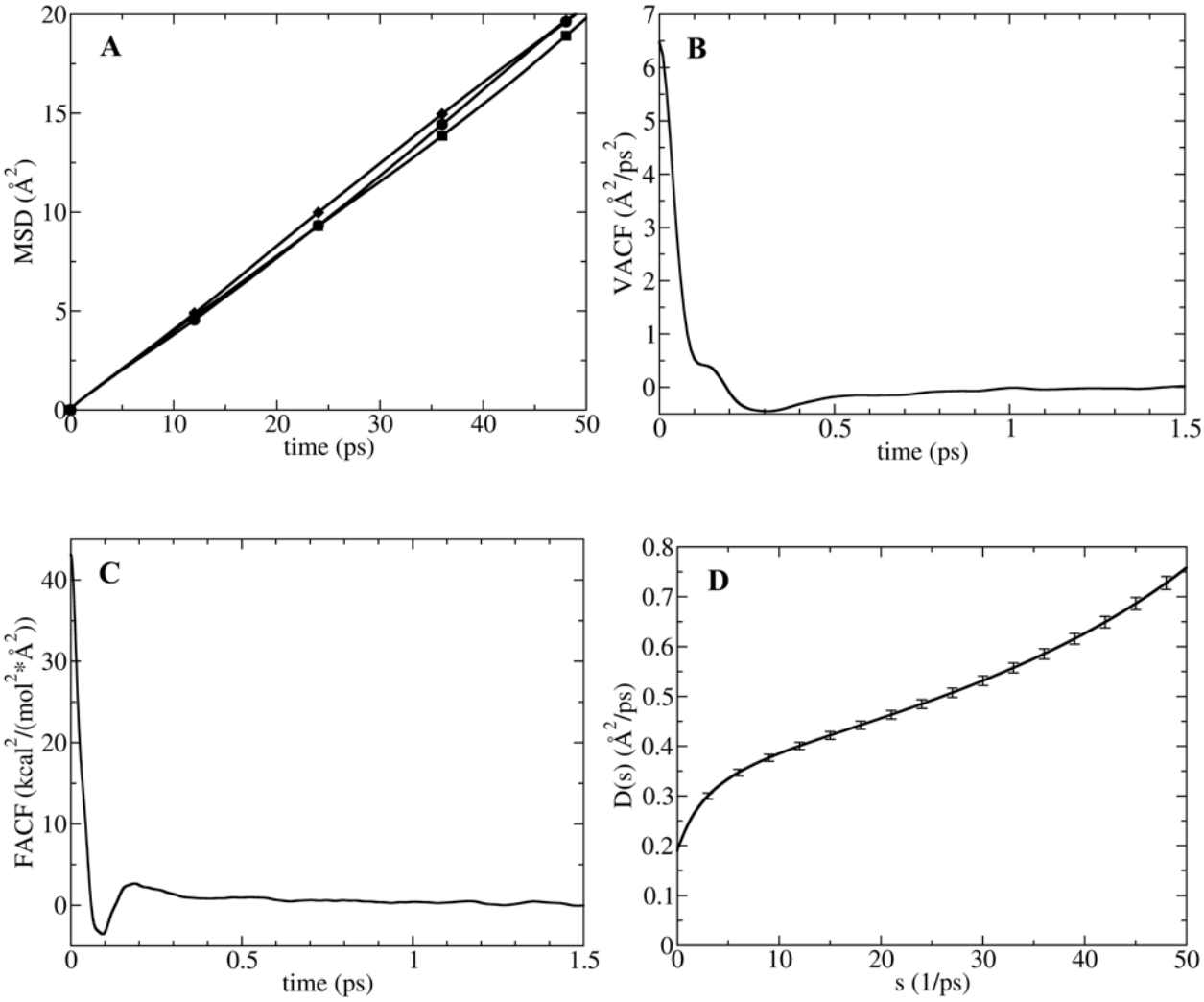

Figure 18. Calculation of K^+ diffusion constants in bulk water using four methods described in the Theory section. (A) MSD plots in x (circles), y (squares) and z (diamonds) direction. (B) VACF in z direction. (C) FACF in z direction. (D) $\hat{D}(s)$ function (with error bars) in z direction.

3.4.2 Analytic test of $\hat{D}(s)$ behavior at small *s* in bulk water

The behavior of $\hat{D}(s)$ as $s \to 0$ has been further investigated by extracting it analytically from an appropriate functional representation of the memory function according to Eq. 3.10. In particular, an analytic form of the *M(t)* function determined by fitting the memory function which is extracted from MD simulation of the force autocorrelation function with the ion fixed in space; cf. Eq. 3.5. A function composed of two damped cosine waves with six parameters $M(t) \cong a_0 e^{-a_1 t}\cos(a_2 t) + a_3 e^{-a_4 t}\cos(a_5 t)$ was found to give a good fit (cf. Figure 19A) using the regression analysis feature of the GRACE program (http://plasma-gate.weizmann.ac.il/Grace/). The optimal fit parameters for this fitting function are given in Table 7. $\hat{D}(s)$ obtained from MD using the GLE-HO method (Eq. 3.12) is compared in Figure 19B with the version of $\hat{D}(s)$ obtained by analytical Laplce transformation of our functional fit to $M(t)$ (cf. Eq. 3.10), which we will term the "analytic" $\hat{D}(s)$. Both $\hat{D}(s)$ functions have the same linear shape in the 10<*s*<30 range and bend down towards the same value at *s*=0. *No singularity was observed for the analytic* $\hat{D}(s)$ *function*, which provides further evidence that the singularity obtained in Figure 19D is a numerical artifact.

Using Eq. 3.9 associated with the GLE-HO method, the normalized VACF *C(t)* can be found by inverse Laplace transformation of a function that contains the Laplace transform of the memory function, namely:

$$C(t) = L^{-1}\left\{\frac{1}{s + \frac{k}{ms} + \frac{\hat{M}(s)}{m}}\right\}. \qquad (3.14)$$

We calculated $C(t)$ using the above equation with the analytic form of $\hat{M}(s)$ described above. Alternatively, $C(t)$ was calculated directly from MD simulations of K^+ restrained with the same harmonic force constant as used to calculate $C(t)$ analytically (i.e., Eq. 3.14). These functions compare well, as shown in Figure 19C.

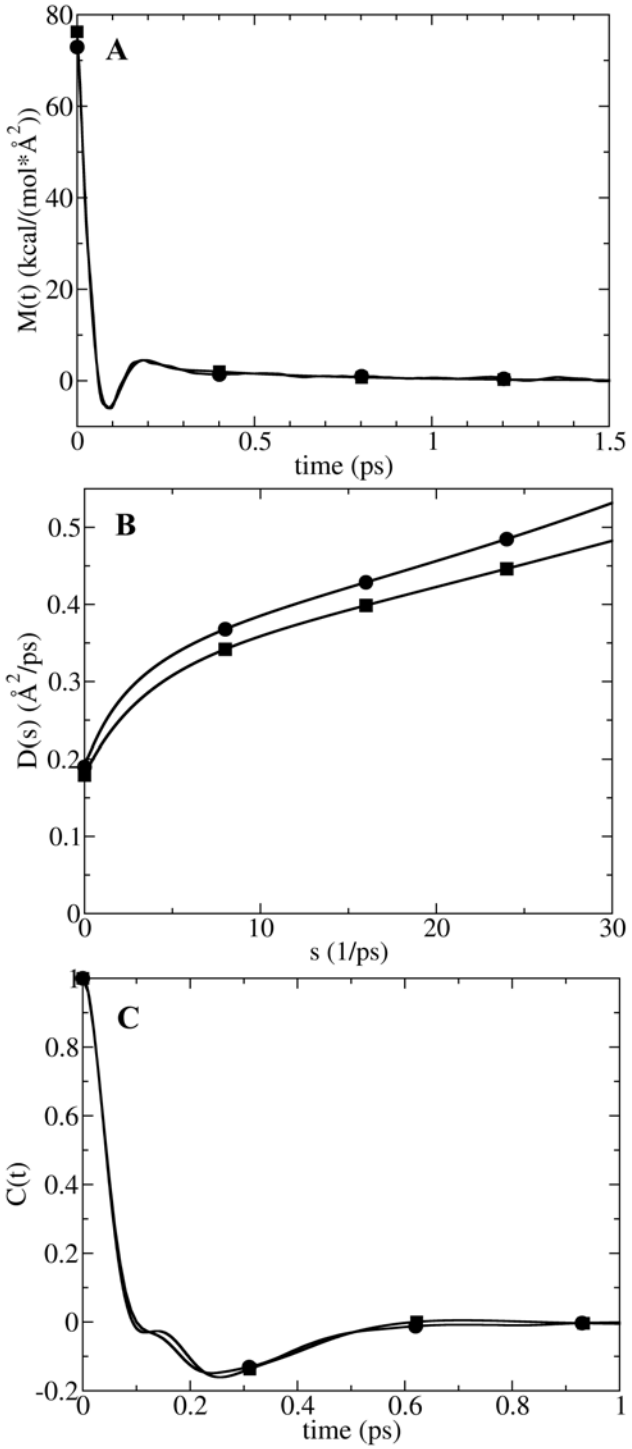

Figure 19. Analytic test of $\hat{D}(s)$ behavior at small s for K^+ in bulk water.

(A) Memory function calculated using SFDT method i.e. Eq. 3.5, from fixed ion MD simulations (circles) (corresponds to FACF illustrated in Figure 18C) and its analytically fitted analog (squares). (B) $\hat{D}(s)$ function calculated from MD using GLE-HO method i.e. Eq. 3.12 (circles) and analytically derived using Eq. 3.10 from

analytic $\hat{M}(s)$ (squares). (C) $C(t)$ calculated directly from MD for a harmonically restrained K^+ (circles) and analytically derived using GLE-HO analysis i.e. Eq. 3.14 from analytic $\hat{M}(s)$ (squares).

Table 7. Best fit parameters for analytic memory function of K^+ in bulk SPC/E water fitted from fixed ion MD simulations (cf. Eq. 3.5).

a_0	a_1	a_2	a_3	a_4	a_5
70.92	19.86	-28.97	5.343	2.472	-0.0007743

3.4.3 Calculation of K^+ PMF in the GA channel

The PMF profile of K^+ along the z (channel) axis inside GA is shown in Figure 20: $z = 0$ corresponds to the middle of the channel. It can be seen that there is some periodicity in the PMF profile, which is related to the helical structure of the GA channel. The maximum barrier for a K^+ ion inside the channel is 7.5 kcal/mol. The PMF of K^+ inside GA has been calculated previously using the CHARMM PARAM27 force field and TIP3P water model [65]. Both PMFs exhibit similar features such as periodicity and a maximum barrier of approximately 7 kcal/mol. This demonstrates that both force fields predict similar behavior for K^+ inside the GA channel.

According to the Smoluchowski Equation, in the absence of an externally applied electric field and ion-ion interactions an ion diffuses in the force field implied by its PMF. Thus, it is instructive to consult the PMF when calculating the position-dependent diffusion constant as will be described in the next subsection.

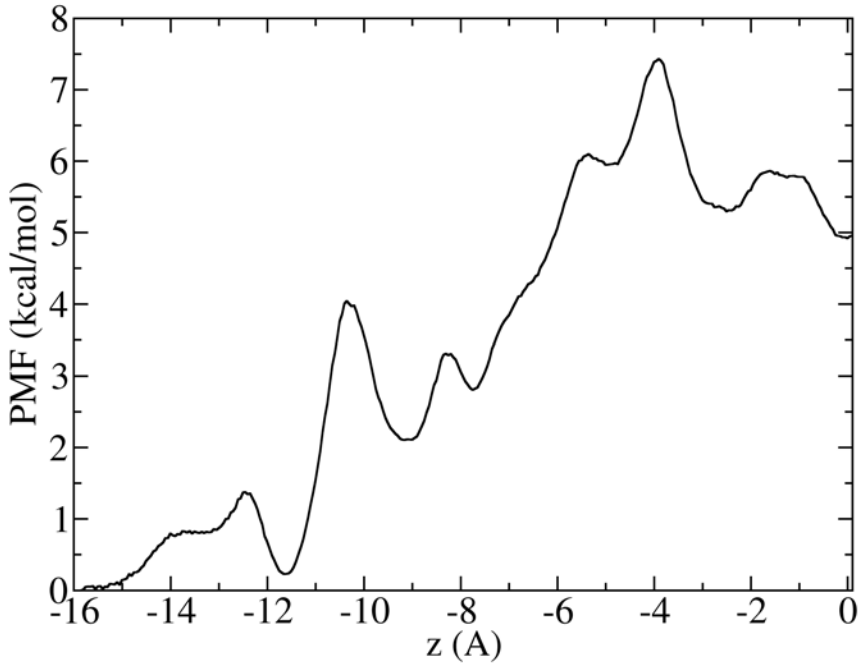

Figure 20. PMF profile of K^+ along *z* (channel) direction inside GA. The origin of the coordinate system coincides with in the center of the channel.

3.4.4 Calculation of the K^+ diffusion constant inside the GA channel

The main results of our calculations of K^+ diffusion constants inside the GA channel are summarized in Table 8. MSDs in *x*, *y* and *z* directions are illustrated in Figure 21A. At short times up to 1 ps all MSDs have the same slope. This is the average time over which K^+ is unconstrained by the cage formed by the walls of the channel in the *x* and *y* directions and neighboring water molecules in the *z* direction. This "free diffusion" time period is nearly the same because the size of the cage is similar in *x*, *y* and *z* directions. A diffusion constant calculated from these data reflects the (nearly) free diffusion properties of the ion inside the cage and therefore cannot be used to represent its long time behavior. MSDs in the *x* and *y* direction (perpendicular to the channel) reach a plateau at several picoseconds because of the channel wall constraints. The MSD plot in the *z* direction continues to increase with time. We tested how the shape of the MSD in the *z* direction depends on the location at which K^+ is released inside GA. MSD plots in *z* direction of K^+ released at five different locations are illustrated in Figure 21B. All MSDs have the same slope up to ca. 10 ps and then diverge at longer time. This strong dependence of MSD on the ion's release location reflects the spatial inhomogeneity of the PMF (see, Figure 20) which governs motion of the ion inside the channel.

When the ion was released at the center and at 2.4 Å from the middle of the channel, the MSD in z direction had the same shape for up to 250 ps (Figure 21B) because the ion moved in the same free energy basin (see, Figure 20). These MSDs deviate from each other after 250 ps because in the 2.4 Å release case the ion traveled further away from the release location. The long time dynamics saturates with time for all these MSDs. Due to strong position dependence of the MSD functions, estimation of diffusion constants is difficult. We estimated the lower and the upper limit of the calculated diffusion constant. An upper limit for the diffusion constant, calculated from the largest MSD slope corresponding to the 10-250 ps region (i.e., prior to saturation of the MSD for the ion released at the center and 2.4 Å away from the center of the channel), was found to be 0.0146 $Å^2$/ps - approximately 14 times smaller than in the bulk. A lower limit of the diffusion constant was calculated from the slope of the 200-1000 ps region of the MSD function for the K^+ ion released 5 Å away from the middle of the channel. The

diffusion constant in this case is close to zero because the ion remained within a narrow local free energy well during the whole simulation time.

Now let us examine results of applying the VACF method, i.e. Eq. 3.3, for calculating the diffusion constant of K^+ inside GA. In Figure 22A the VACF of the ion inside the channel is compared with its bulk water analog. The z-component of the VACF inside the channel has a more complex shape characterized by two major minima, one occurring at 0.07 ps and the other at 0.18 ps. The negative part of the VACF is more pronounced than in bulk water. This suggests that there is a larger back scattering of the ion from the neighboring water molecules although the decorrelation time is the same, ca. 1 ps. Comparison of the VACF inside the channel in the *z* direction with that in the *x* and *y* directions is shown in Figure 22B. Again, the VACF in the *z* direction has a more complex shape: the VACFs in the *x* and *y* directions have only one minimum and do not have a flat region. The complex shape of the VACF in the *z* direction compared to bulk water analog and the internal ion VACF in the *x* and *y* directions suggests a more complex character of the correlations between particles moving in single file where the motions of individual molecules are coupled in a non-trivial way with the motion of the single file chain.

Diffusion constants calculated using the VACF method for K^+ released at different locations inside GA are reported in Table 9. When the ion is released in the center and at 2.4 Å the diffusion constants are the same, namely, ca. 26 times smaller compared to the bulk. When the ion is released 5 Å away from the middle of the channel the diffusion constant is 550 times smaller (nearly zero) than in the bulk. When the ion is released at 8.2 Å and 9.2 Å away from the center the diffusion constants are the same and ca. 72 times smaller than in the bulk. This dependence of the diffusion constant on the location of release has the same trend as calculated using MSD method, although the absolute value of the diffusion constants calculated by VACF method is on average two times smaller.

FACFs and integrals of the FACF for K^+ fixed at three different locations inside GA are shown in Figure 23. We found that the FACFs inside the channel have much longer correlation tails (namely, ca. 80 ps) than in the bulk. This suggests that there are much longer correlation (or memory) effects inside the channel. Comparison of the mean values of the squared random forces in bulk and in the channel is provided in Table 10. We found that mean of the squared random force in the channel is ca. 1.6 times larger than in the bulk. This is another manifestation

of stronger interactions between K^+ and water molecules in the channel. It was found that the error bars for integrals of the FACFs are very large (also shown in Figure 23) although they were calculated from long MD simulations of ca. 40 ns. (We could not do much longer MD sampling due to computer time limitations.) The diffusion constant calculated as the arithmetic average of three integrals (corresponding to three positions along the channel axis, as described in the caption for Figure 23) is 9 times smaller compared to bulk with the lower limit being 5.7 and the upper limit 12.3 times smaller than in the bulk. We have identified that the two main reasons for such a large depression of the diffusion constant inside the channel are larger mean square random forces and longer random force correlation time. Other workers have reached the same conclusion about the depression of diffusion constants of ions inside model hydrophobic channels [71].

Now let us look at the results calculated using the GLE-HO method, i.e. Eq. 3.12. The $\hat{D}(s)$ function of K^+ restrained in the center of GA is compared with the one in bulk water in Figure 24. For both systems the $\hat{D}(s)$ function bends down at $s < 10$ ps^{-1}. We encountered the same singularity of $\hat{D}(s)$ function at small s as in the bulk water simulations and were able to shift it to smaller s by increasing the simulation time. As our analytical test above showed, this singularity is almost certainly a numerical artifact and therefore is ignored in extrapolating the numerical $\hat{D}(s)$ function to $s \to 0$.

We tested how the strength of the harmonic restraint in the $4 \le k \le 40$ kcal/mol/Å^2 range affects the behavior of $\hat{D}(s)$ function, as illustrated in Figure 25. It was found that a harmonic restraint of $k < 20$ kcal/mol/Å^2 resulted in a low diffusion constant, ca. 40 times smaller than in the bulk (Figure 25A). When a stronger harmonic restraint was used, $20 \le k \le 40$ kcal/mol/Å^2 then the diffusion constant was found to be ca. 13 times smaller compared to bulk (Figure 25B). The purpose of a harmonic restraint is to overwhelm the influence of the actual systematic force on the dynamics of the ion by a harmonic force. The reason for this is that it is difficult to accurately calculate the actual position dependent systematic force. It is thus advantageous to replace the full systematic force by a known harmonic oscillator force that can later be easily unbiased using GLE-HO analysis to extract a diffusion constant. If the harmonic restraint is weak it cannot effectively overcompensate for the effect of the systematic force. This can leads to a large error in diffusion constant.

We also calculated the $\hat{D}(s)$ function for harmonic restraints applied at several different locations inside the channel, as illustrated in Figure 26. At all locations it leads to a diffusion constant significantly (4-13 times) smaller than in the bulk.

Calculation of the diffusion constant of K^+ in bulk TIP3P water and inside GA channel has been carried out by other researchers [65]. In their work a 10 kcal/mol/Å^2 harmonic restraint was used for K^+ and the function $\hat{D}(s)$ was extrapolated to s=0 from 15<s<35 range. They found that the diffusion constant inside GA is 66 % of the bulk value. Our computations show that the $\hat{D}(s)$ function significantly bends down at s<15 and thus that extrapolation from the 15<s<35 range results in a significant overestimation of the diffusion constant, namely, a value about 66 % of the bulk - the same as in Ref [65]. Such an extrapolation of $\hat{D}(s)$ from the 15<s<35 range to $s \cong 0$ is shown in Figure 24 for K^+ in bulk water (squares) and in the center of GA (circles). The fact that this function bends to such small values of $\hat{D}(s)$ is another manifestation of long time correlation effects inside GA.

As noted above, the diffusion constants of K^+ inside GA predicted by the different methods are collected in Table 9. For MSD and VACF methods we give the lower and the upper limit of the diffusion constant. Of the methods investigated here, SFDT and GLE-HO predicted a similar diffusion constant roughly 10 times smaller compared to the bulk. This value of the diffusion constant is in good agreement with results predicted by other workers as noted in the Introduction section [71, 141]. The results of our study strongly suggest that SFDT and GLE-HO are the two most reliable extant methods for calculating the diffusion constant of ions inside narrow ion channels. We found that MSD and VACF methods are not reliable because of their strong dependence on the position along the channel from which the ion is released. But, perhaps surprisingly, the upper limit (0.0145 Å^2/ps) predicted by MSD method is not very far from the diffusion constant predicted by SFDT and GLE-HO methods.

Table 8. Diffusion constants of K^+ inside the Gramicidin A channel calculated using the four methods describes in the Theory section.

	MSD	VACF	SFDT	GLE-HO
D (Å^2/ps)	~0-0.0145	0.000035-0.0075	0.019±0.008	0.016±0.004

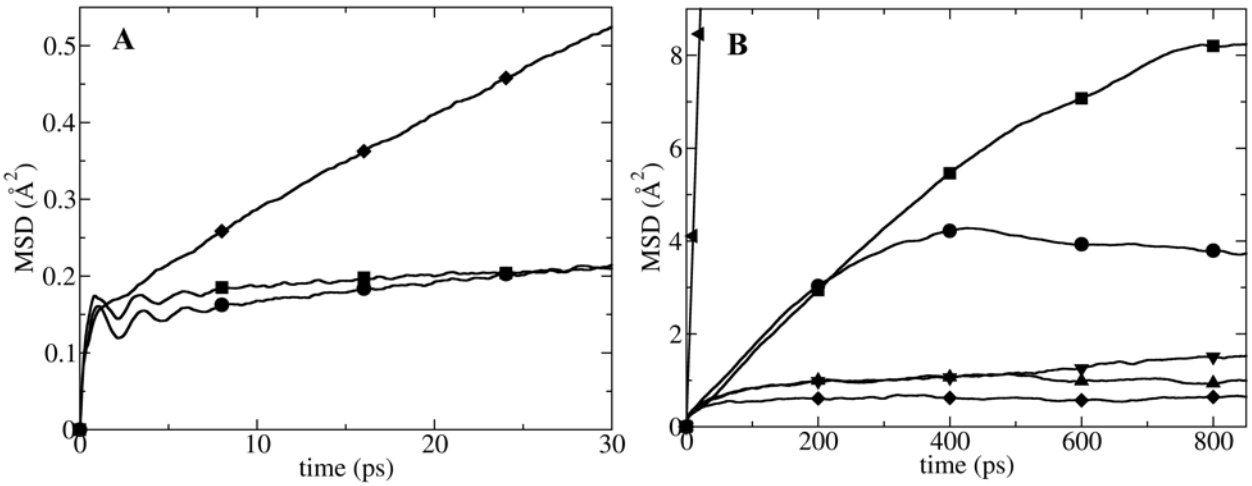

Figure 21. MSDs of K^+ released at several different locations inside GA.
(A) MSD in *x* (circles), *y* (squares) and *z* (diamonds) direction when K^+ was released in the center of the channel. (B) MSDs in *z* (channel) direction for K^+ released in the center (circles), 2.4 Å away from the center (squares), 5 Å away from the center (diamonds), 8.4 Å away from the center (triangles up) and 9.2 Å away from the center (triangles down) of the channel. They are compared to one dimensional MSD of K^+ in bulk water (triangles left).

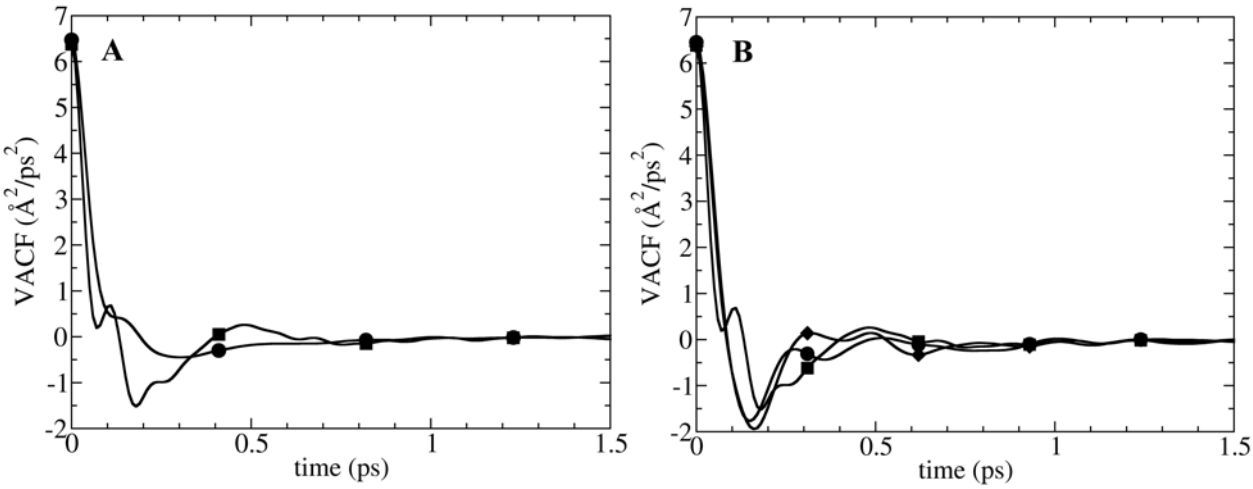

Figure 22. (A) Velocity Autocorrelation Function (VACF) of K^+ in z direction in bulk water (circles) and in the center of GA (squares). (B) VACF in *x* (circles), *y* (diamonds) and *z* (squares) direction for K^+ released in the center of GA.

Table 9. Diffusion constants of K^+ inside the Gramicidin A channel calculated using the four methods describes in the Theory section.

	MSD	VACF	SFDT	GLE-HO
D ($Å^2$/ps)	~0-0.0145	0.000035-0.0075	0.019±0.008	0.016±0.004

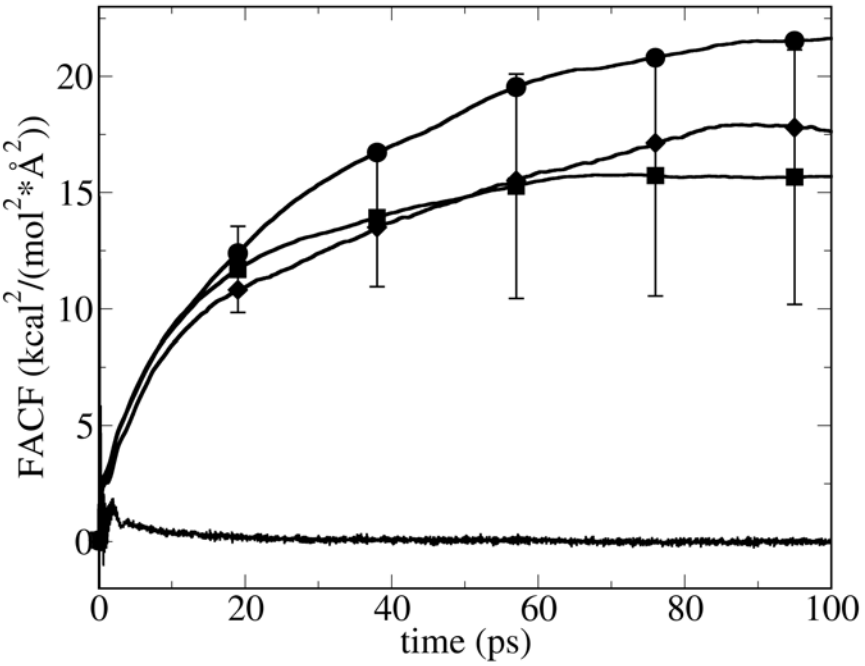

Figure 23. Force Autocorrelation Function (FACF) (jagged line on the bottom) for K^+ fixed in the center of GA, and integrals of the FACF with error bars for K^+ fixed in the center of the channel (squares), 2.5 Å away from the center of the channel (circles), and 11.5 Å away from the center of the channel (diamonds).

Table 10. Comparison of the mean value of the squared random force in bulk SPC/E water and inside GA.

	Bulk water	Center of GA
$\langle R^2 \rangle$, kcal^2/mol^2/Å^2	43.1	69.5

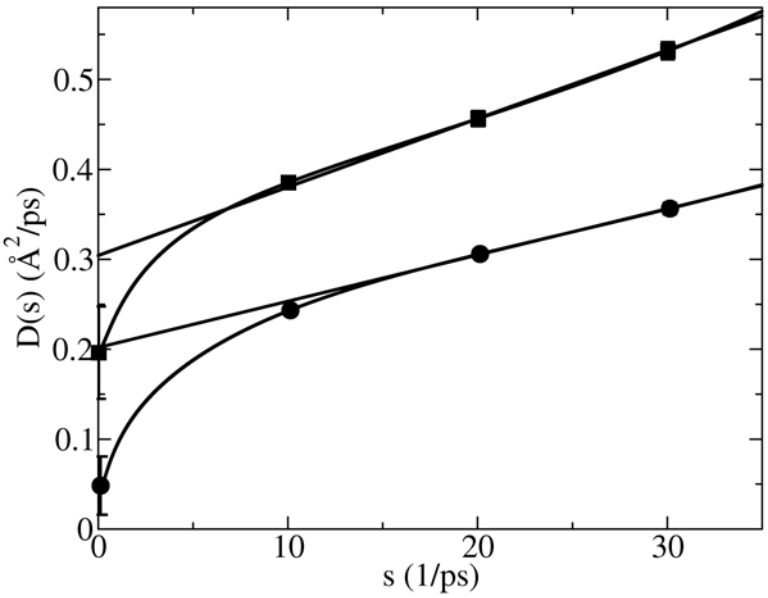

Figure 24. $\hat{D}(s)$ function calculated using GLE-HO method for K^+ in bulk water (squares) and in the center of GA (circles) along with extrapolations from 15<s<35 range (the extrapolation range used in Ref. [65]).

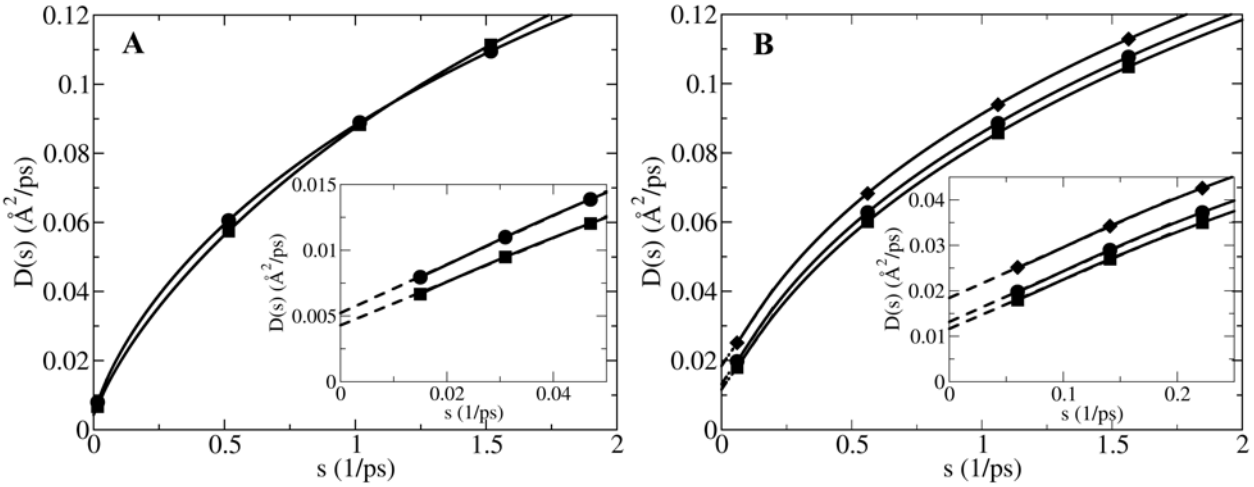

Figure 25. $\hat{D}(s)$ function calculated using GLE-HO method i.e. Eq. 3.12, for K^+ restrained with different harmonic restraints in the center of GA.

(A) k=4 kcal/mol/Å^2 (squares) and k=8 kcal/mol/Å^2 (circles). (B) k=24 kcal/mol/Å^2 (diamonds), k=32 kcal/mol/Å^2 (squares) and k=40 kcal/mol/Å^2 (circles). A blowup of the $\hat{D}(s)$ functions at small *s* is shown in the insets. The broken line represents where the $\hat{D}(s)$ function was linearly extrapolated to *s*=0 (broken lines).

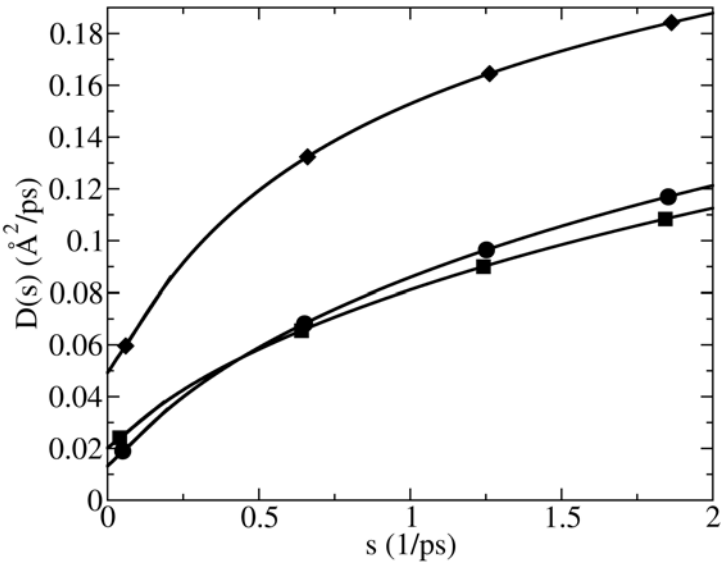

Figure 26. $\hat{D}(s)$ function calculated using GLE-HO method for K^+ restrained at three different locations along the channel (z axis) with harmonic constant of 40 kcal/mol/Å^2: 5.2 Å away from the center (diamonds), 2.4 Å away from the center (squares) and in the center of the channel (circles).

3.5 CONCLUSIONS

There are two main conclusions of this study. The first conclusion is that all four methods predict that diffusion constant of K^+ inside the GA channel is significantly (at least 4 times) smaller than in bulk water. We have identified a possible explanation for the large diffusion constant of K^+ inside GA calculated by GLE-HO method reported recently [65], namely extrapolation of $\hat{D}(s)$ to s=0, based on its "intermediate s" behavior (which misses critical details of $\hat{D}(s)$ near s=0; see Figure 24).

The second conclusion is that of the four methods considered here, SFDT and GLE-HO predict a similar diffusion constant which is ca. 10 times smaller than in bulk water. The other two methods, MSD and VACF, predict a much smaller diffusion constant compared to the bulk. We attribute this to the fact that SFDT and GLE-HO methods correctly unbias the influence of the systematic force on the diffusion properties of the ion, while MSD and VACF do not. Therefore, the MSD and VACF methods inject unwanted information about the systematic force (manifested in the PMF), resulting in predicted diffusion constants which are quite different than when calculated by SFDT and GLE-HO methods.

3.6 ACKNOWLEDGMENTS

The work of ABM and RDC was supported in part by grants from NSF (Grant CHE0092285) and ARO-MURI (grant DADD19-02-1-0227). MGK's research was supported in part by the NIH (Grant GM067962).

4.0 MODELING THE FAST GATING MECHANISM IN CLC CHLORIDE CHANNELS

Mamonov, A. B., J. W. Dukes, H. Cheng, and R. D. Coalson. Manuscript in preparation.

4.1 ABSTRACT

A simplified three-dimensional ClC chloride model channel is constructed to couple the permeation of Cl^- ions to the motion of a glutamate side chain which acts as the putative fast gate in the ClC-0 channel. The gate is treated as a single spherical particle attached by a rod to a pivot point. This particle moves in a one-dimensional arc under the influence of a bi-stable potential, which mimics the isomerization process by which the glutamate side chain moves from an open state (not blocking the channel pore) to a closed state (blocking the channel pore, at a position which also acts as a binding site for Cl^- ions moving through the channel). A Dynamic Monte Carlo (DMC) technique is utilized to perform Brownian Dynamics simulations in order to investigate the dependence of the gate closing rate on both internal and external chloride concentration, and the gate charge as well. To accelerate the simulation of gate closing to a time scale which can be accommodated with current methodology and compute power, i.e. microseconds, parameters that govern the motion of the bare gate (i.e., in the absence of coupling to the permeating ions) are chosen appropriately. Our simulation results are in qualitative agreement with experimental observations and consistent with the "foot-in-the-door" mechanism [74, 75], although the absolute time scale of gate closing in the real channel is much longer (millisecond time scale). A simple model based on the fractional occupation probability of the Cl^- binding site that is ultimately blocked by the fast gate suggests straightforward scalability of

simulation results for the model channel considered herein to experimentally realistic time scales.

4.2 INTRODUCTION

The ClC family of ion channels primarily regulates the flow of Cl^- across cell membranes. By doing so, ClC channels control a variety of important physiological functions, such as skeletal muscle excitability (ClC-1), renal and intravascular transport (ClC-K and ClC-5), and cell volume regulation (ClC-2 and ClC-3). The presence of a double-barreled channel was first suggested by early electrophysiological recordings from *Torpedo electroplax* ClC-0 channel [156], and was recently confirmed by X-ray crystallography [20, 77]. Opening and closing of these two pores appear to be regulated by two distinct mechanisms, corresponding to a fast and a slow gate. Slow gating involves structural changes of both monomers, and thus opens or closes both pores simultaneously. The slow gate operates on a time scale of seconds. Fast gating is controlled separately by each individual pore and occurs on a time scale of milliseconds. It was observed experimentally that both gating mechanisms are regulated by Cl^- concentrations [75, 76, 157]. Changing the concentrations of Cl^- on the intracellular and extracellular sides of the membrane affects the fast gating in different ways. Increasing the extracellular concentration increases the rate of fast gate opening but has little effect on the closing rate [75, 76]. In contrast, increasing the intracellular concentration reduces the rate of fast gate closing but has a much smaller effect on the rate of fast gate opening [74, 75]. Thus, it was suggested that the opening and closing of the fast gate are coupled to ion permeation and regulated by two different mechanisms. To explain the dependence of the fast gate closing rate on the internal concentration, a foot-in-the-door mechanism was proposed [74, 75]. According to this mechanism a permeating Cl^- ion blocks the fast gate from closing by occupying a binding site that would be occupied by the fast gate in the closed state. Recently, Dutzler et al. [77] presented a structural basis for this mechanism and suggested a possible way of coupling ion permeation to ClC channel gating. The authors solved the x-ray structure of a channel-antibody complex for the wild type channel at 2.5 Å resolution that allowed identification of two Cl^- binding sites: one located close to intracellular and the other in the center of the channel. However, the passage to

the extracellular side was blocked by the glutamate E148 residue. In the next step the authors solved the structures of two mutants in which the glutamate E148 residue was replaced with alanine and glutamine. In both cases the side chains of the mutated residues pointed away towards the extracellular side and the position of the carboxyl group found in the wild type channel was occupied by a Cl^- ion. Based on this study the authors suggested a gating mechanism in which the permeant Cl^- ions compete with the carboxyl group of E148 for the binding site located closest to the extracellular side.

The goal of the present study is to test the proposed foot-in-the-door mechanism for the dependence of the fast gate closing rate on internal and external [Cl^-] using numerical modeling. With currently available computational power, a fully atomistic simulation of ion permeation is intractable on the time scales relevant for studying the fast-gating mechanism of ClC channels. Coarse-grained models sacrifice some realism, but by virtue of their relative simplicity make it possible to calculate ion permeation kinetics on currently available computing platforms to predict the rate of ion permeation through a variety of open channels. Among such models**,** Poisson-Nernst-Planck theory [48], Brownian dynamics [56, 98] and the dynamic Monte Carlo (DMC) technique [50, 140] have been extensively applied. However, modeling gating of ion channels remains challenging for two reasons: 1) gating often involves large structural changes and 2) gating times far exceed the amount of time the most powerful computers are able to simulate via MD. To account for this, in the present study we have developed a coarse-grained model which couples the ion permeation to fast gating.

The outline of this paper is as follows. In "Methods" section, we discuss the protocol and rationale for constructing a numerical model channel which mimics ion permeation and the fast (glutamate) gate in ClC channels. We also outline a DMC method for carrying out Brownian Dynamics (BD) simulations of both ion permeation and the motion of the gate in our model system. In "Results and Discussion" section, we discuss our simulation results and present a simple quasi-analytical model to address the "foot-in-the-door" mechanism. Finally, our conclusions are presented in "Conclusions" section.

4.3 METHODS

4.3.1 Model channel

The ClC gate model channel is depicted schematically in Figure 27. The membrane is 32 Å wide. The selectivity filter is 12 Å long and 2 Å in radius, and is connected to two cone-like vestibules on each side of the channel. The widest part of these vestibules is 6 Å in radius. This geometry was designed to mimic the ClC-0 channel based on its crystallographic structure [20, 77]. Three binding sites for Cl^- ions were positioned inside the channel to represent experimentally determined Cl^- binding sites in ClC-0 [77]. In our model, the Cl^- binding sites are asymmetrically located at -6 Å, 1 Å and 6 Å relative to the center of the channel.

Since the fast-gate is linked to non-equilibrium chloride permeation through the ClC channel, to model this mechanism, both the dynamics of the fast gate and permeation of chloride ions must simultaneously be taken into account. In the present study, we invoke a minimalist model for the fast gate, in which a spherical particle is attached to a lever whose pivot is located in the wall of the pore (cf. Figure 27). The gate particle is allowed to swing from the extracellular vestibule of the channel into the selectivity filter of the channel, thus blocking chloride permeation.

The gate particle has a radius of 2 Å and mimics the side chain of the glutamate residue E148, which was determined experimentally to be the residue most likely responsible for the fast gating in the ClC-0 channel [77]. The pivot of the model gate lever was positioned inside the membrane 6 Å away from the center of the channel in the *z* direction and -4 Å in the *x* direction. The length of the lever is 4 Å. The gate particle undergoes Brownian motion in a bistable potential, as shown in Figure 28. Results of preliminary MD simulations of the ClC channel [158] indicated that the two dihedral angles of E148 contribute most significantly to the closing and opening of the gate. Let us adopt the nomenclature that dihedral angle 1 is closest to the peptide backbone and dihedral angle 2 is adjacent to dihedral angle 1 (closer to the terminal carboxyl group). The dihedral coordinate in our simple model corresponds roughly to dihedral angle 1 of the E148 side chain. The wells of our bistable potential correspond to the stable states where the steric hindrance between the substituents is minimum while the barrier corresponds to sterically hindered conformations between substituents. The shape of the bistable potential was

chosen to mimic the shape of the dihedral energy functions employed in the description of torsional potentials in standard MD force fields [59]. We have chosen the following equation to describe the bistable potential $\frac{E_{act}((\theta-60)^2-60^2)^2}{60^4}$, where E_{act} is height of the energy barrier and θ is the angle of the gate lever. The closed state of the gate corresponds to θ=0° angle. In this state the gate lever is perpendicular to the channel (z) axis. The open state of the gate is located at θ=120°. The maximum barrier height of the gate is at θ=60°. In our computational study we employed several sets of parameters, which are reported in Table 11. The choice of parameters will be discussed at length below.

The radii of mobile ions Cl^- and Na^+ were taken to be 1.8 Å and 1 Å, respectively. Inside the channel they moved in the single ion free energy profiles shown in Figure 29. The Na^+ PMF was calculated based on the numerical solution of the Poisson equation for a model ClC system in which the Cl^- binding sites were represented by three rings of dipoles [158]. The magnitude of dipole rings were fit to reproduce the same Cl^- binding energies as reported in Ref. [159]. This energy profile completely excluded the passing of Na^+ through the model channel. The Cl^- PMF has three energy wells, which mimic experimentally determined Cl^- binding sites in ClC-0 [77]. Following a procedure described in Ref. [141], the well depths and barrier heights of Cl^- PMF were adjusted to reproduce a saturation behavior of the gate open time with internal [Cl^-] by approximating the binding energies reported in Ref. [159]. The diffusion coefficient for both Na^+ and Cl^- was set to 0.2 $Å^2$/ps in the bulk [131] and assumed to be 10 times smaller than this inside the channel.

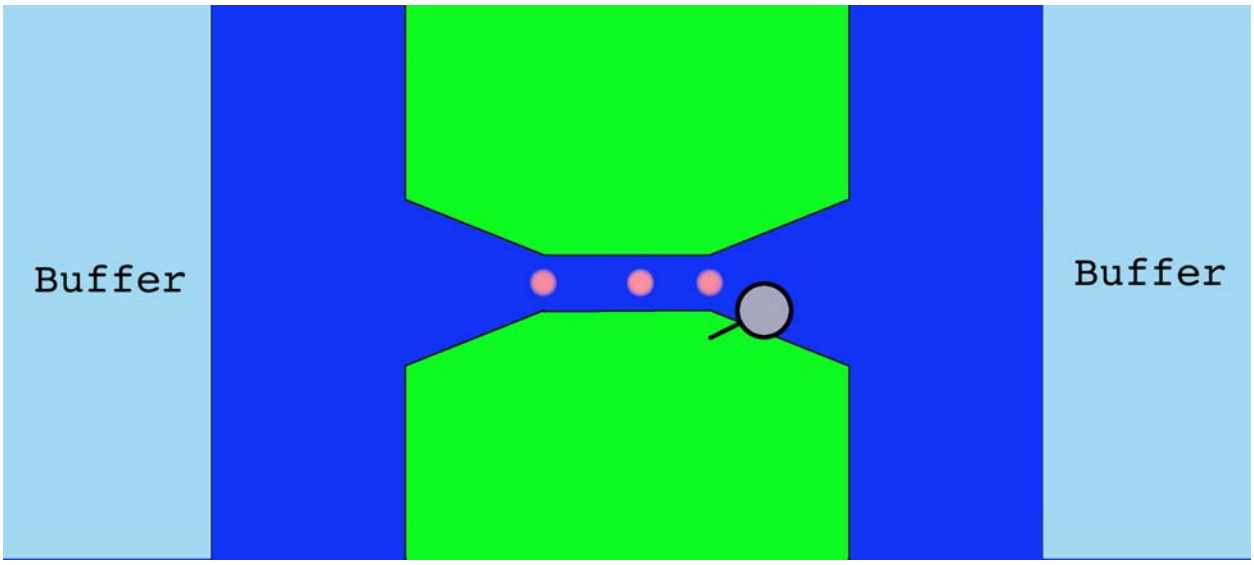

Figure 27. Schematic depiction of the DMC simulation model.

The membrane is shown in green. The gate is represented by a gray particle connected to a pivot rod. Three Cl^- binding sites in the middle of the channel are shown in pink. In the buffer regions, a constant number of ions is maintained during DMC simulations. During simulations of the ion motion, the bath concentrations are monitored in order to assess the performance of the imposed constant concentration boundary conditions.

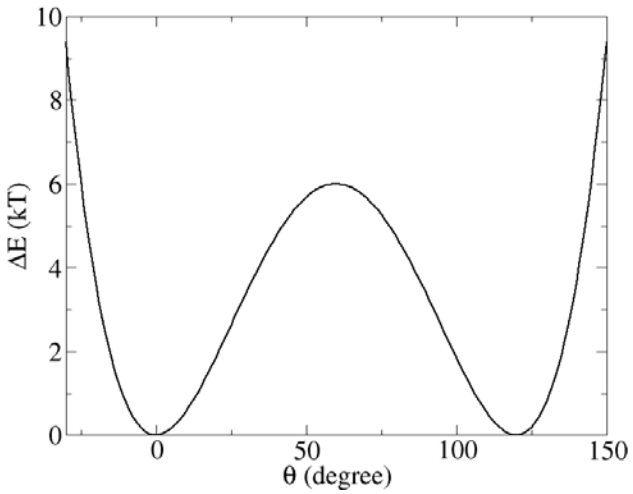

Figure 28. Free energy profile of the fast gate used in our model. θ=0 degrees corresponds to the closed state and θ=120 degrees to the open state of the fast gate.

Table 11. Parameters used in our DMC simulations. Rate constant was calculated using Eq. 4.9.

	Set 4.6	Set 6	Set 6.7	Set 8
E_{act} , k_BT	4.6	6	6.7	8
D_{gate} , Å^2/ps	0.02	0.061	0.02	0.061
k_{esc} , ns^{-1}	0.04732	0.04633	0.008424	0.008377

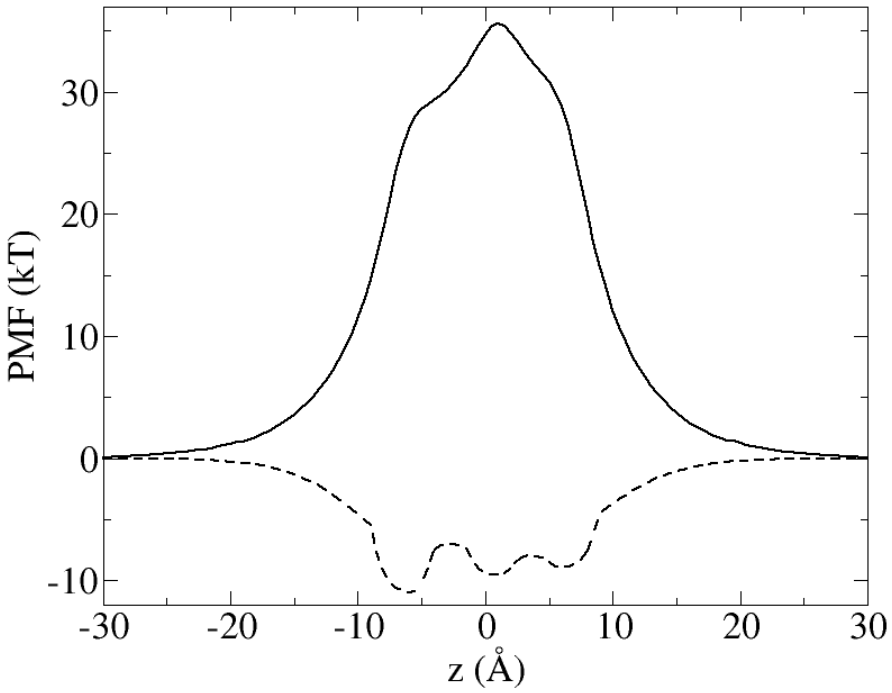

Figure 29. 1D Potential of mean force (PMF) of Na^+ (solid line) and Cl^- (dashed line) along the channel (z) axis. The Na^+ PMF was calculated based on numerical solution of the Poisson equation for a model ClC system in which Cl^- binding sites were represented by three rings of dipoles [158]. The magnitude of dipole rings and location of binding sites were fit to reproduce the same binding energies and geometries as reported in Ref. [159]. The Cl^- PMF was calculated by adjusting the depths and barriers of the binding sites to reproduce a saturation behavior of the gate open time with internal [Cl^-] by approximating binding energies reported in Ref. [159].

4.3.2 Dynamic Monte Carlo

We used Dynamic Monte Carlo (DMC) method to simulate ion permeation and motion of the gate. Complete computational details of our DMC algorithm and its application to ion permeation through protein channels can be found in Refs. [50, 57, 95, 140]. Here we will give a brief review of our computational model.

In a DMC algorithm for ion permeation [50, 57, 95], configurations are generated by random changes of the ion positions. The total number of ions is characterized by $N = N_L + N_R + N_I + N_v$. Here N_L and N_R are the fixed numbers of ions on the left and right boundaries (buffers in

Figure 27), which are obtained by integrating the given boundary concentrations C_L and C_R over the volumes of the boundary layers. In this study, the constant concentration boundary condition is imposed by uniformly distributing N_L or N_R ions in the buffers at each Monte Carlo (MC) step. N_I is the number of ions inside the system and N_v is the number of virtual ions. The total number of ions N is fixed and N_I fluctuates. N_v is introduced only for counting purposes and is included to account for dynamic fluctuation of the number of ions in the interior of the system, and ensure the proportionality of Monte Carlo cycles to real time (characterizing time evolution under the corresponding multi-ion Smoluchowski Equation). For example, in DMC simulation that involved the ionic concentration of 0.135 M NaCl on both sides of the membrane, the number of ions in the left buffer was the same as in the right N_L=N_R=4 (2 for Cl^- and 2 for Na^+ to make the buffer neutral), the number of ions in the internal system was N_I=8 and the virtual number of ions N_v=2; so that the total number of ions used was N=18.

One MC cycle consists of N steps. At each step, one ion k is randomly chosen to move $\pm h$ in one direction (x, y, or z) if the chosen ion is not a virtual one, where h is a position-dependent displacement. In the present implementation, this new configuration is accepted if $Rand < \exp(-\beta \Delta W)$, where $Rand$ is a uniform random number that belongs to the interval [0, 1] and $\beta = (k_B T)^{-1}$; ΔW is the energy change between the old and the new configurations based on the chosen ions k with charge q_k [140]. In the present study, ΔW is calculated as:

$$\Delta W = W_k^{new} - W_k^{old} \tag{4.1}$$

$$W_k = \phi_k^{stat} + \sum_{j \neq k} \frac{q_k q_j}{\varepsilon_w} \phi^{coul}(r_{kj}) + \frac{q_k q_{gate}}{\varepsilon_w} \phi^{coul}(r_{kg}) - k_B T \ln(D(z)/D_0), \tag{4.2}$$

where q_j and q_{gate} are charges of ion j and the gate particle, respectively. D_0 and $D(z)$ are the diffusion constants of ion in the bulk and at position z, respectively. The first term in the right hand side of Eq. 4.2 is the PMF (cf. Figure 29) of ion k. The second term represents Coulombic interactions between pairs of ions in an environment characterized by the (uniform) water dielectric constant ε_w. The third term is Coulombic interactions between the gate particle and the chosen ion k. The effect of the dielectric inhomogeneity of the channel environment on the ion-ion and ion-gate electrostatic interactions was not included in this study. The last term in Eq. 4.2 is incorporated to reflect the effect of non-uniform diffusion constant of ions. While this term can be applied to treat any given three dimensional inhomogeneous diffusion constant profile, in the

model considered in this paper the diffusivity varies only along the channel direction. The diffusion constants and the associated ion displacement steps taken in one DMC step obey the relation:

$$h_z^2 / D(z) = h_0^2 / D_0 \tag{4.3}$$

where h_0 and h_z are the associated ion displacement in the bulk and at the position z, respectively. The total simulation time T_s for ions is related to the number of the Monte Carlo cycles N_c as

$$T_s = \frac{h_0^2 N_c}{6D_0} \tag{4.4}$$

The putative gate is assumed to undergo one-dimensional angular motion. At one MC cycle, the gate moves $\pm\Delta$ angle. This new configuration is accepted if $Rand < \exp(-\beta \Delta W_g)$, where ΔW_g is the energy change of the gate between these two configurations. The energy of the gate is calculated in the following way:

$$W_g = \phi_g(\theta) + \sum_j \frac{q_g q_j}{\varepsilon_w} \phi^{coul}(r_{gj}), \tag{4.5}$$

where $\phi_g(\theta)$ is the angular dependent potential of the gate (cf. Figure 28) and the second term represents the Coulombic interactions between the gate particle and the ions. The total simulation time for the gate particle T_g is related to the number of the Monte Carlo cycles N_g as

$$T_g = \frac{(L_g \Delta)^2 N_g}{2D_{gate}}, \tag{4.6}$$

where L_g is the arm of gate and D_{gate} is the diffusivity of the gate. In order to keep the same total MC cycles and the real time as ions, the gate angular displacement is related to the ion displacement in the bulk as follows:

$$(L_g \Delta)^2 / D_{gate} = h_0^2 / 3D_0 \tag{4.7}$$

Unless otherwise explicitly noted, for one MC cycle the angular displacement for the gate was Δ=0.0458 radian (or 2.6241 degrees) for all parameter sets. The displacement of ions in the bulk was set to 0.575 Å for parameter Set 6 and Set 8, and 1.0 Å for parameter Set 4.6 and Set 6.7. For all our simulations, -100 mV external electric potential was applied across the membrane. The gate open time was calculated by counting the time it took for the gate to go from the open state (corresponding to θ=120 degrees) to the closed one (θ=0 degree).

4.4 RESULTS AND DISSCUSION

4.4.1 Test of the gate motion using a simple analytical model

In order to test our DMC algorithm for simulating combined ion permeation/gate particle motion, we first considered one dimensional bistable gate particle motion *in the absence* of any coupling to ion permeation, i.e., the channel was empty of ions. Simulation results for the escape rate (rate of transitions from the initial to the final state well, suppressing any back transitions from the final to the initial state well) were compared to the corresponding predictions of Kramer's theory in the high friction limit, namely [160]

$$k_{esc} = \frac{\omega_w \omega_b}{2\pi\xi} e^{-\frac{E_{act}}{k_B T}}, \tag{4.8}$$

where k_{esc} is Kramer's escape rate constant, E_{act} is height of the energy barrier (activation energy), and ξ is the coefficient of dynamical friction of the escaping particle. Furthermore, ω_w and ω_b are harmonic curvatures describing the energy well and the barrier of the escaping potential, respectively. Specifically, $\omega_w = \sqrt{\frac{k_w}{m}}$, where *m* is the particle mass and k_w>0 is the 2nd derivative of the gate particle potential function evaluated at the bottom of the reactant well; analogously, $\omega_b = \sqrt{\frac{k_b}{m}}$ with k_b>0 being the negative of the 2nd derivative of the gate particle potential evaluated at the top of the barrier. Using Einstein's relation $D = \frac{k_B T}{m\xi}$, Eq. 4.8 reads

$$k_{esc} = \frac{D_{gate}\sqrt{k_w k_b}}{2\pi k_B T} e^{-\frac{E_{act}}{k_B T}}, \tag{4.9}$$

where D_{gate} is the diffusion constant of the gate particle. Note that the mass of the particle does not appear in Eq. 4.9 because it gets incorporated into the diffusion constant. Comparison of Kramer's formula, which is essentially exact when $E_{act}/k_B T >> 1$, to the corresponding DMC simulation results for several different sets of D_{gate} and E_{act} is shown in Table 11 (discussion of D_{gate} and E_{act} values used in our model is presented below in the subsection "Effect of D_{gate} and

E_{act}"). Transition of the gate particle from the open to the closed state is analogous to a first order chemical reaction, where the open state corresponds to the reactant side and the closed state to the product side. Therefore, the survival probability of the gate to be open is [161]

$$p_o(t) = e^{-k_{esc}t}, \tag{4.10}$$

where $p_o(t)$ is the probability for the gate to be open at time t. We calculate p_o analytically via Eqs. 4.9 and 4.10 and then compare to the corresponding numerical calculation using the DMC method, as illustrated in Figure 30. There is excellent agreement between them.

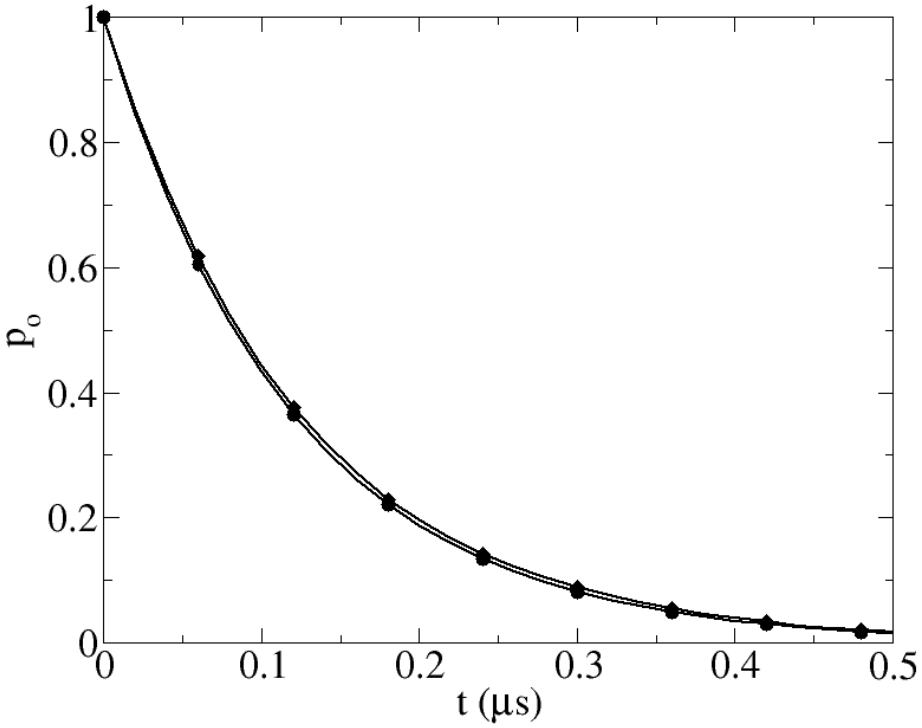

Figure 30. Dependence of the neutral gate probability to be open on time for parameter Set 6 (Table 11) calculated using Kramer's rate theory (circles) and DMC (diamonds). The error bars for DMC data are smaller than symbol labels.

4.4.2 Dependence of the gate open time on internal and external [Cl^-]

To validate computationally the foot-in-the-door mechanism for the ClC channel, we studied two main relationships that were measured experimentally [74, 75]: the dependence of the gate open time on internal [Cl^-] while keeping external [Cl^-] constant at 0.135 M and the dependence of the gate open time on external [Cl^-] while keeping internal [Cl^-] constant at 0.135 M. Results of the open time dependence on internal [Cl^-] for parameter Set 6 (Table 11) are shown in Figure 31, for the case of a neutral gate (analogous results for a gate with -1 charge, representing the deprotonated state of E148, are presented below). In order to scan the range of [Cl^-] used in experiments [74, 75], the following set of constant concentrations was imposed in the internal buffer boundary (cf. Figure 27): 0.135 M, 0.270 M, 0.54 M, 0.81 M, 1.22 M, and 2.02 M. The average bath (cf. Figure 27) concentrations fluctuate as: 0.1397±0.006 M, 0.2708±0.008 M, 0.5297±0.011 M, 0.7907±0.011 M, 1.179±0.0128 M, 1.982±0.015 M, indicating successfully implemented constant boundary conditions in our simulation systems. A smooth saturation of the open time is observed when the internal [Cl^-] is increased from 0 M to 2 M, which is in qualitative agreement with experimental observations [74] shown in the inset of Figure 31. This saturation behavior observed in our simulations is consistent with the "foot-in-the-door" mechanism proposed by Chen and Miller [74]: at low [Cl^-], the probability of S_{ext} being occupied by a Cl^- ion (thus preventing the gate from closing) increases linearly with internal [Cl^-], since the flux through the channel scales linearly with bathing solution concentration at low concentration. At higher concentration, S_{ext} becoming "clogged" with Cl^-, and further increase of the bath concentration of Cl^- does not increase the probability that S_{ext} will be occupied by Cl^-. Thus a saturated gate open time is observed, as would be expected for this model.

Results of DMC calculations for the dependence of gate open time on external [Cl^-] are shown in Figure 32. Our simulations show a relatively weak dependence of gate open time on the external [Cl^-], qualitatively consistent with experimental measurements [74, 75], Such behavior might be expected in the model channel explored here, since the ions are being driven from the internal to external by the applied membrane potential, and thus should be less sensitive to the ion concentration in the external compartment.

The dependence of gate open time on the external [Cl^-] was not further investigated because of the speculated presence of a fourth binding site on the extracellular side whose existence could significantly affect how a extracellular Cl^- ions regulate opening and closing of the gate [74]. The location of the fourth binding site has not been identified yet and, therefore, the fourth binding site was not included in our model.

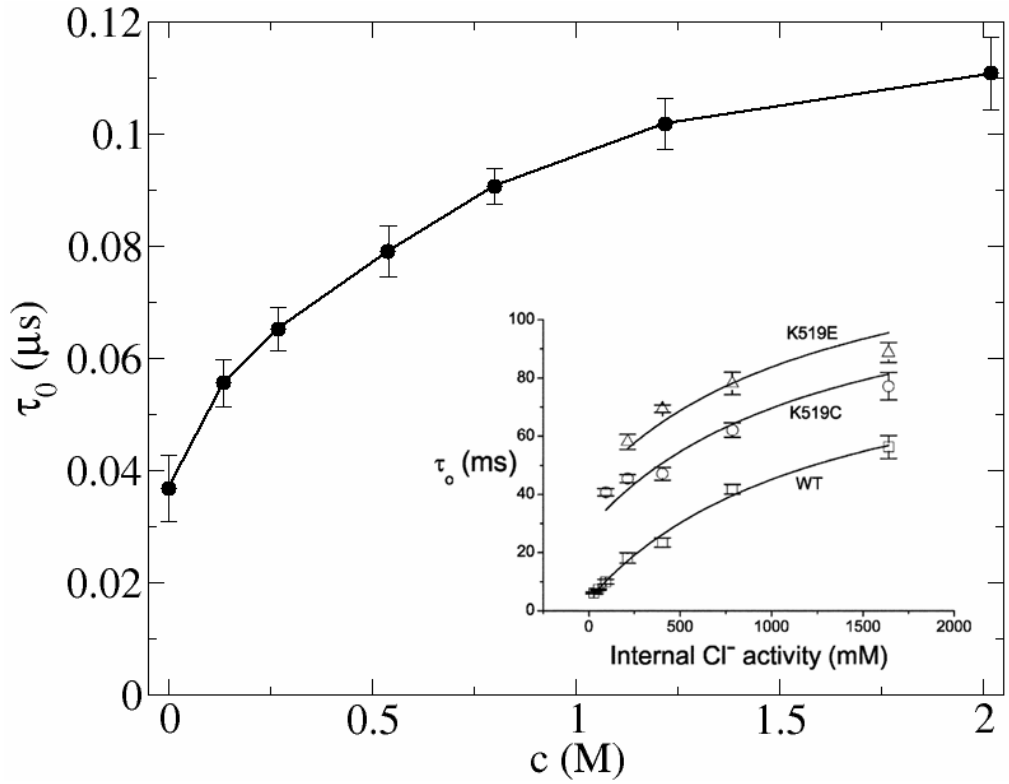

Figure 31. Dependence of the gate open time on the internal [Cl^-] for the neutral gate and parameter Set 6 (Table 11) calculated using DMC. Result of the experimental measurements [74] are shown in the inset.

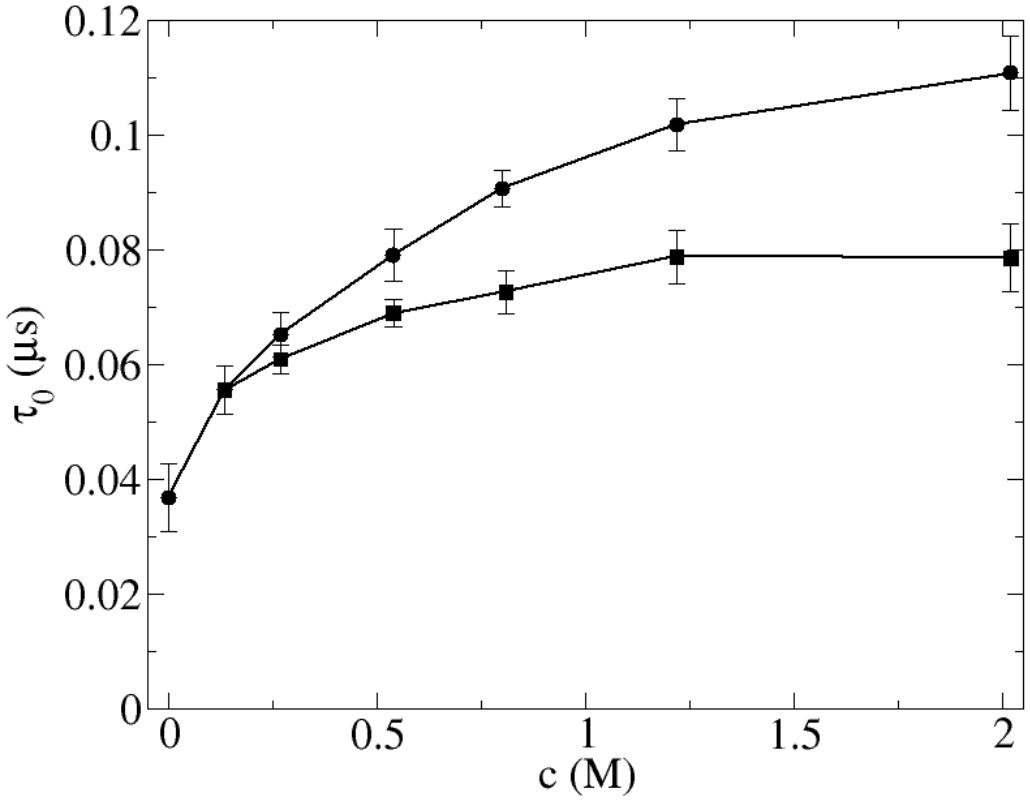

Figure 32. Dependence of the gate open time on the external [Cl^-] (squares) for neutral gate with parameter Set 6 (Table 11) calculated using DMC. For comparison, dependence of the gate open time on the internal [Cl^-] is also shown (circles).

4.4.3 Effect of a negatively charged gate on the gate open time

There is at present no consensus in the biophysical literature whether the glutamate residue in the ClC channel is charged or not [162-164]. Using our DMC model, we studied how a -1 *e* negative charge on the gate particle affects the gate open time. Results of DMC simulations for the neutral and charged gate are shown in Figure 33. For the negatively charged gate the open time is slightly larger than for the neutral one, but the saturation effect is still observed. The longer open time for the charged gate is consistent with the expected consequence of electrostatic repulsion between the gate and the Cl^- in the external binding site, which pushes the gate away from the closed state and increases the open time. The effect of the negative charge on the gate open time

is rather small (cf. Figure 33) in our simulation since we calculated the ion-gate interaction in water bath with ε_w=80. It should be noted that ignoring the effect of dielectric constant discontinuities on charge-charge interactions is in some sense a significant oversimplification of reality; nonetheless, given all the other uncertainties in our model, as well as the large additional computational cost of including dielectric inhomogeneity effects, the simple calculation of the ion-gate interaction used in the present study serves a reasonable zeroth-order approximation.

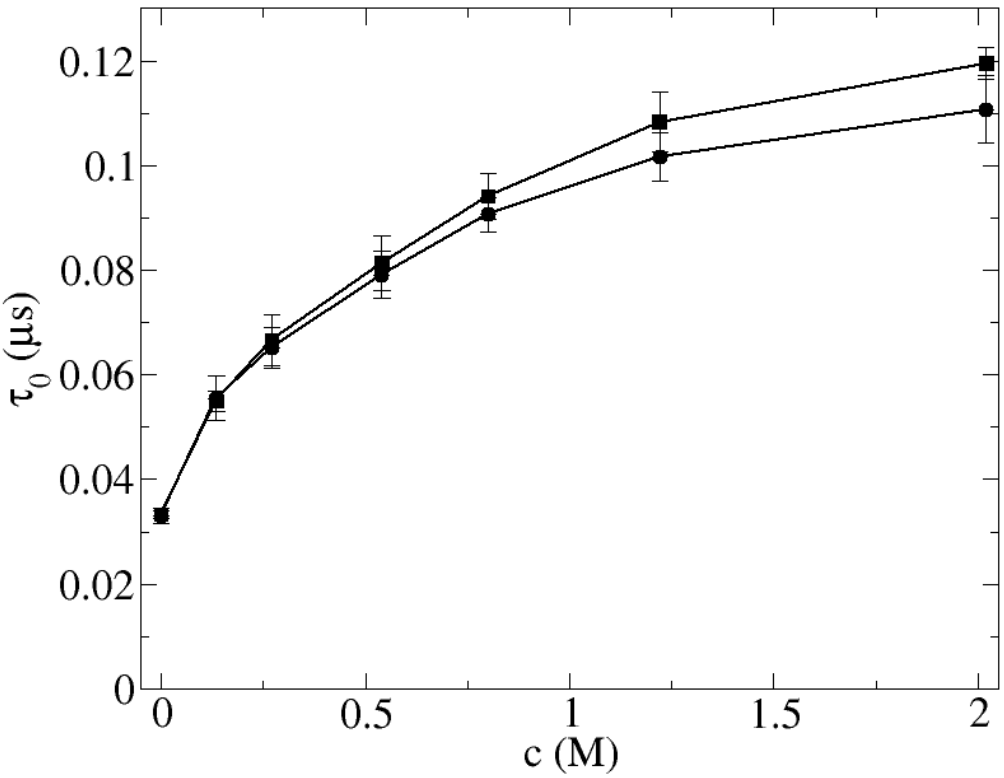

Figure 33. Dependence of the gate open time on the internal [Cl^-] for neutral gate (circles) and negatively charged gate (squares) calculated using DMC with parameter Set 6 (Table 11).

4.4.4 Effect of D_{gate} and E_{act}

Figure 31 illustrates the qualitative agreement between our numerical simulations and experiments. However, the absolute values of calculated gate open time are ca. 4 orders of magnitude smaller than the experimentally measured ones. In reality, the gate open time for the fast gate of the ClC channel is in the multi-ms time-scale, well beyond the time scale which can be computationally accessed at present (recall that in 3D Brownian Dynamic simulations of ion channel permeation kinetics, data is typically collected for several μs). Our model is crude of necessity: there are no experimental measurements of the gate diffusion constant in the ClC channel and the magnitude of the activation energy for the ClC gate is not known either. Therefore, we treated them as adjustable input parameters for our DMC calculations and appropriately chose these gate parameters (i.e., D_{gate} and E_{act}) in order to accelerate the simulation of gate closing to a time scale accommodated with current methodology and compute power. There are four sets of D_{gate} and E_{act} parameters used in our DMC simulations (see, Table 11). These parameters were selected to study the combined influence of D_{gate} and E_{act} based on what value of k_{esc} they correspond to. Two different values of D_{gate} were selected: 0.061 Å^2/ps and 0.02 Å^2/ps, which are, respectively, 3 and 10 times smaller than the diffusion constant of ions in the bulk solution. It should be noted that this is our crude estimate of the diffusion constant of the Glu-148 side chain responsible for the fast gating in our model. According to Stoke's equation the friction constant of a spherical particle immersed in the fluid is $\gamma = 6\pi a\eta$ [59], where γ is the friction coefficient, a is the radius of the particle and η is the fluid viscosity. There is a linear dependence between the friction coefficient and the radius of the particle. The size of the glutamate residue is much larger than the size of a single ion. Therefore, a smaller diffusion constant for the gate should be expected compared to the ion diffusion constant.

Four different values of E_{act} were selected: 4.6 k_BT, 6 k_BT, 6.7 k_BT and 8 k_BT. This magnitude of E_{act} was chosen to satisfy the lower limit of the high friction Kramer's theory (*ca.* 1 k_BT) and at the same time to be computationally inexpensive. The diffusion constants and E_{act}

were selected such that Set 4.6 and Set 6 had a similar k_{esc} and Set 6.7 and Set 8 had a similar k_{esc} (see, Table 11).

Results of the gate open time on internal [Cl^-] for parameter Set 4.6 and Set 6 are shown in Figure 34A. The saturation behavior is the same for both parameter sets. Results of the gate open time on the internal [Cl^-] for parameter Set 6.7 and Set 8 are shown in Figure 34B. Both parameter sets predict the same saturation behavior. Based on these results we can conclude that saturation behavior of the gate does not depend strongly on D_{gate} and E_{act} individually, but only on their combined influence on k_{esc}.

We also compared the saturation behavior of the gate open time on internal [Cl^-] for parameter sets with much different k_{esc} (Table 11). For the sake of comparison we normalized the gate open time for parameter Set 6 and Set 8 and plotted them on the same graph (Figure 35): normalization was done by dividing the open time by that at internal [Cl^-]=0. Both sets predicted the same saturation behavior. This result implies that k_{esc} simply scales the curve of the gate open time but the curve shape is determined by some "universal" mechanism. This mechanism relies on saturation of external binding site (S_{ext}) with Cl^- as the internal [Cl^-] increases (This mechanism is further discussed in subsection "Approximate Factorization of the Gate Closure Mechanism"). An important corollary of this observation is that if k_{esc} was much slower (comparable to the experimentally measured values), we would expect the same normalized curve for the gate open time and, therefore, our model would be able to account semi-quantitatively for the experimentally measured saturation of the gate open time with internal [Cl^-].

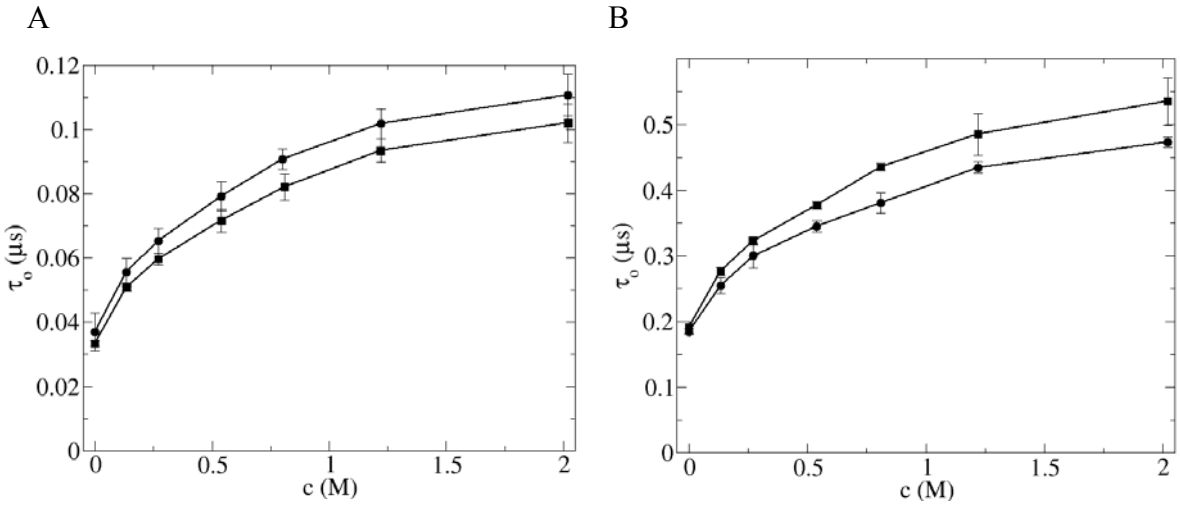

Figure 34. Dependence of the gate open time on the internal [Cl^-] for neutral gate calculated using DMC.
(A) Results of parameter Set 6 (circles) are compared with results of parameter Set 4.6 (squares). (B) Results of parameter Set 6.7 (circles) are compared with results of parameter Set 8 (squares). See, Table 11 for parameter values.

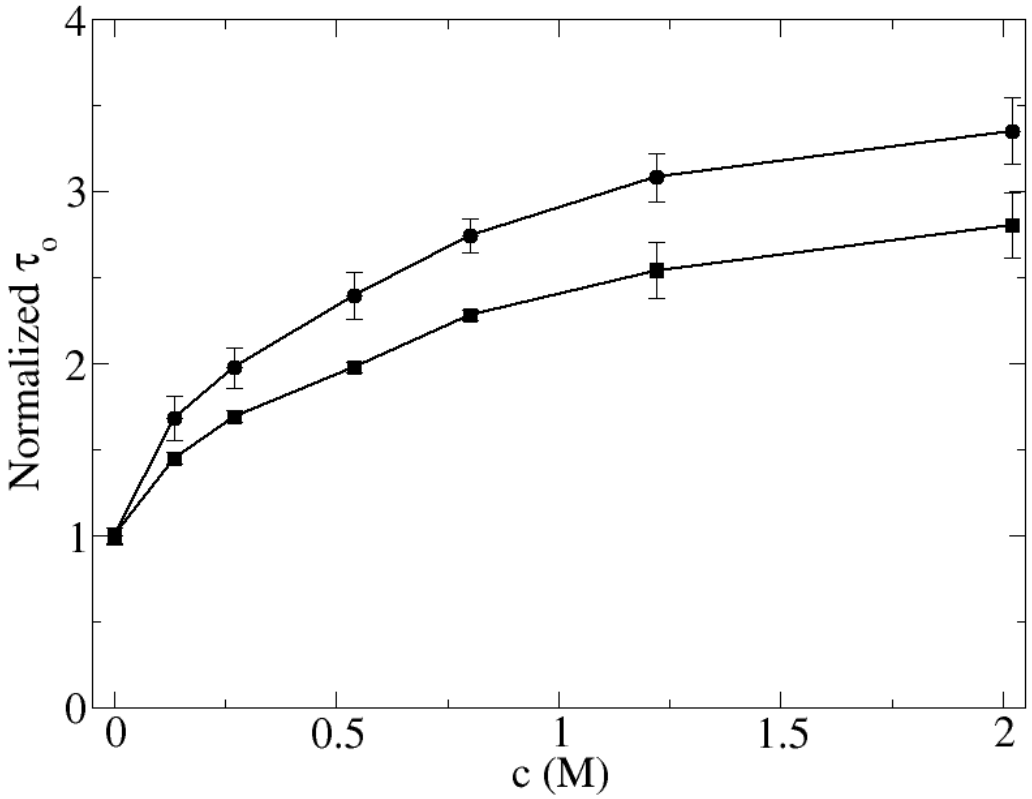

Figure 35. Dependence of the normalized neutral gate open time on internal [Cl^-] calculated using DMC. Results for parameter Set 6 (circles) are compared with parameter Set 8 (squares). See, Table 11 for parameter values. Open time was normalized by dividing it by open time at internal [Cl^-]=0.

4.4.5 Approximate Factorization of the Gate Closure Mechanism

The saturation behavior of gate open time with internal [Cl^-], implies that as the internal [Cl^-] increases, the S_{ext} site of the channel pore is occupied to an increasing extent at any particular time by a Cl^- ion, thus preventing the gate from occupying the same site, i.e., closing. This is the essence of the foot-in-the-door mechanism. Saturation of the gate open time is then exerted to be correlated directly with saturation of the occupation probability (i.e., fractional occupation time) of the S_{ext} site by Cl^- ions, which is anticipated on the basis of chemical kinetics principles when there is an intermediate state which becomes "clogged" as more an more particles are forced to traverse the reaction pathway. To quantify these ideas in the context of the present model of coupled gate particle/ion motion, we can think of the "bare" escape rate along the 1D reaction

coordinate traversed by the gate particle as providing the rate of successful traversal of the reaction barrier. For a metastable 1D potential well, any particle that makes it over the barrier is captured in the product state (assuming that the product well is replaced by a probability sink), corresponding in our system to a gate closing event. However, in the full model under investigation here, in which gate closing is coupled to ion permeation through the channel pore, some of the barrier crossing events described above will be blocked by the presence of a Cl^- ion in the product well region. This will cause the observed closing rate to be reduced from the value given by Kramer's escape rate constant, roughly by a factor of $(1-f_{S_{ext}}(c))$, where $f_{S_{ext}}(c)$ is the fractional occupation probability that the S_{ext} site is occupied by a Cl^- ion, which is in turn a function of the internal chloride concentration $c=[Cl^-]_{int}$. With increasing c, $f_{S_{ext}}(c)$ saturates to some maximum value less than unity, and thus the observed gate closing rate saturates to a corresponding minimum value. Furthermore, it is reasonable to expect that the function $f_{S_{ext}}(c)$ will be largely independent of the dynamics of the gate particle in its open state, because in this configuration the gate particle is relatively far away from the channel pore and the S_{ext} site in particular. If all the elements of the scenario just described are valid, then the exact values of the activation barrier and diffusion constants of the reaction coordinate for the gate particle are not critical for describing the dependence of gate closing time on internal $[Cl^-]$, in the sense that this curve scales proportionally to Kramer's k_{esc}, and the scaling of k_{esc} with details of the gate particle reaction coordinate is well-understood (cf. Eq. 4.9). In the following section, we examine the validity of this mechanistic factorization scheme by carrying out appropriate numerical simulation studies on our model system.

4.4.6 Factorized model for gate closure mechanism

We compared results of gate open time calculated using DMC method with the simple factorized mechanism. In this model the gate open time is related to occupation probability of Cl^- in the external binding site according to:

$$\tau_o(c) = \tau_{o,0}/(1-f_{S_{ext}}(c)), \tag{4.11}$$

where $\tau_{o,0} = 1/k_{esc}$ is the gate open time without Cl^- in the system. In practice $f_{S_{ext}}(c)$ was calculated from DMC simulations by integrating the average number of Cl^- ions occupying the positions $\left|z_{Cl^-} - z_{S_{ext}}\right| \le R_{gate}$ where z_{Cl^-} is the z coordinate of Cl^- center, $z_{S_{ext}}$ is z coordinate of the center of the external binding site, and R_{gate} is the radius of the gate particle. $f_{S_{ext}}(c)$ saturated to the maximum value of 0.72 at internal $[Cl^-]$=2.02 M. The dependence of the ion density inside the channel system on internal $[Cl^-]$ is shown in Figure 36. Gate open times calculated directly from full all-ion plus gate potential DMC simulations are compared with factorized mechanism in Figure 37. Reasonable agreement is found.

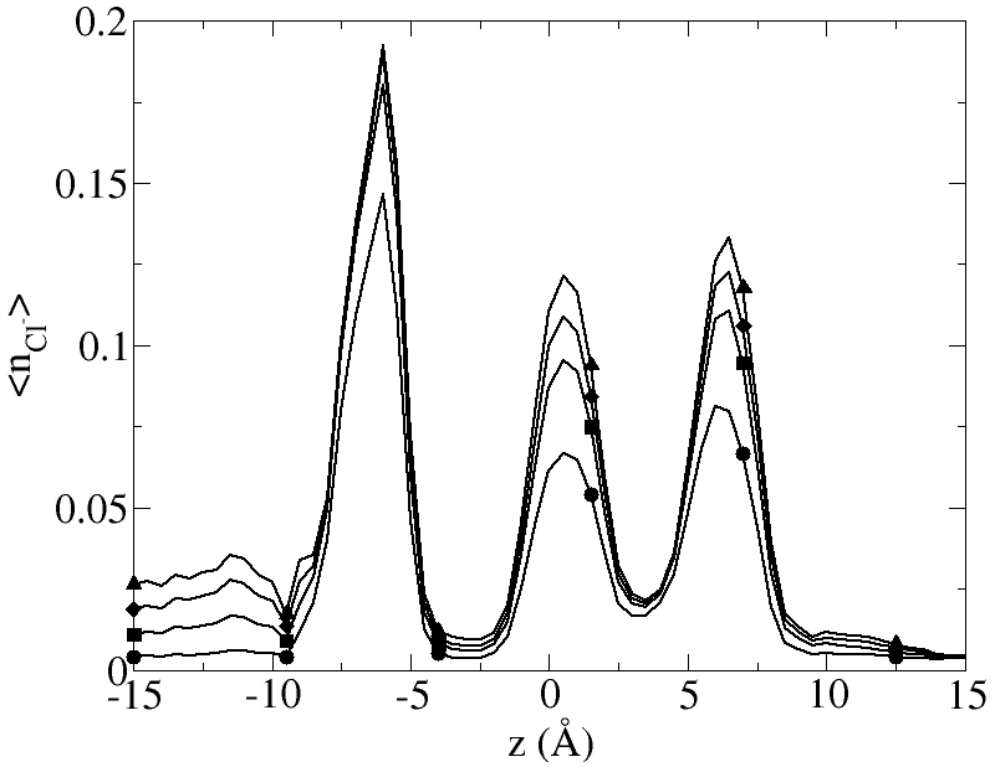

Figure 36. The average number of Cl^- ions along the channel axis for several different internal Cl^- concentrations calculated using DMC for parameter Set 6 (Table 11).

Internal [Cl^-] was set to 0.135 M (circles), 0.54 M (squares), 1.0 M (diamonds) and 2.02 M (triangles). The same external electric potential of -100 mV was used for all concentration calculations. Similar profiles were observed in other parameter sets.

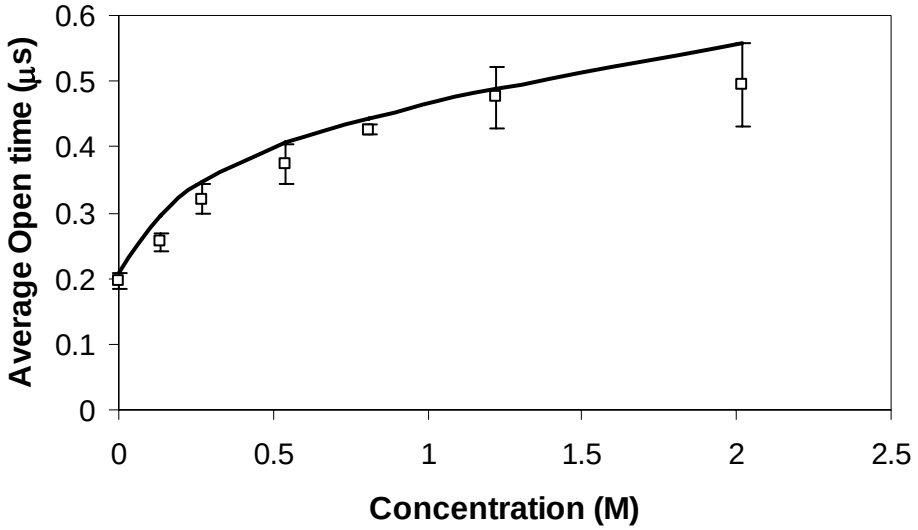

Figure 37. Dependence of gate open time on the internal [Cl^-] for neural gate and parameter Set 8 (Table 11). Results of DMC simulations (open squares) are compared with analytical model using Eq. 4.11 (solid line).

4.5 CONCLUSIONS

We have constructed a simplified three-dimensional model channel that mimics the ClC channel in several important respects regarding geometry, energetics and position/function of the fast gate. Using a Dynamic Monte Carlo simulation technique, we calculated the dependence of the gate closing rate on both internal Cl^- concentration (holding the external Cl^- concentration fixed) and external Cl^- concentration (holding the internal Cl^- concentration fixed). Our simulation results show saturation of the gate open time with the increase of the internal [Cl^-], in qualitative agreement with experiments [74, 75]. External [Cl^-] concentration also regulates the fast gate, but the effect is less prominent on the closing rate of the fast gate. This saturation behavior is consistent with the foot-in-the-door mechanism and would be predicted by our simple kinetic model embodied by Eq. 4.11.

The work presented here suggests future avenues of research on fast-gating in ClC channels that can focus on both more molecular detail and less. In the direction of increased molecular detail, our representation of the E148 as a "ball on a stick" is clearly an

oversimplification. The glutamate side chain is a complicated and somewhat flexible molecular group, whose understanding would profit from careful study via all-atom equilibrium MD simulation the range of conformations accessible to the E148 side chain. Computations of the PMF as a function of one coordinate (dihedral angle 1) and two coordinates (dihedral angles 1 and 2) would help to illuminate the energetic and mechanistic pathways by which the fast gate closes.

It would also be instructive to proceed in the direction of reduced atomic resolution, by taking advantage of the three deep minima ("binding sites") that characterize the single-particle potential seen by permeating Cl^- ions to make a discrete-state model governed by kinetic master equations that can be solved efficiently via kinetic Monte Carlo, or by more deterministic (matrix-based) analysis. This reduction is motivated by the observation that even the minimalist 3D Brownian Dynamics model developed in the present work strains available computational resources. To develop conceptual understanding of the mechanisms of fast-gate coupled ion permeation in ClC-type channels, it would be useful to have a mathematical model which enables rapid understanding of the relation between input parameters (e.g., concentration of ions in the reservoirs, depth of binding sites, relative time scale of motion of ion motion through the channel vs. that of the open/close transition of the gate particle coordinate, etc.) and output (ion currents, gating times, etc.). The well-defined binding sites of the narrow channel suggest a 3-site model for ions in the channel – each site can be occupied by zero or one ion. In addition, the gate particle has two stable states (open and closed), and makes transitions between these. The closed state of the gate particle corresponds to the same geometric site as the S_{ext} binding site. With this effective state space, use of kinetic Monte Carlo simulation or Markov chain theory could be carried out with relative ease. As is clear from the results presented in this paper, 3D BD simulations of ion permeation with the additional fast gating coordinate can only be run for 10's of microseconds, which is not even enough time to monitor the initial closing of a channel started in the open state, let alone to follow multiple opening and closing transitions. By contrast, a discrete state model can easily yield this information and hence the distribution of opening and closing times (from which the mean dwell time can be extracted). Of course, one needs to input rate constants that connect various pairs of states in the state space, which will be difficult to obtain from first principles. However, all-atom simulations of PMF's should be able

to provide effective activation barriers, etc., which will hopefully allow estimation of these critical input parameters.

5.0 WATER AND DEUTERIUM OXIDE PERMEABILITY THROUGH AQUAPORIN 1: MD PREDICTION AND EXPERIMENTAL VERIFICATION

Mamonov, A. B., R. D. Coalson, M. L. Zeidel, and J. C. Mathai. Manuscript in preparation.

5.1 ABSTRACT

Osmotic (p_f) and diffusion (p_d) permeabilities of H_2O and D_2O in Aquaporin 1 (AQP1) were calculated using Molecular Dynamics (MD) simulations and subsequently, the osmotic permeabilities of H_2O and D_2O were measured experimentally. For MD simulations the force field parameters of D_2O model were reparameterized from the TIP3P water model to reproduce the experimentally observed difference in the bulk self diffusion constant between H_2O and D_2O. Two MD systems (one for each solvent) were constructed, each containing explicit palmitoyl-oleoyl-phosphatidyl-ethanolamine (POPE) phospholipid molecules, solvent and AQP1. It was found that the calculated p_f and p_d are similar for H_2O and D_2O along with large error bars. Bovine AQP1 was reconstituted into palmitoyl-oleoyl-phosphatidylcholine (POPC) liposomes and it was found that the measured osmotic permeability of D_2O is *ca.* 21 % lower than for H_2O. The combined computational and experimental results suggest that deuterium oxide permeability through AQP1 is similar to that of water. The slightly lower osmotic permeability of D_2O compared to H_2O in AQP1 is most likely due to the lower self diffusion constant of D_2O.

5.2 INTRODUCTION

Aquaporins belong to a family of membrane proteins that passively transport water, glycerol and other small molecules [165]. The archetypical water channel AQP1 has been shown to be highly specific for water and excludes protons, ammonia and sugars such as glycerol [166, 167]. The specificity of the channel arises from the presence of two highly conserved NPA motifs (asn-pro-ala residues) that form the narrow constriction of the pore region, which acts as a molecular sieve. Crystallographic studies suggest that the pore is narrow at the constriction and lets only water diffuse through it [168, 169]. Molecular dynamics simulation studies suggest the presence of another energy barrier that offers both steric and electrostatic selectivity, named the aromatic (ar/R) constriction, which is formed by the following four amino acids: Phe-56, His-180, Cys-189 and Arg-195 (rat AQP1) in water selective aquaporins [170-172]. In aquaglyceroporins this constriction region is wider, as His-180 is usually replaced by Gly which allows for water and glycerol to pass through as shown in GlpF [173]. The positively charged arginine residue is thought to prevent the passage of protons through the channel while allowing water molecules to traverse it [174, 175].

To assess whether such a finely tuned channel allows the passage of deuterium oxide (D_2O), a close analogue of water, we measured the permeability of D_2O in AQP1 reconstituted proteoliposomes. D_2O differs from H_2O in the following respects: D_2O is more polar, has a stronger O-D bond compared to O-H and exhibits a higher viscosity [88]. Further, its self diffusion coefficient is 18.6 % lower than that of water [176]. Since water is thought to interact with specific residues Phe-56 and Agr-195 in the pore via hydrogen bonding [174], it would be interesting to study the passage of D_2O which has a stronger hydrogen bond. In addition, to check the predictive power of molecular dynamics simulations, we computed the osmotic permeability of deuterium oxide through AQP1 by MD simulations and compared it to experimental results. Both MD simulations and experimental results suggest that D_2O and H_2O permeate AQP1 at similar rates.

5.3 METHODS

5.3.1 MD simulations

Molecular Dynamics (MD) simulations were used to calculate the diffusion and osmotic permeability of H_2O and D_2O through AQP1. The X-ray structure of bovine AQP1 was downloaded from the Protein Data Bank (www.rcsb.org) with pdb code 1J4N [168]. The tetrameric structure was assembled from the coordinates of the monomer using transformation matrices provided in the pdb file. The tetramer was then embedded in a pre-equilibrated patch of 177 palmitoyl-oleoyl-phosphatidyl-ethanolamine (POPE) molecules and solvated by 15,079 CHARMM modified TIP3P water molecules [177, 178] (referred to here as TIP3P), so that the total system contained 80,434 atoms. This system was energy minimized and equilibrated for 3 ns at 298 K and 1 atm. To construct the AQP1/D_2O system, the TIP3P water model was replaced with a TIP3P-HW model (described below) and equilibrated for 1 ns at 298 K and 1 atm.

Diffusion permeabilities were calculated for both AQP1/H_2O and AQP1/D_2O systems from *ca.* 40 ns equilibrium MD simulations at constant volume and constant temperature of 298 K. A weak harmonic restraining potential of 0.12 kcal/mol/Å^2 was applied in all 3 dimensions to AQP1 backbone alpha carbons to prevent the protein form drifting. Diffusion permeability was calculated using the following equation [66]:

$$p_d = \frac{V_W}{N_A} q_0 = v_w q_0 , \tag{5.1}$$

where p_d is the diffusion permeability, V_W is the molar volume of the solvent, N_A is the Avogadro's number, q_0 is the unidirectional permeation rate and v_w is the volume of a single solvent molecule. q_0 was calculated by counting the number of H_2O or D_2O molecules passing from one side to the other of the channel per unit time. The pore region was chosen to be the narrow central section of the channel, 22 Å in length, where water molecules pass in single file or nearly single file fashion.

Osmotic permeabilities were calculated by following the non-equilibrium MD method described in Ref. [66]. A hydrostatic pressure gradient was established across the membrane by applying extra force to a layer of solvent molecules parallel to the membrane interface. Applied

pressure MD simulations of different time length were carried out at 50 MPa and 100 MPa for AQP1/H_2O system and at 25 MPa, 50 MPa, 100 MPa and 200 MPa for AQP1/D_2O system. A force of 0.013445 kcal/mol/Å, 0.02689 kcal/mol/Å, 0.05378 kcal/mol/Å and 0.10756 kcal/mol/Å was applied to oxygen atoms of H_2O/D_2O within an 8 Å solvent layer to generate 25 MPa, 50 MPa, 100 MPa and 200 MPa pressure, respectively. To prevent the protein and the lipid bilayer from moving under the influence of this external force a harmonic restraint of 0.12 kcal/mol/Å^2 was applied in all 3 dimensions to the backbone alpha carbons of the protein and a harmonic restraint of 0.8 kcal/mol/Å^2 was applied to the phosphorus atoms of the POPE molecules. The net flux of H_2O/D_2O through AQP1 was calculated by averaging the number of molecules that crossed 3 planes located 5 Å away from each other inside the channel per monomer per unit time. Osmotic permeabilities were calculated from the best fit slope line of H_2O/D_2O flux versus applied hydrostatic pressure according to the following equation [66]:

$$p_f = \frac{j}{\Delta P} RT \,, \tag{5.2}$$

where p_f is the osmotic permeability, j the solvent flux, ΔP the applied hydrostatic pressure, R the ideal gas constant, and T the absolute temperature.

For MD simulations we used the CHARMM 27 force field [179] that was derived to be consistent with the TIP3P model [178]. For the parameterization of deuterium oxide we started with the TIP3P model as a reference, doubled the mass of the hydrogen atoms and adjusted the partial charges of both the deuterium and oxygen atoms. It is well known that TIP3P water considerably overestimates (by more than a factor of 2) the self diffusion constant of water [180, 181]. That is why as a target for parameterization we have chosen to reproduce the experimentally measured 18.6 % difference in the self diffusion constants of H_2O vs. D_2O [176] rather than the experimental self diffusion constant of heavy water. A similar re-parameterization of the SPC/E model for deuterium oxide has been reported recently in which only the mass and partial charges of hydrogen atoms where changed in order to reproduce the experimental self diffusion constant, the molar volume and the potential energy of heavy water[182]. For our re-parameterization a simulation box of 3921 TIP3P water molecules was constructed, minimized and equilibrated at 298 K and 1 atm. The mass of hydrogen atoms was set to 2 amu and atomic partial charges were incremented by fractions of a percent. The system was equilibrated for 0.5 ns followed by 1 ns production runs carried out at a constant temperature of 298 K and a constant

pressure of 1 atm. The self diffusion constant was calculated from the collected coordinate time series using the mean-square-displacement (MSD) method [183]. Adjustment of D_2O atomic partial charges along with recalculation of self diffusion constant was repeated until we generated a diffusion coefficient *ca*. 18 % smaller than the value obtained with TIP3P under the same conditions.

All MD simulations were carried out using the NAMD package [184] version 2.5. For long range electrostatics the Particle Mesh Ewald method [185] was used as implemented in the NAMD program along with periodic boundary conditions. The MD time step was set to 2 fs and all the bonds between each hydrogen atom and its mother atom were fixed via the SHAKEH algorithm [184] to the nominal bond length given in the parameter file. MD coordinates of AQP1 simulations were saved every 1 ps and for the parameterization of TIP3P-HW water model every 100 fs. Most simulations were carried out on Lemieux supercomputer at the Pittsburgh Supercomputing Center (www.psc.edu). It took *ca.* 4.6 hours to run 1 ns of AQP1 simulations on 160 CPUs of Lemieux. All visualizations and analysis of MD trajectories were made with the VMD program[186].

5.3.2 Reconstitution of AQP1 into liposomes.

Purified bovine AQP1 was a kind gift from Dr. Jan J. Enghild and Dr. Niels Chr. Nielsen, University of Aarhus, Denmark. The AQP 1 reconstitution procedure was similar to that described earlier [167]. Briefly, 6-8 mg of POPC lipids (Avanti lipids, Alabama) was bath sonicated for 3 cycles of 3 min duration at 4 mW setting in 20 mM MOPS, pH 7.4. N-Octylglucoside (OG) was added to the sonicated lipids to achieve a final concentration of 1.2% (v/v). To this, 50-60 µg of AQP1 in 1.5 % OG was added and incubated for 30 minutes on ice. The mixture was diluted 25 fold into reconstitution buffer (150 mM NaCl, 20 mM MOPS pH 7.4) containing 10 mM carboxyfluorescein (CF). The proteoliposomes formed were collected by centrifugation at 100,000xg for 1 hour. The external CF was removed by 2 additional centrifugal washes. The final pellet was resuspended in 300 µl of reconstitution buffer and used for permeability studies.

5.3.3 Measurement of osmotic water permeability.

Osmotic H_2O and D_2O permeabilities were measured as described earlier [167]. Briefly, the proteoliposomes were subjected to a doubling of external osmotic pressure in a stopped-flow fluorimeter (Applied Photophysics, SX.17 MV, Leatherhead, United Kingdom) and the fluorescence decrease of CF due to self quenching caused by shrinkage of the vesicle was measured as a function of time. The data were fit using a single exponential function. P_f was calculated by comparing the single-exponential time constants fitted to a family of numerically integrated curves generated using the water permeability equation in which P_f was varied to that obtained experimentally. MathCad was used to simulate the water permeability equation:

$$\frac{dV_r(t)}{dt} = P_f \times r_{SV} \times V_w \times \left(\frac{C_{in}}{V_r(t)} - C_{out} \right). \tag{5.3}$$

In Eq. 5.3, $V_r(t)$, is the relative volume of the vesicle at time t, (i.e., volume at time t, divided by the initial volume), P_f (cm/s) is the osmotic water permeability coefficient, r_{SV} is the surface area to volume ratio of a vesicle; C_{in} and C_{out} are initial solute concentrations inside and outside the vesicle respectively. The size of the vesicles was measured by laser light scatter using a DynaPro particle sizer.

5.4 RESULTS AND DISCUSSION

Earlier studies prior to discovery of aquaporins showed that permeation of D_2O across erythrocytes and red cell ghosts was mercury inhibitable [187, 188]. However, mercurial compounds are nonspecific and do not inhibit the AQP1 channel completely [166]. In teleost and elasmobronchs, gill vesicle preparations when treated with mercury do not behave as an ideal osmometer, which renders them unsuitable for volume measurements (personal observations). In this study we have performed a quantitative permeability measurement using purified AQP1, reconstituted into proteoliposomes, which eliminates the background permeability due to other proteins [189, 190]. Figure 38 shows the time course of relative volume change of liposomes on application of an osmotic gradient, causing the efflux of H_2O (Figure 38A) or D_2O (Figure 38B).

It was found that the measured osmotic permeability of D_2O ($1.8x10^{-2}\pm 0.42x10^{-2}$ cm/s) is *ca.* 21% lower than that for H_2O ($2.3x10^{-2}\pm0.31x10^{-2}$ cm/s). This difference in permeability can be attributed to higher viscosity and lower self diffusion coefficient of D_2O of 18.6 % compared to water [176]. In red blood cells, prior to discovery of aquaporins, the decreased permeability of D_2O was attributed to higher viscosity of D_2O [188]. A similar decrease of ion conductance through Gramicidin in D_2O was also attributed to higher viscosity of D_2O [191]. The osmotic permeabilities of H_2O and D_2O through POPC lipid vesicles were 0.0032 cm/s and 0.0034 cm/s respectively.

The force field parameters of our TIP3P-HW (D_2O) model are summarized in Table 12. In MD simulations the TIP3P-HW was characterized by b bulk diffusion coefficient of $4.00x10^{-5}$ cm^2/s, which is 18.7 % smaller than that of the TIP3P model of water ($4.92x10^{-5}$ cm^2/s). This difference is in good agreement with the 18.6 % difference between H_2O and D_2O measured experimentally [176]. The densities of TIP3P and TIP3P-HW models were found to be 1.00 g/cm^3 and 1.13 g/cm^3 respectively. This is also in a good agreement with experimental densities of 0.997 g/cm^3 for H_2O and 1.104 g/cm^3 for D_2O [192]. These solvent models were subsequently used to calculate the osmotic and diffusion permeabilities of H_2O and D_2O in AQP1.

A snapshot of the AQP1/H_2O system from the equilibrium MD trajectory is illustrated in Figure 39, with only one monomer and channel shown for the sake of clarity. The single file arrangement and dipole rotation of water which are unique properties of AQP family [63, 78] are correctly reproduced in our simulations. The concentration profile of H_2O across the channel system at equilibrium conditions is compared with that obtained at 100 MPa applied hydrostatic pressure in Figure 40. When hydrostatic pressure was applied the concentration of water became slightly higher on the left side and lower on the right side of the membrane due to the compressibility of water. The main results of our equilibrium MD simulations for H_2O and D_2O are summarized in Table 13. The unidirectional permeation rate (q_0) of H_2O was found to be 0.26, which is 30 % higher than the value predicted by another AQP study reported in Ref. [78]. This difference can be attributed to the fact that they used a different (lower resolution) structure of AQP1 and a different water model. Also, there is some uncertainty about where to assign planes that define when a water molecule crosses the channel from one side of the membrane to the other. We found that q_0 for D_2O is *ca.* 8 % higher than for H_2O. Furthermore, the error bars are large because we could not run much longer MD simulations.

Results of our osmotic pressure simulations are reported in Table 14 and Figure 41A for H_2O, and in Table 15 and Figure 41B for D_2O. We found that the osmotic permeability of D_2O (7.8×10^{-14} cm^3/s/monomer) is *ca.* 12 % lower than that of H_2O (8.2×10^{-14} cm^3/s/monomer). This difference compares well with the experimentally measured difference of *ca.* 21 %. The large error bars were found for MD results because of the limited MD sampling allowed by available computational resources. We could not compare the individual values of the osmotic permeabilities because of the experimental uncertainty in the number of channels per proteoliposome. The osmotic permeability of H_2O 8.2×10^{-14} cm^3/s/monomer obtained in our MD simulations is similar to that predicted by another MD study where a value of 7.1×10^{-14} cm^3/s/monomer was reported [66]. It also compares well with the experimentally measured unit osmotic conductance of $11.7 \times 10^{-14} \pm 1.8 \times 10^{-14}$ cm^3/s/monomer reported in Ref. [167]. Since water moves in a single file fashion through the AQP1 channel, the $\frac{p_f}{p_d}$ ratio should give the number of solute molecules lining the pore [193]. The calculated $\frac{p_f}{p_d}$ ratios for H_2O and D_2O are 10.5 and 9.3 respectively. The $\frac{p_f}{p_d}$ ratio of H_2O is in good agreement with 11.9 predicted in Ref. [66] and 13.2 measured experimentally [194].

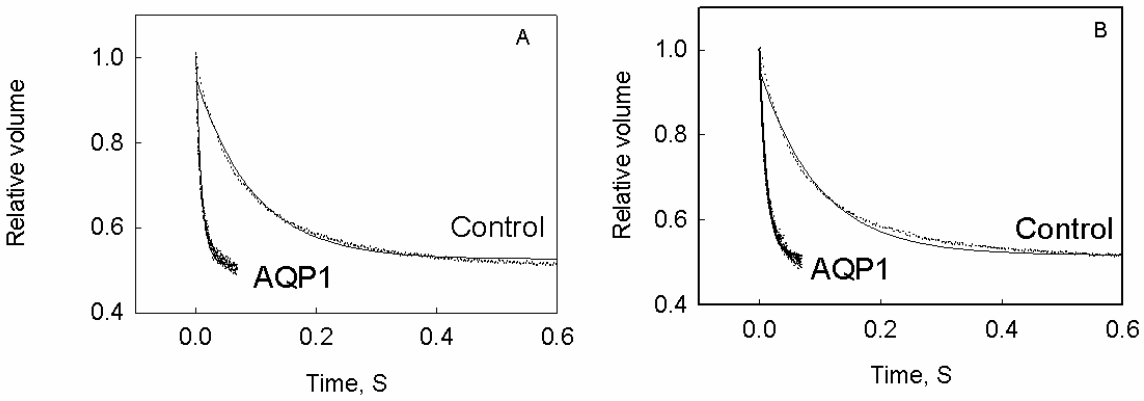

Figure 38. Osmotic permeability of H_2O and D_2O. Shown is the time course of relative volume (volume at time *t* divided by initial volume) change of AQP1 containing vesicles and control lipid vesicles on abrupt exposure to a doubling of external osmotic pressure in H_2O (A) and D_2O (B).

Table 12. Force field parameters of TIP3P-HW model.

$r_{\min}^{OO}$ (Å)	$r_{\min}^{DD}$ (Å)	ε^{OO} (kcal/mol)	ε^{DD} (kcal/mol)	q^{O} (e units)	q^{D} (e units)	b^{OD} (Å)	θ^{DOD} (deg)
3.5365	0.449	0.1521	0.046	-0.842	-0.421	0.9572	104.52

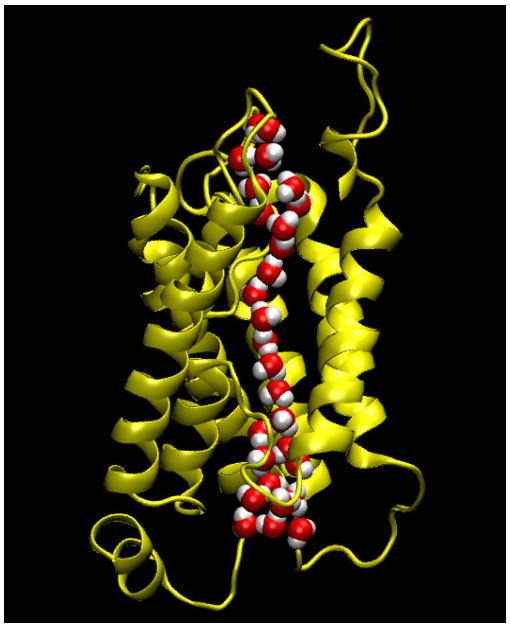

Figure 39. A snapshot from MD simulation of AQP1/H_2O system. Only one monomer and channel water is shown. Note the single file arrangement of water molecules inside the channel.

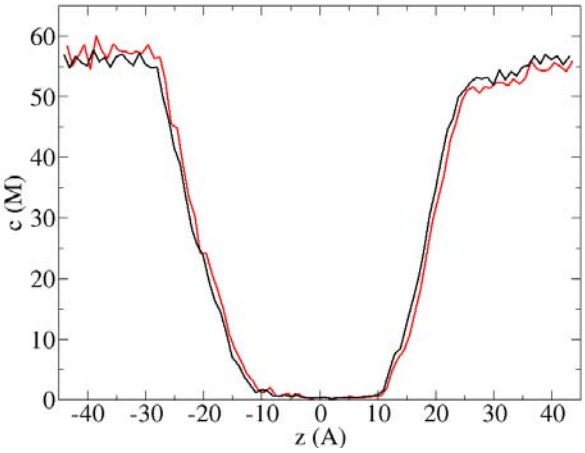

Figure 40. Concentration profile of H_2O along z axis (channel axis) at equilibrium conditions (black line) and 100 MPa applied hydrostatic pressure (red line). Note the low concentration region between approximately z=-11 Å and z=+11 Å: this is the "channel pore region" discussed in the text.

Table 13. Results of equilibrium MD simulations.

	Time (ns)	No. of permeations	q_0 (molecules/ns/monomer)	p_d x10^{15} (cm^3/s/monomer)
H_2O	21.6	46	0.26±0.05	7.8±1.5
D_2O	20.4	45	0.28±0.12	8.4±3.6

A B

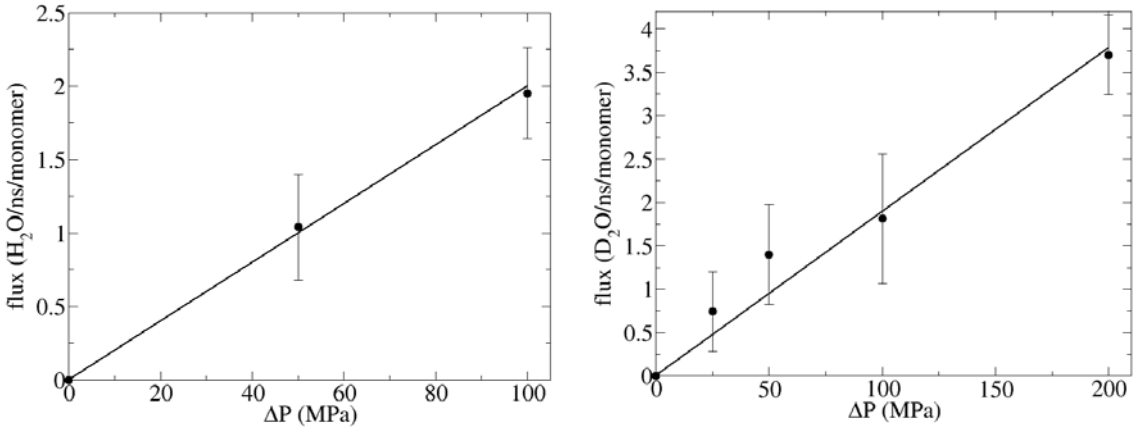

Figure 41. Flux versus applied hydrostatic pressure with error bars for H_2O (A) and D_2O (B). Circles represent the calculated (average) data point values, which are shown along with the best-fit line.

Table 14. Results of applied pressure MD simulations for H_2O.

Applied pressure (MPa)	Time (ns)	No. of H_2O permeations	flux (H_2O/ns/monomer)	p_f x10^{14} (cm^3/s/monomer)
50	22.85	92	1.04±0.40	8.2
100	21.87	171	1.95±0.30	

Table 15. Results of applied pressure MD simulations for D_2O.

Applied pressure (MPa)	Time (ns)	No. of D_2O permeations	flux (D_2O/ns/monomer)	p_f x10^{14} (cm^3/s/monomer)
25	7.0	20.6	0.74	7.8
50	22.25	126	1.41	
100	33.84	239	1.81	
200	10	147.3	3.68	

5.5 CONCLUSIONS

A new TIP3P-HW model for D_2O was developed for simulation of D_2O transport through AQP1. This model reproduces the experimental differences observed in density and the self diffusion coefficient between H_2O and D_2O. Both MD simulations and experimental measurements confirm that D_2O and H_2O permeate the AQP1 channel. The observed lower permeability of D_2O is attributed to the lower self diffusion coefficient and higher viscosity of D_2O compared to H_2O. Our study showed that MD could accurately predict the permeability properties of D_2O in AQP1 in advance of experimental measurements. This study will be helpful for designing MD

simulations to study permeation of solutes through AQP1 that are not easily amenable to experiments such as carbon dioxide, hydrogen sulfide and oxygen.

5.6 ACKNOWLEDGMENTS

The authors acknowledge computer time provided by PSC grant MCB030021P. MLZ and JCM are supported by a grant from NIH, DK 43955. We would like to thank Zuzana Valnickova, Jan Enghild, Niels Chr. Nielsen, and Astrid C. Sivertsen for AQP1 purification.

BIBLIOGRAPHY

1. Hille, B., *Ion channels of excitable membranes*. 2001, Sunderland. Sinauer Associates, Inc.
2. Jordan, P.C., *Fifty years of progress in ion channel research.* IEEE Trans. Nanobioscience, 2005. 4: p. 3-9.
3. Cole, K.S., *Dynamic electrical characteristics of the squid axon membrane.* Arch. Sci. Physiol, 1949. 3: p. 253-258.
4. Hodgkin, A.L., A.F. Huxley, and B. Katz, *Ionic currents underlying activity in the giant axon of the squid.* Arch. Sci. Physiol, 1949. 3: p. 129-150.
5. Hodgkin, A.L. and A.F. Huxley, *Currents carried by sodium and potassium ions through the membrane of the giant axon of Loligo.* J. Physiol. (Lond.), 1952. 116: p. 449-472.
6. Hodgkin, A.L. and A.F. Huxley, *The components of membrane conductance in the giant axon of Loligo.* J. Physiol. (Lond.), 1952. 116: p. 473-496.
7. Hodgkin, A.L. and A.F. Huxley, *A quantitative description of membrane current and its application to conduction and excitation in nerve.* J. Physiol. (Lond.), 1952. 117: p. 500-544.
8. Narahashi, T., J.M. Moore, and W.R. Scott, *Tetrodotoxin blockage of sodium conductance increase in lobster giant axon.* J. Gen. Physiol., 1964. 47: p. 965-974.
9. Armstrong, C.M. and L. Binstock, *Anomalous rectification in the squid giant axon injected with tetraethylammonium chloride.* J. Gen. Physiol., 1965. 48: p. 859-872.
10. Hladky, S.B. and D.A. Haydon, *Ion transfer across lipid membranes in the presence of Gramicidin A. I. Studies of the unit conductance channel.* Biochim. Biophys. Acta., 1972. 274: p. 294-312.
11. Neher, E. and B. Sakmann, *Single-channel currents recorded from membrane of denervated frog muscle fibers.* Nature, 1976. 260: p. 799-802.
12. Hamill, O.P., A. Marty, E. Neher, B. Sakmann, and F.J. Sigworth, *Improved patch-clamp techniques for high-resolution current recording from cells and cell-free membrane patches.* Pflugers Arch., 1981. 391: p. 85-100.
13. Noda, M., H. Takahashi, T. Tanabe, M. Toyosato, Y. Furutani, T. Hirose, M. Asai, S. Inayama, T. Miyata, and S. Numa, *Primary structure of alpha-subunit precursor of Torpedo californica acetylcholine receptor deduced from cDNA sequence.* Nature, 1982. 299: p. 793-797.
14. Chou, P.Y. and G.D. Fasman, *Empirical predictions of protein conformation.* Annu. Rev. Biochem., 1978. 47: p. 251-276.

15. Hopp, T.P. and K.R. Woods, *Prediction of protein antigenic determinants from amino acid sequences.* Proc. Natl. Acad. Sci. U. S. A., 1981. 78: p. 3824-3828.
16. Noda, M., H. Takahashi, T. Tanabe, M. Toyosato, S. Kikyotani, Y. Furutani, T. Hirose, H. Takashima, S. Inayama, T. Miyata, and S. Numa, *Structural homology of Torpedo californica acetylcholine receptor subunits.* Nature, 1983. 302: p. 528-532.
17. Imoto, K., C. Busch, B. Sakmann, M. Mishina, T. Konno, J. Nakai, H. Bujo, Y. Mori, K. Fukuda, and S. Numa, *Rings of negatively charged amino acids determine the acetylcholine receptor channel conductance.* Nature, 1988. 335: p. 645-648.
18. Arseniev, A.S., I.L. Barsukov, V.F. Bystrov, A.L. Lomize, and A. Ovchinnikov Yu, *1H-NMR study of gramicidin A transmembrane ion channel. Head-to-head right-handed, single-stranded helices.* FEBS Lett., 1985. 186: p. 168-174.
19. Doyle, D.A., J. Morais Cabral, R.A. Pfuetzner, A. Kuo, J.M. Gulbis, S.L. Cohen, B.T. Chait, and R. MacKinnon, *The structure of the potassium channel: molecular basis of K+ conduction and selectivity.* Science, 1998. 280: p. 69-77.
20. Dutzler, R., E.B. Campbell, M. Cadene, B.T. Chait, and R. MacKinnon, *X-ray structure of a ClC chloride channel at 3.0 A reveals the molecular basis of anion selectivity.* Nature, 2002. 415: p. 287-294.
21. Miller, C. and M.M. White, *A voltage-dependent chloride conductance channel from Torpedo electroplax membrane.* Ann. N. Y. Acad. Sci., 1980. 341: p. 534-551.
22. Orlova, E.V. and H.R. Saibil, *Structure determination of macromolecular assemblies by single-particle analysis of cryo-electron micrographs.* Curr. Opin. Struct. Biol., 2004. 14: p. 584-590.
23. Miyazawa, A., Y. Fujiyoshi, and N. Unwin, *Structure and gating mechanism of the acetylcholine receptor pore.* Nature, 2003. 423: p. 949-955.
24. Ludtke, S.J., I.I. Serysheva, S.L. Hamilton, and W. Chiu, *The pore structure of the closed RyR1 channel.* Structure, 2005. 13: p. 1203-1211.
25. Wolf, M., A. Eberhart, H. Glossmann, J. Striessnig, and N. Grigorieff, *Visualization of the domain structure of an L-type Ca2+ channel using electron cryo-microscopy.* J. Mol. Biol., 2003. 332: p. 171-182.
26. Sato, C., Y. Ueno, K. Asai, K. Takahashi, M. Sato, A. Engel, and Y. Fujiyoshi, *The voltage-sensitive sodium channel is a bell-shaped molecule with several cavities.* Nature, 2001. 409: p. 1047-1051.
27. Korn, S.J. and J.G. Trapani, *Potassium channels.* IEEE Trans. Nanobioscience, 2005. 4: p. 21-33.
28. Andersen, O.S., R.E. Koeppe, and B. Roux, *Gramicidin channels.* IEEE Trans. Nanobioscience, 2005. 4: p. 10-20.
29. Im, W. and B. Roux, *Ion permeation and selectivity of OmpF porin: A theoretical study based on molecular dynamics, brownian dynamics, and continuum electrodiffusion theory.* J. Mol. Biol., 2002. 322: p. 851-869.
30. Agre, P. and D. Kozono, *Aquaporin water channels: molecular mechanisms for human diseases.* FEBS Lett., 2003. 555: p. 72-78.
31. Preston, G.M. and P. Agre, *Isolation of the cDNA for erythrocyte integral membrane protein of 28 kilodaltons: member of an ancient channel family.* Proc. Natl. Acad. Sci. U. S. A., 1991. 88: p. 11110-11114.
32. Preston, G.M., T.P. Carroll, W.B. Guggino, and P. Agre, *Appearance of water channels in Xenopus oocytes expressing red cell CHIP28 protein.* Science, 1992. 256: p. 385-387.

33. Benga, G., *Birth of water channel proteins-the aquaporins.* Cell Biol. Int., 2003. 27: p. 701-709.
34. King, L.S., D. Kozono, and P. Agre, *From structure to disease: the evolving tale of aquaporin biology.* Nat. Rev. Mol. Cell Biol., 2004. 5: p. 687-698.
35. Parsegan, A., *Energy of an ion crossing a low dielectric membrane: Solutions to four relevant electrostatic problems.* Nature, 1969. 221: p. 844-846.
36. Levitt, D.G., *Electrostatic calculations for an ion channel. I. Energy and potential profiles and interactions between ions.* Biophys. J., 1978. 22: p. 209-219.
37. Cooper, K., E. Jakobsson, and P. Wolynes, *The theory of ion transport through membrane channels.* Prog. Biophys. Molec. Biol., 1985. 46: p. 51-96.
38. Lauger, P., *Ion transport through pores: A rate-theory analysis.* Biochim. Biophys. Acta., 1973. 311: p. 423-441.
39. Crozier, P.S., D. Henderson, R.L. Rowley, and D.D. Busath, *Model channel ion currents in NaCl-extended simple point charge water solution with applied-field molecular dynamics.* Biophys. J., 2001. 81: p. 3077-3089.
40. Crozier, P.S., R.L. Rowley, N.B. Holladay, D. Henderson, and D.D. Busath, *Molecular dynamics simulation of continuous current flow through a model biological membrane channel.* Phys. Rev. Lett., 2001. 86: p. 2467-2470.
41. Nernst, W., *Zur kinetik der in losung befindlichen korper: theorie der diffusion.* Z. Phys. Chem., 1888. 4: p. 613-637.
42. Planck, M., *Ueber die erregung von elektricitat und warme in elektrolyten.* Ann. Phys. Chem., Neue. Folge., 1890. 39: p. 161-186.
43. Goldman, D.E., *Potential, impedance, and rectification in membranes.* J. Gen. Physiol, 1943. 27: p. 37-60.
44. Hodgkin, A.L. and B. Katz, *The effect of sodium ions on the electrical activity of the giant axon of the squid.* J. Physiol. (Lond.), 1949. 108: p. 37-77.
45. de Levie, R., N.G. Seidah, and H. Moreira, *Transport of ions of one kind through thin membranes. I. Nonequilibrium steady-state behavior.* J. Membr. Biol, 1972. 10: p. 171-192.
46. Levitt, D.G., *General continuum theory for multiion channel I. Theory.* Biophys. J., 1991. 59: p. 271-277.
47. Coalson, R.D. and M.G. Kurnikova, *Poisson-Nernst-Planck theory approach to the calculation of current through biological ion channels.* IEEE Trans. Nanobioscience, 2005. 4: p. 81-93.
48. Kurnikova, M.G., R.D. Coalson, P. Graf, and A. Nitzan, *A lattice relaxation algorithm for three-dimensional Poisson- Nernst-Planck theory with application to ion transport through the gramicidin A channel.* Biophys. J., 1999. 76: p. 642-656.
49. Corry, B., S. Kuyucak, and S.H. Chung, *Tests of continuum theories as models of ion channels. II. Poisson-Nernst-Planck theory versus Brownian dynamics.* Biophys. J., 2000. 78: p. 2364-2381.
50. Graf, P., A. Nitzan, M.G. Kurnikova, and R.D. Coalson, *A dynamic lattice Monte Carlo model of ion transport in inhomogeneous dielectric environments: Method and implementation.* J. Phys. Chem. B, 2000. 104: p. 12324-12338.
51. Miloshevsky, G.V. and P.C. Jordan, *Permeation in ion channels: the interplay of structure and theory.* Trends in Neurosciences, 2004. 27: p. 308-314.

52. Kramers, H.A., *Brownian motion in a field of force and the diffusion model of chemical reactions.* Physica, 1940. 40: p. 284-304.
53. Levitt, D.G., *Interpretation biological ion channel flux data-Reaction rate versus Continuum Theory.* Annu. Rev. Biophys. Biophys. Chem., 1986. 15: p. 29-57.
54. Ermak, D.L. and J.A. McCammon, *Brownian dynamics with hydrodynamic interactions.* J. Chem. Phys., 1978. 69: p. 1352-1360.
55. McQuarrie, D.A., *Statistical Mechanics*. 1976, New York. Harper & Collins.
56. Chung, S.H., M. Hoyles, T. Allen, and S. Kuyucak, *Study of ionic currents across a model membrane channel using Brownian dynamics.* Biophys. J., 1998. 75: p. 793-809.
57. Cheng, H.Y. and R.D. Coalson, *An accurate and efficient empirical approach for calculating the dielectric self-energy and ion-ion pair potential in continuum models of biological ion channels.* J. Phys. Chem. B, 2005. 109: p. 488-498.
58. Szabo, A. and N.S. Ostlund, *Modern Quantum Chemistry*. 1996, Mineola. Dover Publications, Inc.
59. Leach, A.R., *Molecular modelling. Principles and applications*. 2001, Dorchester. Pearson Education Limited.
60. Mackay, D.H.J., P.H. Berens, and K.R. Wilson, *Structure and dynamics of ion transport through Gramicidin A.* Biophys. J., 1984. 46: p. 229-248.
61. Cohen, J. and K. Schulten, *Mechanism of anionic conduction across ClC.* Biophys. J., 2004. 86: p. 836-845.
62. Aksimentiev, A. and K. Schulten, *Imaging alpha-hemolysin with molecular dynamics: Ionic conductance, osmotic permeability, and the electrostatic potential map.* Biophys. J., 2005. 88: p. 3745-3761.
63. Tajkhorshid, E., P. Nollert, M.O. Jensen, L.J. Miercke, J. O'Connell, R.M. Stroud, and K. Schulten, *Control of the selectivity of the aquaporin water channel family by global orientational tuning.* Science, 2002. 296: p. 525-530.
64. Berneche, S. and B. Roux, *Energetics of ion conduction through the K+ channel.* Nature, 2001. 414: p. 73-77.
65. Allen, T.W., O.S. Andersen, and B. Roux, *Energetics of ion conduction through the gramicidin channel.* Proc. Natl. Acad. Sci. U. S. A., 2004. 101: p. 117-122.
66. Zhu, F.Q., E. Tajkhorshid, and K. Schulten, *Theory and simulation of water permeation in aquaporin-1.* Biophys. J., 2004. 86: p. 50-57.
67. Roux, B. and M. Karplus, *Ion transport in a gramicidin-like channel: dynamics and mobility.* J. Phys. Chem., 1991. 95: p. 4856-4868.
68. Koneshan, S., R.M. Lynden-Bell, and J.C. Rasaiah, *Friction coefficients of ions in aqueous solution at 25 degrees C.* J. Am. Chem. Soc., 1998. 120: p. 12041-12050.
69. Chang, T.M. and L.X. Dang, *Detailed study of potassium solvation using molecular dynamics techniques.* J. Phys. Chem. B, 1999. 103: p. 4714-4720.
70. Koneshan, S., J.C. Rasaiah, and L.X. Dang, *Computer simulation studies of aqueous solutions at ambient and supercritical conditions using effective pair potential and polarizable potential models for water.* J. Chem. Phys., 2001. 114: p. 7544-7555.
71. LyndenBell, R.M. and J.C. Rasaiah, *Mobility and solvation of ions in channels.* J. Chem. Phys., 1996. 105: p. 9266-9280.
72. Allen, T.W., S. Kuyucak, and S.H. Chung, *Molecular dynamics estimates of ion diffusion in model hydrophobic and KcsA potassium channels.* Biophys. Chem., 2000. 86: p. 1-14.

73. Smith, G.R. and M.S.P. Sansom, *Effective diffusion coefficients of K+ and Cl- ions in ion channel models.* Biophys. Chem., 1999. 79: p. 129-151.
74. Chen, T.Y., M.F. Chen, and C.W. Lin, *Electrostatic control and chloride regulation of the fast gating of ClC-0 chloride channels.* J. Gen. Physiol., 2003. 122: p. 641-651.
75. Chen, T.Y. and C. Miller, *Nonequilibrium gating and voltage dependence of the ClC-0 Cl- channel.* J. Gen. Physiol., 1996. 108: p. 237-250.
76. Pusch, M., U. Ludewig, A. Rehfeldt, and T.J. Jentsch, *Gating of the voltage-dependent chloride channel CIC-0 by the permeant anion.* Nature, 1995. 373: p. 527-531.
77. Dutzler, R., E.B. Campbell, and R. MacKinnon, *Gating the selectivity filter in ClC chloride channels.* Science, 2003. 300: p. 108-112.
78. de Groot, B.L. and H. Grubmuller, *Water permeation across biological membranes: Mechanism and dynamics of aquaporin-1 and GlpF.* Science, 2001. 294: p. 2353-2357.
79. Mamonov, A.B., R.D. Coalson, J.C. Mathai, and M.L. Zeidel, *Manuscript in preparation.*
80. Andersen, O.S. and R.E. KoeppeII, *Molecular determinants of channel function.* Physiol. Rev., 1992. 72: p. S89-S158.
81. Dorman, V., M.B. Partenskii, and P.C. Jordan, *A semi-microscopic Monte Carlo study of permeation energetics in a gramicidin-like channel: The origin of cation selectivity.* Biophys. J., 1996. 70: p. 121-134.
82. Eisenberg, R.S., *From structure to function in open ionic channels.* J. Membr. Biol., 1999. 171: p. 1-24.
83. Hille, B., C.M. Armstrong, and R. MacKinnon, *Ion channels: From idea to reality.* Nature Med., 1999. 5: p. 1105-1109.
84. Roux, B., S. Berneche, and W. Im, *Ion channels, permeation, and electrostatics: Insight into the function of KcsA.* Biochemistry, 2000. 39: p. 13295-13306.
85. Kuyucak, S., O.S. Andersen, and S.H. Chung, *Models of permeation in ion channels.* Rep. Progr. Phys., 2001. 64: p. 1427-1472.
86. Nilius, B. and G. Droogmans, *Ion channels and their functional role in vascular endothelium.* Physiol. Rev., 2001. 81: p. 1415-1459.
87. Lerche, H., K. Jurkat-Rott, and F. Lehmann-Horn, *Ion channels and epilepsy.* Amer. J. Med. Genet., 2001. 106: p. 146-159.
88. Antonov, S.M., *Transporters of neurotransmitters: receptive, transport, and channel functions.* J. Evol. Biochem. Physiol., 2001. 37: p. 328-334.
89. Marban, E., *Cardiac channelopathies.* Nature, 2002. 415: p. 213-218.
90. Koprowski, P. and A. Kubalski, *Bacterial ion channels and their eukaryotic homologues.* Bioessays, 2001. 23: p. 1148-1158.
91. Allen, T.W., M. Hoyles, S. Kuyucak, and S.H. Chung, *Molecular and Brownian dynamics study of ion selectivity and conductivity in the potassium channel.* Chem. Phys. Let., 1999. 313: p. 358-365.
92. Cardenas, A.E., R.D. Coalson, and M.G. Kurnikova, *Three-dimensional Poisson-Nernst-Planck theory studies: Influence of membrane electrostatics on gramicidin A channel conductance.* Biophys. J., 2000. 79: p. 80-93.
93. Tieleman, D.P., P.C. Biggin, G.R. Smith, and M.S.P. Sansom, *Simulation approaches to ion channel structure-function relationships.* Q. Rev. Biophys, 2001. 34: p. 473-561.
94. Crozier, P.S., D. Henclerson, R.L. Rowley, and D.D. Busath, *Model channel ion currents in NaCl-extended simple point charge water solution with applied-field molecular dynamics.* Biophys. J., 2001. 81: p. 3077-3089.

95. Graf, P., M.G. Kurnikova, R.D. Coalson, and A. Nitzan, *Comparison of dynamic lattice Monte Carlo simulations and the dielectric self-energy Poisson-Nernst-Planck continuum theory for model ion channels.* J. Phys. Chem. B, 2004. 108: p. 2006-2015.
96. Corry, B., T.W. Allen, S. Kuyucak, and S.H. Chung, *Mechanisms of permeation and selectivity in calcium channels.* Biophys. J., 2001. 80: p. 195-214.
97. Chung, S.H., T.W. Allen, M. Hoyles, and S. Kuyucak, *Permeation of ions across the potassium channel: Brownian dynamics studies.* Biophys. J., 1999. 77: p. 2517-2533.
98. Im, W., S. Seefeld, and B. Roux, *A grand canonical Monte Carlo-Brownian dynamics algorithm for simulating ion channels.* Biophys. J., 2000. 79: p. 788-801.
99. Burykin, A., C.N. Schutz, J. Villá, and A. Warshel, *Simulations of ion current in realistic models of ion channels: the KcsA potassium channel.* Proteins: Struct., Funct., Genet., 2002. 43: p. 265-280.
100. Mashl, R.J., Y.Z. Tang, and J. Schnitzer, *Hierarchical approach to predicting permeation in ion channels.* Biophys. J., 2001. 81: p. 2473-2483.
101. Dieckmann, G.R., J.D. Lear, Q.F. Zhong, M.L. Klein, W.F. DeGrado, and K.A. Sharp, *Exploration of the structural features defining the conduction properties of a synthetic ion channel.* Biophys. J., 1999. 76: p. 618-630.
102. Roux, B. and M. Karplus, *Ion transport in the gramicidin channel: free-energy of the solvated right-handed dimer in a model membrane.* J. Am. Chem. Soc., 1993. 115: p. 3250-3262.
103. Mackay, D.H.J., P.H. Berens, K.R. Wilson, and A.T. Hagler, *Structure and dynamics of ion-transport through Gramicidin A.* Biophys. J., 1984. 46: p. 229-248.
104. Partenskii, M.B. and P.C. Jordan, *Theoretical perspectives of ion-channel electrostatics, continuum and microscopic approach.* Q. Rev. Biophys, 1992. 91: p. 477-510.
105. Berneche, S. and B. Roux, *Molecular dynamics of the KcsA K+ channel in a bilayer membrane.* Biophys. J., 2000. 78: p. 2900-2917.
106. Woolf, T.B. and B. Roux, *The binding site of sodium in the gramicidin A channel: Comparison of molecular dynamics with solid-state NMR data.* Biophys. J., 1997. 72: p. 1930-1945.
107. Barcilon, V., D.P. Chen, and R.S. Eisenberg, *Ion flow through narrow membrane channels: Part II.* SIAM J. Appl. Math., 1992. 53: p. 1405-1425.
108. Chen, D.P. and R.S. Eisenberg, *Charges, currents, and potentials in ionic channels of one conformation.* Biophys. J., 1993. 64: p. 1405-1421.
109. Chen, D.P. and R.S. Eisenberg, *Flux, coupling, and selectivity in ionic channels of one conformation.* Biophys. J., 1993. 65: p. 727-746.
110. Schuss, Z., B. Nadler, and R.S. Eisenberg, *Derivation of Poisson and Nernst-Planck equations in a bath and channel from a molecular model.* Phys. Rev. E, 2001. 64: p. 036116(1-14).
111. Sharp, K.A. and B.H. Honig, *Electrostatic interactions in macromolecules: theory and applications.* Ann. Rev. Biophys. Biophys. Chem., 1990. 19: p. 301-332.
112. Luty, B.A., M.E. Davis, and J.A. McCammon, *Solving the finite-difference non-linear Poisson-Boltzmann equation.* J. Comp. Chem., 1992. 13: p. 1114-1118.
113. Partenskii, M.B., V. Dorman, and P.C. Jordan, *Influence of a channel-forming peptide on energy barriers to ion permeation, viewed from a continuum dielectric perspective.* Biophys. J., 1994. 67: p. 1429-1438.

114. Kollman, P.A., I. Massova, C. Reyes, B. Kuhn, S.H. Huo, L. Chong, M. Lee, T. Lee, Y. Duan, W. Wang, O. Donini, P. Cieplak, J. Srinivasan, D.A. Case, and T.E. Cheatham, *Calculating structures and free energies of complex molecules: Combining molecular mechanics and continuum models.* Acc. Chem. Res., 2000. 33: p. 889-897.
115. Elber, R., D. Rojewska, D.P. Chen, and R.S. Eisenberg, *Sodium in Gramicidin - an example of a permion.* Biophys. J., 1995. 68: p. 906-924.
116. Roux, B. and S. Berneche, *On the potential functions used in molecular dynamics simulations of ion channels.* Biophys. J., 2002. 82: p. 1681-1684.
117. Vorobjev, Y.N. and J. Hermans, *ES/IS: Estimation of conformational free energy by combining dynamics simulations with explicit solvent with an implicit solvent continuum model.* Biophys. Chem., 1999. 78: p. 195-205.
118. Aqvist, J. and A. Warshel, *Energetics of ion permeation through membrane channels.* Biophys. J., 1989. 56: p. 171-182.
119. Roux, B. and R. MacKinnon, *The cavity and pore helices the KcsA K+ channel: Electrostatic stabilization of monovalent cations.* Science, 1999. 285: p. 100-102.
120. Doyle, D.A., J.M. Cabral, R.A. Pfuetzner, u. , A. , J.M. Gulbis, S.L. Cohen, B.T. Chait, and R. MacKinnon, *The structure of the potassium channel: Molecular basis of K^+ conduction and selectivity.* Science, 1998. 280: p. 69-77.
121. Cornell, W.D., P. Cieplak, C.I. Bayly, I.R. Gould, K.M. Merz, D.M. Ferguson, D.C. Spellmeyer, T. Fox, J.W. Caldwell, and P.A. Kollman, *A second generation force field for the simulation of proteins, nucleic acids, and organic molecules.* J. Am. Chem. Soc., 1996. 118: p. 2309-2309.
122. Aqvist, J., *Ion water interaction potentials derived from free-energy perturbation simulations.* J. Phys. Chem., 1990. 94: p. 8021-8024.
123. Dasent, W.E., *Inorganic energetics*. 1982, NY. Cambridge University Press.
124. Simonson, T. and C.L. Brooks, *Charge screening and the dielectric constant of proteins: Insights from molecular dynamics.* J. Am. Chem. Soc., 1996. 118: p. 8452-8458.
125. Warshel, A. and S.T. Russell, *Calculations of electrostatic interactions in biological-systems and in solutions.* Q. Rev. Biophys, 1984. 17: p. 283-422.
126. Arsen'ev, A.S., A.L. Lomize, I.L. Barsukov, and V.F. Bystrov, *Gramicidin A transmembrane ion-channel. Three-dimensional structure reconstruction based on NMR spectroscopy and energy refinement.* Biol. Membr., 1986. 3: p. 1077-1104.
127. King, G., F.S. Lee, and A. Warshel, *Microscopic simulations of macroscopic dielectric-constants of solvated proteins.* J. Chem. Phys., 1991. 95: p. 4366-4377.
128. Gilson, M.K. and H. B.H., *The dielectric constant of a folded protein.* Biopolymers, 1986. 25: p. 2097-2119.
129. Schutz, C.N. and A. Warshel, *What axe the dielectric "constants" of proteins and how to validate electrostatic models?* Proteins: Struct., Funct., Genet., 2001. 44: p. 400-417.
130. Tang, Y.Z., W.Z. Chen, and C.X. Wang, *Molecular dynamics simulations of the gramicidin A- dimyristoylphosphatidylcholine system with an ion in the channel pore region.* Eur. Biophys. J. Biophys. Lett., 2000. 29: p. 523-534.
131. Lide, D.R. and H.V. Kehiaian, *CRC handbook of thermophysical and thermochemical data*. 1994, Boca Raton. CRC Press.
132. Lynden-Bell, R.M. and J.C. Rasaiah, *Mobility and solvation of ions in channels.* J. Chem. Phys., 1996. 105: p. 9266-9280.

133. Busath, D.D., C.D. Thulin, R.W. Hendershot, L.R. Phillips, P. Maughan, C.D. Cole, N.C. Bingham, S. Morrison, L.C. Baird, R.J. Hendershot, M. Cotten, and T.A. Cross, *Noncontact dipole effects on channel permeation. I. Experiments with (5F-Indole)Trp(13) gramicidin A channels.* Biophys. J., 1998. 75: p. 2830-2844.
134. Hollerbach, U., D.P. Chen, D.D. Busath, and B. Eisenberg, *Predicting function from structure using the Poisson-Nernst- Planck equations: Sodium current in the gramicidin A channel.* Langmuir, 2000. 16: p. 5509-5514.
135. Lomize, A.L., V. Orekhov, and A.S. Arsenev, *Refinement of the spatial structure of the gramicidin A ion channel.* Bioorg. Khim., 1992. 18: p. 182-200.
136. Song, L., M.R. Hobaugh, C. Shustak, S. Cheley, H. Bayley, and J.E. Gouaux, *Structure of staphylococcal alpha-hemolysin, a heptameric transmembrane pore.* Science, 1996. 274: p. 1859-1866.
137. Mamonov, A.B., R.D. Coalson, A. Nitzan, and M.G. Kurnikova, *The role of the dielectric barrier in narrow biological channels: A novel composite approach to modeling single-channel currents.* Biophys. J., 2003. 84: p. 3646-3661.
138. Noskov, S.Y., W. Im, and B. Roux, *Ion permeation through the alpha-hemolysin channel: Theoretical studies based on Brownian dynamics and Poisson-Nernst-Plank electrodiffusion theory.* Biophys. J., 2004. 87: p. 2299-2309.
139. Hollerbach, U. and R.S. Eisenberg, *Concentration-dependent shielding of electrostatic Potentials inside the gramicidin A channels.* Langmuir, 2002. 18: p. 3626-3631.
140. Cheng, M.H., M. Cascio, and R.D. Coalson, *Theoretical studies of the M2 transmembrane segment of the Glycine receptor: models of the open pore structure and current-voltage characteristics.* Biophys. J., 2005. 89: p. 1669-1680.
141. Edwards, S., B. Corry, S. Kuyucak, and S.H. Chung, *Continuum electrostatics fails to describe ion permeation in the gramicidin channel.* Biophys. J., 2002. 83: p. 1348-1360.
142. Allen, T.W., O.S. Andersen, and B. Roux, *On the importance of atomic fluctuations, protein flexibility, and solvent in ion permeation.* J. Gen. Physiol., 2004. 124: p. 679-690.
143. Burykin, A., M. Kato, and A. Warshel, *Exploring the origin of the ion selectivity of the KcsA potassium channel.* Proteins, 2003. 52: p. 412-426.
144. Kubo, R., *Many-body theory*. 1966, Tokyo. Syokabo and Benjamin.
145. Straub, J.E., M. Borkovec, and B.J. Berne, *Calculation of dynamic friction on intramolecular degrees of freedom.* J. Phys. Chem., 1987. 91: p. 4995-4998.
146. Crouzy, S., T.B. Woolf, and B. Roux, *A molecular dynamics study of gating in dioxolane-linked Gramicidin A channels.* Biophys. J., 1994. 67: p. 1370-1386.
147. Berendsen, H.J., J.R. Grigera, and T.P. Straatsma, *The missing term in effective pair potentials.* J. Phys. Chem., 1987. 91: p. 6269-6271.
148. Pearlman, D.A., D.A. Case, J.W. Caldwell, W.S. Ross, T.E. Cheatham, S. Debolt, D. Ferguson, G. Seibel, and P. Kollman, *Amber, a Package of Computer-Programs for Applying Molecular Mechanics, Normal-Mode Analysis, Molecular-Dynamics and Free-Energy Calculations to Simulate the Structural and Energetic Properties of Molecules.* Comput. Phys. Commun., 1995. 91: p. 1-41.
149. Wang, J.M., P. Cieplak, and P.A. Kollman, *How well does a restrained electrostatic potential (RESP) model perform in calculating conformational energies of organic and biological molecules?* J. Comput. Chem., 2000. 21: p. 1049-1074.
150. Cornell, W.D., P. Cieplak, C.I. Bayly, I.R. Gould, K.M. Merz, D.M. Ferguson, D.C. Spellmeyer, T. Fox, J.W. Caldwell, and P.A. Kollman, *A second generation force field*

for the simulation of proteins, nucleic acids, and organic molecules. J. Am. Chem. Soc., 1995. 117: p. 5179-5197.
151. Wilson, M.A., A. Pohorille, and L.R. Pratt, *Molecular dynamics test of the Brownian description of Na+ motion in water.* J. Chem. Phys., 1985. 83: p. 5832-5836.
152. Torrie, G.M. and J.P. Valleau, *Nonphysical Sampling Distributions in Monte Carlo Free-Energy Estimation: Umbrella Sampling.* J. Comput. Phys., 1977. 23: p. 187-199.
153. Kumar, S., D. Bouzida, R.H. Swendsen, P.A. Kollman, and J.M. Rosenberg, *The Weighted Histogram Analysis Method for Free-Energy Calculations on Biomolecules. I. The Method.* J. Comput. Chem., 1992. 13: p. 1011-1021.
154. Schumaker, M.F., R. Pomes, and B. Roux, *A combined molecular dynamics and diffusion model of single proton conduction through gramicidin.* Biophys. J., 2000. 79: p. 2840-2857.
155. Hummer, G., *Position-dependent diffusion coefficients and free energies from Bayesian analysis of equilibrium and replica molecular dynamics simulations.* New J. Phys., 2005. 7: p. 1-14.
156. Miller, C., *Open-state substructure of single chloride channels from Torpedo electroplax.* Philos. Trans. R. Soc. Lond. B. Biol. Sci., 1982. 299: p. 401-11.
157. Richard, E.A. and C. Miller, *Steady-state coupling of ion-channel conformations to a transmembrane ion gradient.* Science, 1990. 247: p. 1208-1210.
158. Dukes, J.W. and R.D. Coalson, *Unpublished results.*
159. Faraldo-Gomez, J.D. and B. Roux, *Electrostatics of ion stabilization in a ClC chloride channel homologue from Escherichia coli.* J. Mol. Biol., 2004. 339: p. 981-1000.
160. Chandrasekhar, S., *Stochastic, statistical, and hydromagnetic problems in physics and astronomy*. 1989, Chicago. University of Chicago Press.
161. Atkins, P.W. and J. De Paula, *Atkins' physical chemistry*. 2002, Oxford. Oxford University Press.
162. Bostick, D.L. and M.L. Berkowitz, *Exterior site occupancy infers chloride-induced proton gating in a prokaryotic homolog of the ClC chloride channel.* Biophys. J., 2004. 87: p. 1686-1696.
163. Bisset, D., B. Corry, and S.H. Chung, *The fast gating mechanism in CIC-0 channels.* Biophys. J., 2005. 89: p. 179-186.
164. Chen, M.F. and T.Y. Chen, *Different fast-gate regulation by external Cl- and H+ of the muscle-type CIC chloride channels.* J. Gen. Physiol., 2001. 118: p. 23-32.
165. Nielsen, S., J. Frokiaer, D. Marples, T.H. Kwon, P. Agre, and M.A. Knepper, *Aquaporins in the kidney: from molecules to medicine.* Physiol. Rev., 2002. 82: p. 205-244.
166. Zeidel, M.L., S.V. Ambudkar, B.L. Smith, and P. Agre, *Reconstitution of functional water channels in liposomes containing purified red cell CHIP28 protein.* Biochemistry, 1992. 31: p. 7436-7440.
167. Zeidel, M.L., S. Nielsen, B.L. Smith, S.V. Ambudkar, A.B. Maunsbach, and P. Agre, *Ultrastructure, pharmacologic inhibition, and transport selectivity of aquaporin channel-forming integral protein in proteoliposomes.* Biochemistry, 1994. 33: p. 1606-1615.
168. Sui, H.X., B.G. Han, J.K. Lee, P. Walian, and B.K. Jap, *Structural basis of water-specific transport through the AQP1 water channel.* Nature, 2001. 414: p. 872-878.
169. Murata, K., K. Mitsuoka, T. Hirai, T. Walz, P. Agre, J.B. Heymann, A. Engel, and Y. Fujiyoshi, *Structural determinants of water permeation through aquaporin-1.* Nature, 2000. 407: p. 599-605.

170. de Groot, B.L., T. Frigato, V. Helms, and H. Grubmuller, *The mechanism of proton exclusion in the aquaporin-1 water channel.* J. Mol. Biol., 2003. 333: p. 279-293.
171. Chakrabarti, N., E. Tajkhorshid, B. Roux, and R. Pomes, *Molecular basis of proton blockage in aquaporins.* Structure, 2004. 12: p. 65-74.
172. Chen, H., Y. Wu, and G.A. Voth, *Origins of proton transport behavior from selectivity domain mutations of the aquaporin-1 channel.* Biophys. J., 2006. 90: p. L73-L75.
173. Fu, D., A. Libson, L.J. Miercke, C. Weitzman, P. Nollert, J. Krucinski, and R.M. Stroud, *Structure of a glycerol-conducting channel and the basis for its selectivity.* Science, 2000. 290: p. 481-486.
174. Miloshevsky, G.V. and P.C. Jordan, *Water and ion permeation in bAQP1 and GlpF channels: a kinetic Monte Carlo study.* Biophys. J., 2004. 87: p. 3690-3702.
175. Vidossich, P., M. Cascella, and P. Carloni, *Dynamics and energetics of water permeation through the aquaporin channel.* Proteins, 2004. 55: p. 924-931.
176. Mills, R., *Self-diffusion in normal and heavy water in the range 1-45.* J. Phys. Chem., 1973. 77: p. 685-688.
177. Jorgensen, W., J. Chandrasekhar, and J. Madura, *Comparison of simple potential functions for simulating liquid water.* J. Chem. Phys., 1983. 79: p. 926-935.
178. Neria, E., S. Fischer, and M. Karplus, *Simulation of activation free energies in molecular systems.* J. Chem. Phys., 1996. 105: p. 1902-1921.
179. MacKerell, A.D., D. Bashford, M. Bellott, R.L. Dunbrack, J.D. Evanseck, M.J. Field, S. Fischer, J. Gao, H. Guo, S. Ha, D. Joseph-McCarthy, L. Kuchnir, K. Kuczera, F.T.K. Lau, C. Mattos, S. Michnick, T. Ngo, D.T. Nguyen, B. Prodhom, W.E. Reiher, B. Roux, M. Schlenkrich, J.C. Smith, R. Stote, J. Straub, M. Watanabe, J. Wiorkiewicz-Kuczera, D. Yin, and M. Karplus, *All-atom empirical potential for molecular modeling and dynamics studies of proteins.* J. Phys. Chem. B, 1998. 102: p. 3586-3616.
180. Mark, P. and L. Nilsson, *Structure and dynamics of the TIP3P, SPC, and SPC/E water models at 298 K.* J. Phys. Chem. A, 2001. 105: p. 9954-9960.
181. van der Spoel, D., P.J. van Maaren, and H.J.C. Berendsen, *A systematic study of water models for molecular simulation: Derivation of water models optimized for use with a reaction field.* J. Chem. Phys., 1998. 108: p. 10220-10230.
182. Grigera, J.R., *An effective pair potential for heavy water.* J. Chem. Phys., 2001. 114: p. 8064-8067.
183. Allen, M.P. and D.J. Tildesley, *Computer simulation of liquids*. 1987, Oxford Oxfordshire, New York. Clarendon Press; Oxford University Press.
184. Kale, L., R. Skeel, M. Bhandarkar, R. Brunner, A. Gursoy, N. Krawetz, J. Phillips, A. Shinozaki, K. Varadarajan, and K. Schulten, *NAMD2: Greater scalability for parallel molecular dynamics.* J. Comput. Phys., 1999. 151: p. 283-312.
185. Essmann, U., L. Perera, M.L. Berkowitz, T. Darden, H. Lee, and L.G. Pedersen, *A Smooth Particle Mesh Ewald Method.* J. Chem. Phys., 1995. 103: p. 8577-8593.
186. Humphrey, W., A. Dalke, and K. Schulten, *VMD: Visual molecular dynamics.* J Mol Graphics, 1996. 14: p. 33-38.
187. Ye, R.G. and A.S. Verkman, *Simultaneous optical measurement of osmotic and diffusional water permeability in cells and liposomes.* Biochemistry, 1989. 28: p. 824-9.
188. Karan, D.M. and R.I. Macey, *The permeability of the human red cell to deuterium oxide (heavy water).* J. Cell Physiol., 1980. 104: p. 209-214.

189. Yang, B., T. Ma, and A.S. Verkman, *Erythrocyte water permeability and renal function in double knockout mice lacking aquaporin-1 and aquaporin-3.* J. Biol. Chem., 2001. 276: p. 624-628.
190. Roudier, N., J.M. Verbavatz, C. Maurel, P. Ripoche, and F. Tacnet, *Evidence for the presence of aquaporin-3 in human red blood cells.* J. Biol. Chem., 1998. 273: p. 8407-8412.
191. Tredgold, R.H. and R. Jones, *A study of gramicidin using deuterium oxide.* Biochim. Biophys. Acta., 1979. 550: p. 543-545.
192. *CRC handbook of chemistry and physics*. 1977, CRC Press: Cleveland, Ohio.
193. Finkelstein, A., *Water Movement through Lipid Bilayers, Pores and Plasma Membranes*. 1987, New York. John Wiley & Sons.
194. Mathai, J.C., S. Mori, B.L. Smith, G.M. Preston, N. Mohandas, M. Collins, P.C. van Zijl, M.L. Zeidel, and P. Agre, *Functional analysis of aquaporin-1 deficient red cells. The Colton-null phenotype.* J. Biol. Chem., 1996. 271: p. 1309-1313.